Intermittent turbulence and oscillations in the stable boundary layer over land

Promotor: Prof. dr. A.A.M. Holtslag

Hoogleraar in de meteorologie en luchtkwaliteit

Co-promotor: Dr. H.A.R. de Bruin

Universitair hoofddocent bij de leerstoelgroep
Meteorologie en luchtkwaliteit

Samenstelling promotiecommissie:

Dr. S. H. Derbyshire - Met Office, Bracknell, U.K.

Prof. dr. J. Oerlemans - Universiteit Utrecht

Prof. dr. F. T. M. Nieuwstadt - Technische Universiteit Delft

Prof. dr. ir. G. van Straten - Wageningen Universiteit

Intermittent turbulence and oscillations in the stable boundary layer over land

Bas van de Wiel

Proefschrift
ter verkrijging van de graad van doctor
op gezag van de rector magnificus
van Wageningen Universiteit,
prof. dr. ir. L. Speelman,
in het openbaar te verdedigen
op woensdag 4 december 2002
des namiddags te half twee in de Aula.

ISBN 90-5808-768-9

Voorwoord

Ha, het is zover! En ik mag nu eindelijk het voorwoord schrijven. Deze ‘sluitpost’ is volgens de moderne wetenschapsmaatstaven ook meteen het belangrijkste deel van het proefschrift, aangezien zij in den regel het meest gelezen wordt (stellingen buiten beschouwing latend). Nee, even zonder gekheid: ik vind het erg de moeite waard om stil te staan bij alle ‘support’ die mij gegeven is in de afgelopen tijd. En daarom het volgende dankwoord:

Om te beginnen zou ik graag mijn co-promotor Henk de Bruin bedanken. Hij was het die me zo’n jaar of vijf geleden polste of ik geen interesse had om op een tamelijk fundamenteel en open onderwerp te komen werken. Hoewel ik uit een ander vakgebied kwam, waren de eerdere ervaringen met het enthousiasme van Henk en de groep zodanig, dat ik wel zin had in een dergelijk avontuur. Dank voor je vertrouwen destijds en voor het feit dat je me van begin af aan in contact bracht met overzeesche mensen en instituten. Ik kreeg de mogelijkheid om als theoreet toch deel te nemen aan experimenten om ervaring op te doen en een zekere ‘feeling’ voor metingen op te bouwen. Naast uiteraard de inhoudelijke discussies leerde ik veel op het ‘meta-vlak’ bv. om zaken af te maken (minder zijpaden), strijdbaar om te gaan met kritiek en om compacter te schrijven.

Na een jaar of twee kreeg ik te maken met een nieuwe hoogleraar: Bert Holtslag. Je sloot snel aan bij het onderwerp en weldra bleek het zowel inhoudelijk als persoonlijk te klikken. Je bent altijd erg betrokken geweest bij het onderzoek en aarzelde vaak niet om ook versie X nog scherp onder de loep te nemen hetgeen de kwaliteit zeker ten goede is gekomen. Je inspireerde internationale presentatie & samenwerking en er lijkt een sterke continuering van het onderzoek binnen de groep aanstaande. Daarnaast is het leuk te vermelden dat ook het thuisfront altijd mocht rekenen op je interesse “Hoe is het in Tilburg?”-met zachte G.

Veel dank ben ik verschuldigd aan Arnold Moene. Gaandeweg werd je, min of meer toevallig, in het onderwerp opgezogen. Ik stormde vaak dolenthousiast je kamer binnen, na een (vermeende) vondst gedaan te hebben. Weldra barstten er ongelimiteerde discussies/brainstormsessies uit, elkaar de ruimte gevend voor heldere momenten én flaters. Daarbij verbaasden we onszelf soms met de ontdekking van een nieuwe paradox, een nieuwe onbekende ruimte, waar de tanden dan weer ingezet konden worden (na ons pensioen werken we part IV t/m MCIX wel uit). Naast medespeler in creative interactie ben je ook vaak de ‘advocaat van de duivel’ die tegenwicht biedt tegen al te snelle/slordige resultaten.

Zoals reeds gezegd werd mij de mogelijkheid geboden om mee te lopen met diverse experimenten, onder leiding van de ‘cracks’ Wouter, Oscar en Bert (Heusinkveld) samen met de student-collega’s Joost, Roos & Job. Naast uiteraard de serieuze bezigheden (zoals het ‘per ongeluk opblazen van een laptop’) zal ik de avonturen/gezelligheid van deze experimenten niet snel vergeten: de barre langlauftocht in de sneeuwstorm (Zweden), camperen en ’s nachts zwemmen in de Flevopolder&Italië, en de collega-immitaties, mailverslaving(Sandy) & Steve Vay in Kansas.

In de altijd zoekende, onzekere beginfase van het onderzoek kreeg ik bijval van Reinder Ronda. Op mijn zuchtende woorden dat het programmeren van een bepaald model een schier onmogelijke taak was voor mij, riep hij: “Dat hebben we vanmiddag nog af!”. Vele lunchpauzes hebben we gewandeld over de dijk, al dan niet loerend naar opvallende flora en fauna (met toppers als Bunzing en Ringslang). Many times we had lunch in the main building with Jeff, Jordi, Alexandro, Henk and Bert, enjoying a cup of soup and/or a real ‘Italian’ Cappuccino, that did not even deserve its name, according to our Italian collegue. We had many good laughs, although Jordi still doesn’t seem to realize that Willem II has a much better team than Barça!

Zoals velen wellicht weten zijn de koffiepauzes in Wageningen een gebeurtenis op zich. Dankzij het zelfzet-roestvrij-stalen koffieapparaat en de vernuftige roulatie-schema’s van Willy, varieert de sterkte van de koffie al naar gelang de aangewezen koffiebrouwer van de week (beginnende AIO’s zijn berucht). Een niet nader te noemen persoon met lange blonde haren kreeg het zelfs voor elkaar om, bij wijze van experiment, een week lang caffeïne-vrije koffie te zetten! Allemaal bedankt (zonder eerder genoemden):
Adrie(Stömungslehre-Brabo), Arjan(H. Universalis), Anne-Wim(surfing/BWA-boys), Berenice(Bere-nice), Dirk(Eins-Zwei-Drei,…), Floris(weather-photographer), Frits(Schumacher), Herbert(Slurfmans), Job(Amsterdammer), Jon(pijproker), Joost(Schunnig), Leo(Cleese), Mara(gezellie), Miao(Sjoep), Michaël(Hubble), Peter(Mountaineer I), Rushdi(Imam), Sjaak(politics), Teun(humor), Willy(Vitess’), Wim(master(fore)caster), Wim(Mountaineer II), met ieder zijn eigen-aardigheid. Onze alleskunner Kees bedank ik voor alle ondersteuning met betrekking tot computers en (schijnbare)Microsoft obstakels. En Gerrie (nog zo’n alleskunner) bedank ik voor de soepelheid én doeltreffendheid waarmee vele problemen van administrative/organisatorische aard immer weer werden opgelost (met altijd tijd voor een gezellig praatje).

De collega’s van het IMAU bedank ik voor de prettige samenwerking tussen Wageningen en Utrecht. Daarbij speciaal Prof. Peter Duynkerke (die helaas niet meer onder ons is) voor de prettige, pittige, en voor mij leerzame discussies die we hadden. Als gevolg daarvan las je binnen no time enthousiast (en belangeloos) manuscripten en voorzag ze van commentaar. Weet dat ik je erg graag in de commissie had gehad en ook graag in de toekomst verder had samengewerkt,…

I wish to express gratitude to some collegues from abroad: Michael Magnusson from Un. of Uppsala with whom I had a pleasant collaboration during and after the WINTEX field campaign in Sweden. Also Prof. Dick McNider from Un. of Huntsville (Alabama): you showed special interest in the work, sharing the same philosophy. Therefore, I hope we may continue to collaborate on these system dynamics stuff in the future. Since now you know how to order a “Straffe Hendrik” in our special-beer café, you are always welcome to visit us in Wageningen!

Niet onvermeld mag blijven de waardering voor de afstudeervakkers waar ik mee samen heb mogen werken om sommige aspecten van de stabiele grenslaag mee uit te diepen: Erwin Wolters (Low Level Jets/Cabauw, dank daarbij voor ondersteuning door Fred Bosveld vanuit het KNMI), Gerrit Oosterhuis(intermittency&waveletts), Jan van de Kassteele(mist& ruimtelijke intermittency) en onlangs de immer

enthousiaste Gert-Jan Steeneveld(SBL modellering&parameterisaties), die binnenkort zal aanvangen met een promotie-onderzoek over stabiele grenslagen, waarmee het huidige onderzoek een dubbel vervolg krijgt.

Ik ben ook blij dat ik een financiële bijdrage heb mogen ontvangen, als sponsoring voor de drukkosten van dit boekje: Wageningen Universiteit en METEO CONSULT WAGENINGEN bedankt!!

En dan belanden we uiteindelijk toch in de buitencategorieën waarvan iedereen zal begrijpen dat de belangrijkste facetten niet in woorden zijn uit te drukken en dus houd ik het kort. Op de eerste plaats: pa en moe, jullie zijn er altijd geweest voor ons!! Daarnaast hebben jullie ons van kinds af aan gestimuleerd in onze interesses, en daarmee tegelijkertijd ook de liefde voor de natuur-(kunde) bijgebracht. Mark(broer) & Dianne(schoonzus): jullie zijn altijd in voor een luisterend oor of juist voor een leuke discussie (dat heb je met die onderzoekslui). Enfin, Pa, moe, Mark en Dianne: bedankt voor alles!

Daarnaast bedank ik mijn schoonfamilie (schôn familie?): Jack, Mia en Claudia Kivits voor de belangstelling, de humor en de betrokkenheid bij het doen en laten van Sandy en mij (ondanks dat jullie schoonzoon/zwager weinig betrouwbare weersvoorspellingen bracht; daarvoor moeten jullie dan toch bij Erwin of Helga zijn!).

Aan de complete vriendenclub heb ik heel veel plezier beleefd tijdens de vele weekendjes. Of het nou om zeilen, wandelen, voetballen, mountainbiken, slangen zoeken, of het vieren van een fantastische bruiloft gaat: het is altijd gezellig met jullie. Daarnaast een speciale vermeldig voor mijn logeer-adres in Wageningen, het gezellige ‘Huize Pomona’ van Maurice en Roëlle (en voorheen ook Martin) waar ik ook na onze verhuizing naar Tilburg altijd welkom was. Dit was niet alleen gezellig maar ook vaak heel praktisch wanneer er flink gewerkt moest worden.

Last but not least bedank ik natuurlijk jou, Sandy. We hebben samen een intensieve, spannende periode achter de rug, maar hebben daarnaast gelukkig nog heel veel leuke dingen gedaan, met als hoogtepunt die onvergetelijke bruiloft & huwelijksreis van afgelopen jaar. Je leeft altijd erg met me mee, benieuwd en enthousiast,… en misschien,… ben je zelfs blijer dan ik dat de taak nu volbracht is. Ik ben blij lief en leed met je te mogen delen!

Zo is het voorwoord toch nog lang geworden,…maar dat geeft niet.

Contents

1 General Introduction **1**
1.1 General Terminology 2
1.2 Intermittent turbulence in stable atmospheric boundary layers 3
1.3 The current role of stable boundary layer formulations in weather forecast and climate models 5
1.4 Some physical background 8
1.5 Research questions and contents 13

2 Intermittent turbulence and oscillations in the stable boundary layer over land.
Part I: A bulk model. **17**
2.1 Introduction 18
2.2 Model setup 21
2.2.1 General description 21
2.2.2 Parameterization of turbulent fluxes 23
2.2.3 Parameterization of longwave radiation 24
2.2.4 Parameterization of surface temperature dynamics 25
2.2.5 Model equations and solving 26
2.3 Model results 28
2.3.1 Transient behaviour 28
2.3.2 Flow regimes 29
2.3.3 The oscillatory regime 30
2.3.4 Sensitivity to forcing parameters 32
2.3.5 Sensitivity to local surface parameters 32
2.4 Impact of turbulence parameterization 34
2.4.1 Stability functions 34
2.4.2 Modelled stability functions for the intermittent case 35
2.4.3 Transient runs for different stability functions 36
2.5 Discussion 37
2.5.1 Comparison with previous work 37
2.5.2 Practical/experimental issues 39
2.6 Conclusions 39

3 Intermittent turbulence and oscillations in the stable boundary layer over land.
Part II: A system dynamics approach **45**
3.1 Introduction 46
3.2 The system equations 48
3.3 Stability analysis of the equilibrium solution and derivation of the intermittency parameter 50
3.3.1 The equilibrium solution and its mathematical stability 50
3.3.2 Application of the Hopf-bifurcation technique: derivation of the intermittency parameter 51
3.3.3 An example 52

3 (continued)
3.4 Flow regimes in the SBL: a classification based on dynamics 54
3.4.1 Classification based on SBL dynamics 54
3.4.2 Relation to other SBL classifications 55
3.5 A simplified criterion for instability 57
3.5.1 Introduction 57
3.5.2 Comparison of stability criteria 59
3.6 Discussion 60
3.6.1 Intermittency versus decoupling 60
3.6.2 Impact of the boundary conditions 60
3.6.3 Practical issues 61
3.7 Conclusions 62

4 Intermittent turbulence and oscillations in the stable boundary layer over land.
Part III: A classification for observations during CASES-99 **69**
4.1 Introduction 70
4.2 Data description 72
4.3 Observed flow regimes during CASES99 72
4.3.1 Method 72
4.3.2 Results: a classification of SBL regimes using observations of flux time-series 73
4.3.3 Classification applied to the whole CASES99 dataset 77
4.4 Application of Π: input parameters 78
4.4.1 Introduction 78
4.4.2 Estimation of external forcing parameters 79
4.4.3 Estimation of local system parameters 80
4.4.4 Boundary conditions 82
4.4.5 Other input parameters 82
4.4.6 Summary 82
4.5 Comparison of theory and observations 83
4.5.1 Using full theory (Π) 83
4.5.2 A simplified approach 86
4.6 Discussion 88
4.7 Conclusions 90

5 Summary **93**

6 Perspectives **99**

Appendix A: Background to the basic equations **107**

Appendix B: Outline of the Hopf-Bifurcation technique **111**

Bibliography **115**

Samenvatting **123**

Curriculum Vitae **129**

Chapter 1

General introduction

1 General Introduction

Below the subject of research is defined and its practical relevance in relation to weather and climate prediction is discussed. Also some specific physical background, related to the posed problems, is given. For a general background on the governing equations we refer to Appendix A. Finally, a number of research questions that will be addressed in the remainder of this thesis, is listed.

1.1 General terminology

As indicated by the title, this thesis deals with ***'intermittent turbulence in the atmospheric boundary layer under stable conditions'***. For those not familiar with this subject, some terminology will be explained in this section. The 'intermittency' aspect is discussed separately in the next section.
Loosely defined, we may state that the ***atmospheric boundary layer*** is thát part of the atmosphere that is directly influenced by the presence of the earth's surface (the actual boundary: hence its name). It responds relatively rapid to changing surface forcings (on a time-scale of less than an hour). As a result, this lower part of the atmosphere experiences the largest diurnal variation in temperature. The depth of the boundary layer varies typically between 500m-2km during daytime and 50m-300m during the night. Due to turbulent motion of air the transport of heat, momentum, moisture, carbon-dioxide and other gases within the boundary layer can be very efficient. Here, by **'turbulent motion'** we mean the chaotic motion of air, consisting of irregular, three-dimensional swirls/eddies that (inter)act over a large range of scales.
Generally speaking, the character of turbulence is dissipative, in a sense that turbulence intensity loses strength due to internal friction, caused by viscous forces on the scale of the smallest eddies. Thus turbulence must be generated continuously in order to keep it going. In the atmosphere turbulence is often generated by the mean wind (shear). (Note that from a large-scale perspective, flow of the mean wind, in turn, is driven by horizontal pressure differences, ultimately generated by differential heating of the earth by the sun). In a daytime situation however, turbulence may also be generated by large convective cells/thermals: due surface heating by solar radiation, near-surface air parcels become warmer than their surroundings, causing them to have a lower density than their surroundings. In presence of the Earth's gravity field, this situation is unstable and the air parcels start to rise (forming thermals), thus driven by upward buoyancy forces ('Archimedes' forces). Consequently, these type of boundary layers are called: unstable boundary layers.

How different things are during nighttime. At nighttime, the longwave radiative cooling of the surface (most natural surfaces have a higher emissivity than air) leads to a *cooling* of the near-surface air. A temperature-stratified boundary layer develops with the coldest temperatures near the surface, increasing upwards. Because cold air has a higher density than warm air, buoyancy forces tend to keep air parcels in place, resisting work against gravity-or: a particle displaced vertically tends to get back at its original position. As such the atmosphere is stably stratified, i.e. a **stable boundary layer** (SBL) develops. In this cases turbulence can only be generated by mechanical shear of the mean wind. At the same time, buoyancy forces act to destroy turbulent kinetic energy (together with viscosity). In fact the competition between this generation and destruction of turbulent kinetic energy plays a crucial role in our current understanding of stable boundary layer physics. The potential of turbulence to

mix air parcels in a stable environment is often expressed in terms of a so-called Richardson number (Ri or Rf), representing the ratio of the amount of turbulent kinetic energy (TKE) destructed by buoyancy forces to the amount of TKE generated by wind shear.
Now it becomes clear why the depth of the boundary at nighttime is generally an order of magnitude smaller than during daytime: buoyancy forces counteract vertical motion (and mixing) in stead of generating it, as in the daytime case. As a consequence turbulence intensities are often much smaller during nighttime than in daytime conditions. Moreover, at night the intensity of turbulence may vary strongly in time, in a sense that quiet periods with hardly any turbulence are followed by bursting periods with strong turbulence. This fundamental aspect of stable boundary layers has strong implications for transport of heat, momentum, moisture, carbon-dioxide and pollutants, and forms the core-of-interest of this thesis. Therefore this subject is addressed in more detail in the following sections.

1.2 Intermittent turbulence in stable atmospheric boundary layers.

Most of us are familiar with the fact that, on a clear evening wind speed may drop considerably, and may even totally vanish. In these quiet conditions, hardly any turbulence is present. This absence of turbulent mixing causes a relative thin strongly stratified layer of cold air to built up in the lower atmosphere. The air layers near the surface become very stable and seem to 'stick' at it. This effect can be visually noticed in case of strong radiation fog: a thin, dense layer of fog covers the cattle field and only the cows heads are visible (that is, in a Dutch landschape…). In figure 1.1 fog enters the flood plain area of the River Rhine, in Wageningen. One may also percept this 'sticking'-effect by smelling the undiluted concentration of blossom perfumes, or, alternatively, exhaustfumes.

Figure 1. 1: Mist in the flood plain area of the River Rhine, Wageningen (by courtesy of: F. Bijlsma).

After a certain amount of time however, the wind may suddenly increase, as noted by the moving tree leaves. This sudden increase of wind causes enhanced mixing by mechanical turbulence. The high gas concentrations near the surface are effectively diluted. In a same manner, cold air near the surface is mixed with warmer air from above, causing a significant heat flux to the surface. As a result near-surface temperatures suddenly rise by several degrees. But later, after some period, often the wind drops again, followed by a collapse of turbulence (as before)…and so on.

Naturally the following question comes up:
Where does this strange 'bursting behaviour' of near-surface turbulence come from?

In literature the discontinous behaviour of turbulence mentioned above is referred to as: ***intermittent turbulence*** (Lat.: intermittere ≈ to stop for a while). It is characterized by brief episodes of turbulence with intervening periods of relatively weak or unmeasurable small fluctuations (Mahrt, 1999). An example of such intermittent behaviour of the turbulent heat flux in a particular night is given in Fig. 1.2. The example shows a clear alternation between strongly turbulent periods with large negative heat fluxes and more quiet periods with hardly any heat flux. For comparison also a non-intermittent timeseries is given representing another night at the same location with continous strong winds.

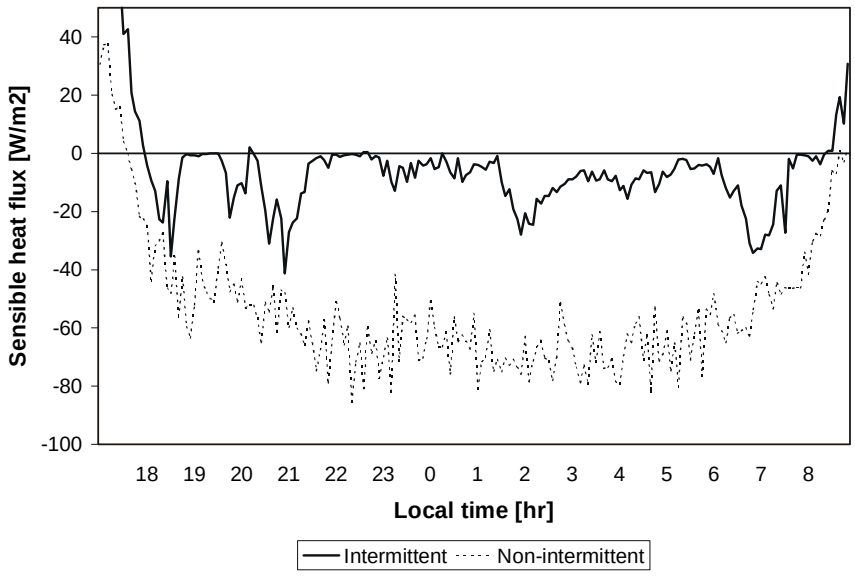

Figure 1. 2: Turbulent heat flux for two different nights observed during CASES-99, Kansas (see: chapter 4). Solid line: a night with intermittent turbulence. Dashed line: a night with continuous turbulence.

The intermittent character of turbulence may have different physical causes, as outlined in the reviews of chapters 2 and 3. The present work focuses on a particular mechanism described below (after Businger (1973) and Turner (1972)):

> On clear nights with weak winds strong radiative surface cooling may built up an intense stratification of temperature. As this stratification increases and becomes large compared to the existing wind shear (thus large Ri) turbulent mixing is strongly suppressed and eventually it cannot longer be maintained and ceases. Turbulent exchange between the atmosphere and the surface vanishes, and the atmosphere *decouples* from the surface. Because in this situation the air experiences hardly any surface friction, the omnipresent

pressure force starts to accelerate the air. Wind speed increases and after some time the wind shear is strong enough to break through the stratification causing large turbulent mixing. This mixing strongly reduces temperature stratification and wind shear. As the wind shear is small little turbulence is generated and the lower atmosphere reaches a quiet state. Now the radiative cooling begins to form a new stratified layer, and the whole situation starts over again. Several of these cycles will cause intermittent bursts of turbulence and an oscillatory-type of behaviour by the mean variables.

Intermittent turbulence seems to occur frequently in real atmospheric boundary layers, and represents a significant transport mechanism between the atmosphere and the surface in stable conditions. Still its physics are poorly understood. This current lack of knowledge about intermittent turbulence and, more general, about stable boundary layer dynamics, has direct implications for the current practice of weather and climate predictions in stable/nocturnal conditions. Some of these implications are discussed in the next section.

1.3 The current role of stable boundary layer formulations in weather forecast and climate models.

This section is mainly based on material from Beljaars and Viterbo (1998) and Viterbo et al. (1999). The representation of the stable boundary layer physics in the ECMWF-model (European Centre for Medium-Range Weather Forecasts) strongly influences our capability to describe large scale weather development, particularly in winter over the Nortern Hemisphere. The evolution of weather patterns is for example strongly dependent on the momentum budgets, which , in turn depend on our description of the surface drag laws. This goes not only on the global scale, where drag from entire continents is felt, but also at the smaller synoptic scales, were surface drag causes damping on low- and high-pressure systems (Ekman damping). Also, the description of stable boundary layer physics in the ECMWF model influences its capability to simulate nighttime and wintertime temperatures. Naturally, this aspect is important for correct frost, fog and sleet predictions (Figs. 1.1/1.3).

Figure 1. 3: rime-frosted grass (photo by courtesy of G.van Aefst)**.**

Despite its relevance for weather prediction issues, the physics of stable boundary layer transport processes are still poorly understood. This lack of knowledge is reflected in the uncapability of current weather and climate models to represent stable boundary layer (SBL) dynamics in an accurate and fysically consistent way. Below some problems with flux parameterization in stable conditions with the ECMWF model are discussed and related to the intermittency issue in the present work.

Traditionally, in numerical weather prediction models, that is for stable conditions, fluxes of heat (H) and momentum (τ) are related to local gradients of the mean wind vector $\mathbf{U}$ and of the mean (potential) temperature T , using some form of K-theory (for background see: Appendix A and section 1.4) :

$$\tau = \rho\left(l^2 F_m(Ri)\left|\frac{\partial \mathbf{U}}{\partial z}\right|\right)\cdot\left|\frac{\partial \mathbf{U}}{\partial z}\right| \qquad (1)$$

$$H = -\rho c_p\left(l^2 F_h(Ri)\left|\frac{\partial \mathbf{U}}{\partial z}\right|\right)\cdot\frac{\partial T}{\partial z} \qquad (2)$$

The diffusion coefficients for momentum K_m and heat K_h (defined through the bracket terms) depend on the local Richardson number (see definitions above) via the stability functions F_m and F_h. Since, presently no universal form of these stability functions exists, various formulations are proposed in literature (see, reviews by Van den Hurk en Holtslag, 1997; De Bruin et al.,2000). In Fig. 1.4a and 1.4b some examples are given.

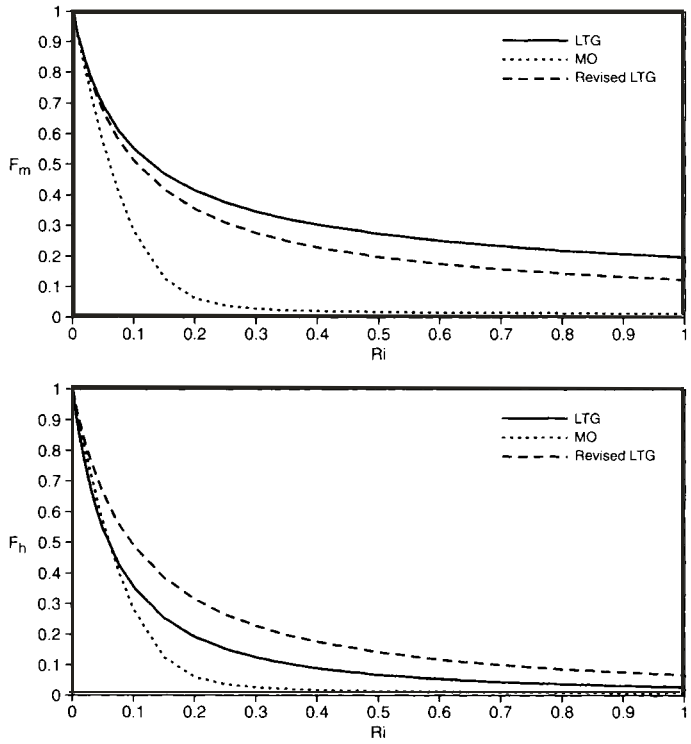

Figure 1. 4a,b: examples of stability function for momentum (upper panel) and heat (lower panel). Dotted line: MO-functions proposed by Beljaars and Holtslag (1991), solid line: Louis, Tiedtke and Geleyn (1982), and the revised version of the latter is given by the dashed line (Viterbo et al, 1999).

A common feature of the stability functions is that they decrease monotonically with increasing stability (indicated by Ri). This represents the fundamental property of the SBL discussed above, namely that vertical mixing is generally speaking less efficient at higher stability, because at larger stability vertical motions have to work harder against gravity. On the other hand, from Fig. 1.4a and 1.4b it occurs that the differences between the proposed stability functions are large. The dotted line represents a stability function derived from Monin-Obukhov similarity theory as suggested by Beljaars and Holtslag (BH,1991). These BH relationships are supported by observations (albeit mostly in the weakly stable part) and is within the range of experimental material reviewed by Högström (1988, 1996). Up till now, however, physically-based MO functions like BH showed not succesfull in numerical weather prediction:
-the simulated surface drag on large scale system is largely underestimated
-the simulated surface temperatures are too cold.
Related to the features above is the observations that NWP simulations using MO relationships often show a definite decoupling between the first model level and the levels above (Beljaars and Viterbo, 1998). In this decoupled cases, turbulent heat flux towards the surface is very low. In the model this causes a runaway of the (near) surface temperature to unrealistic low values, and causes unrealistic low surface drags.

A practical way to prevent this decoupling is to use (artificial) stability functies that allow a significant turbulent heat flux at large Richardson numbers (Fig. 1.4a,b). A well-known stability function was proposed by Louis, Tiedtke and Geleyn (1982; here indicated as LTG). This function largely solved the surface drag problem, but the surface temperatures were still predicted too low. Therefore a revised LTG scheme was introduced (Viterbo et al. 1999) with a larger stability function for turbulent heat exchange. Note that, with this modification the stability function for momentum had to be adjusted to maintain the same surface drag, since the equations of momentum and heat are coupled. To get an impression about the effect of stability functions on average weather/climate prediction, a seasonal integration is shown in Fig. 1.5 (From:Viterbo et al. 1999).

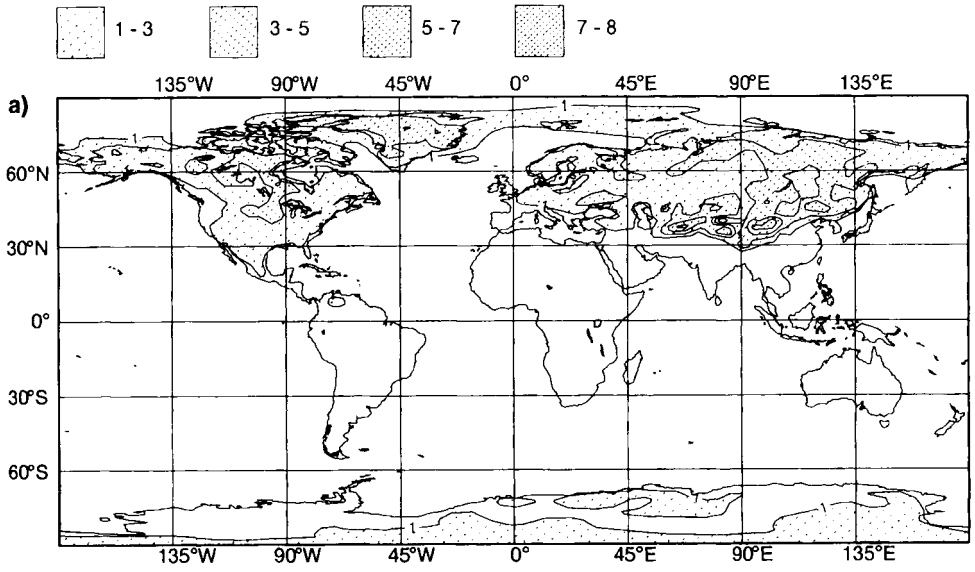

Figure 1. 5: difference in 2m temperature for January 1996, calculated from operational weather analysis, using the LTG scheme and its revised version (from: Viterbo et al., 1999).

Fig. 1.5 shows the difference in 2m temperature for January 1996, between the (relaxed) operational analysis using LTG and the revised LTG scheme. It is observed that the revised LTG scheme increases monthly-mean temperatures by 1 to 3 degree C over large continental areas of the northern hemisphere and over a considerable part of Antarctica (of course, differences are larger for individual days). In view of the shape of the stability functions it is likely that the differences between the MO scheme and the revised LTG scheme would result in even larger differences. From these results it can be concluded that large uncertainties in the describtion of stable boundary layer processes imply large uncertainties in the outcome of weather predictions under stable conditions. This is even more true for long term climate predictions, as with studies on global warming, due to enhanced greenhouse effects. According to our current knowledge, one of the most important consequences of an enhanced greenhouse-effect seems to be the warming of stable boundary layers over land (IPCC, 2001). Just these type of boundary layers are poorly understood.

1.4 Some physical background

The practical problems in NWP indicated above are strongly connected with their scientific counterparts. Most importantly it is recognized that "The LTG functions are not based on observational material but are inspired by model performance" (Beljaars and Viterbo, 1998), which is unsatisfactory from a scientific perspective.
If we aim at a more more reliable and physically based description of the stable boundary layer (SBL) in NWP models , we should investigate the physical cause for this decouping/intermittency behaviour. It is clear (from section 1.2) that both phenomena are real characteristics of the SBL, and that they are probably closely related. Therefore, a more realistic SBL description in NWP models, should try either to explicitly permit decoupling/intermittent behavior or parameterize both processes in a consistent way. In this respect it is doubtfull if any time-average flux-profile relationship, as currently used in NWP, can hold in a situation with intermittent turbulence (see: introduction chapter 2). The same goes for the spatial-averaged equivalent, not adressed here (see e.g. Ronda and De Bruin, 1999 or Acevedo and Fitzjarrald, 2002). But, obviously, an alternative for the current practical approach cannot be found without an understanding of the SBL dynamics in those conditions, explaining the motivation for the present work.

Non-linearity enters the equations
In this section some characteristics of SBL behaviour are discussed by looking at typical diffusion laws describing turbulent exchange processes. The purpose of this section is to show that the non-linear nature of these laws favors complicated/rather dramatic behavior. For this introduction a rather straightforward approach is followed without too much discussion on the exact quantitative characteristics. For a more rigorous treatment of this instability problem we refer to chapters 2,3 and 4. Also, for a formal introduction into the governing equations used in this thesis, we refer to App. A.

As already indicated above, in stable boundary layer studies turbulent fluxes are often expressed in terms of local gradients of the mean quantities using a type of diffusion equation. These relationships implicitely assume that the turbulent kinetic energy budget is determined by local parameters (see: App. A; Duynkerke and De Roode,

2001). In this way the local shear stress and turbulent heat flux can be related to local gradients of temperature and wind speed (standard notation used):

$$\tau = \rho K_m \left| \frac{\partial \mathbf{U}}{\partial z} \right| \qquad (3)$$

$$H = -\rho c_p K_h \frac{\partial T}{\partial z} \qquad (4)$$

with the turbulent exchange coefficients for momentum K_m and heat K_h usually expressed as:

$$K_m = \frac{(\kappa z)^2}{f_m} \left| \frac{\partial \mathbf{U}}{\partial z} \right| \text{ and } K_h = \frac{(\kappa z)^2}{f_h} \left| \frac{\partial \mathbf{U}}{\partial z} \right| \qquad (5)$$

The exchange functions for momentum f_m and heat f_h are often expressed in terms of a local stability parameter z/Λ (as defined by Nieuwstadt, 1984). These relationships $f_m(z/\Lambda)$ and $f_h(z/\Lambda)$ have to be found from experiments such as reviewed by Högström (1996). Alternatively, f_m and f_h can be expressed in terms of another local stability parameter: the gradient Richardson numbe Ri. To gain some physical insight eqs. (3),(4), and (5) are combined using Ri as stability parameter (similar to (1) and (2)):

$$\tau = \rho \left((\kappa z)^2 F_m(Ri) \left| \frac{\partial \mathbf{U}}{\partial z} \right| \right) \cdot \left| \frac{\partial \mathbf{U}}{\partial z} \right| \qquad (6)$$

$$H = -\rho c_p \left((\kappa z)^2 F_h(Ri) \left| \frac{\partial \mathbf{U}}{\partial z} \right| \right) \cdot \frac{\partial T}{\partial z} \qquad (7)$$

with:

$$Ri = \frac{g}{T_{ref}} \frac{\partial T}{\partial z} \Big/ \left| \frac{\partial \mathbf{U}}{\partial z} \right|^2$$

It immediately occurs that the turbulent exchange coefficients, as represented by the bracket terms in (6) and (7), are not material constants (as in laminar flow), but depend on the nature of the flow itself. This is a fundamental property of turbulent flow (Nieuwstadt, 1992). A closer look learns that the exchange coefficients are function of the wind speed and (via Ri) temperature gradients themselves! This property causes the turbulent diffusion to be a non-linear process. As a consequence, governing equations that contain such terms are non-linear differential equations (App. A). This non-linear structure of the equations prevents explicit analytical time-dependent solutions, such as often available for linear differential equations (Seydel, 1988). But the most important and most interesting aspect is the fact that these non-linear type of equations may lead to rather unexpected/dramatic behavior, unlike their linear counterparts. This is illustrated with the example below:

Example

In this example the temporal behavior of a simple surface energy budget is studied for a thin vegetation layer with uniform temperature T_S (similar to Eqs. chapters 2,3 and 4):

$$\rho_v c_v \frac{\partial T_S}{\partial t} = Q_{net} + G_0 - H_0 \qquad (8)$$

with ρ_v the bulk density [kg m^{-3}] and c_v the thermal heat capacity [J kg^{-1} K^{-1}] of the vegetation layer. Q_{net} is the net longwave radiation defined positive downward, G_0 the soil heat flux and H_0 the turbulent heat flux, both positive upward. In 'normal' nighttime conditions Q_{net} is negative (surface energy loss), G_0 is positive and H_0 negative (both surface energy gain). Here we assume Q_{net} and G_0 to have fixed values, neglecting important feedback mechanisms in these terms as discussed in chapter 3.

The surface heat flux is related to the mean profiles of temperature and wind speed similar to Eq. (7). But, in stead of using gradients as in (7), finite differences of temperature and wind speed are used between the surface and a reference height z_{ref}. As such the equation below is derived from an integration of temperature and wind profiles over a finite depth $z_{ref} - z_0$ assuming Monin-Obukhov (MO) theory, as a special case of local similarity, to be valid. This gives (following Businger et al., 1971):

$$H = -\rho c_p \left[c_{Dn} |\mathbf{U}| \cdot F_h(R_b)\right] \cdot (T - T_S) \qquad (9)$$

with c_{Dn}, the neutral drag coefficient (chapter 3). Because finite differences are used, the so-called bulk-Richardson number R_b is taken in stead of the gradient Richardson number Ri (chapter 2).

We now investigate the behavior of the surface energy budget equation, assuming wind speed to be fixed. Of course in reality this assumption is questionable, because the wind speed is not a conservative quantity. In this case, Eq. (9) may simply be written as:

$$H = -\alpha \cdot F_h(R_b) \cdot (T - T_S) \qquad (10)$$

α being a constant [W m^{-2} K^{-1}]. In figure 1.6c the downward turbulent heat flux at the surface is plotted as a function of the temperature difference between the surface and 10m, for a fixed wind speed of 4 [m s^{-1}] at 10m height. Also, the two basic factors of the turbulent heat flux i.e. the 'temperature gradient part' $\alpha(T - T_S)$ and the stability function $F_h(R_b)$ are given as a function of $T - T_S$ in Figs. 1.6a,b.

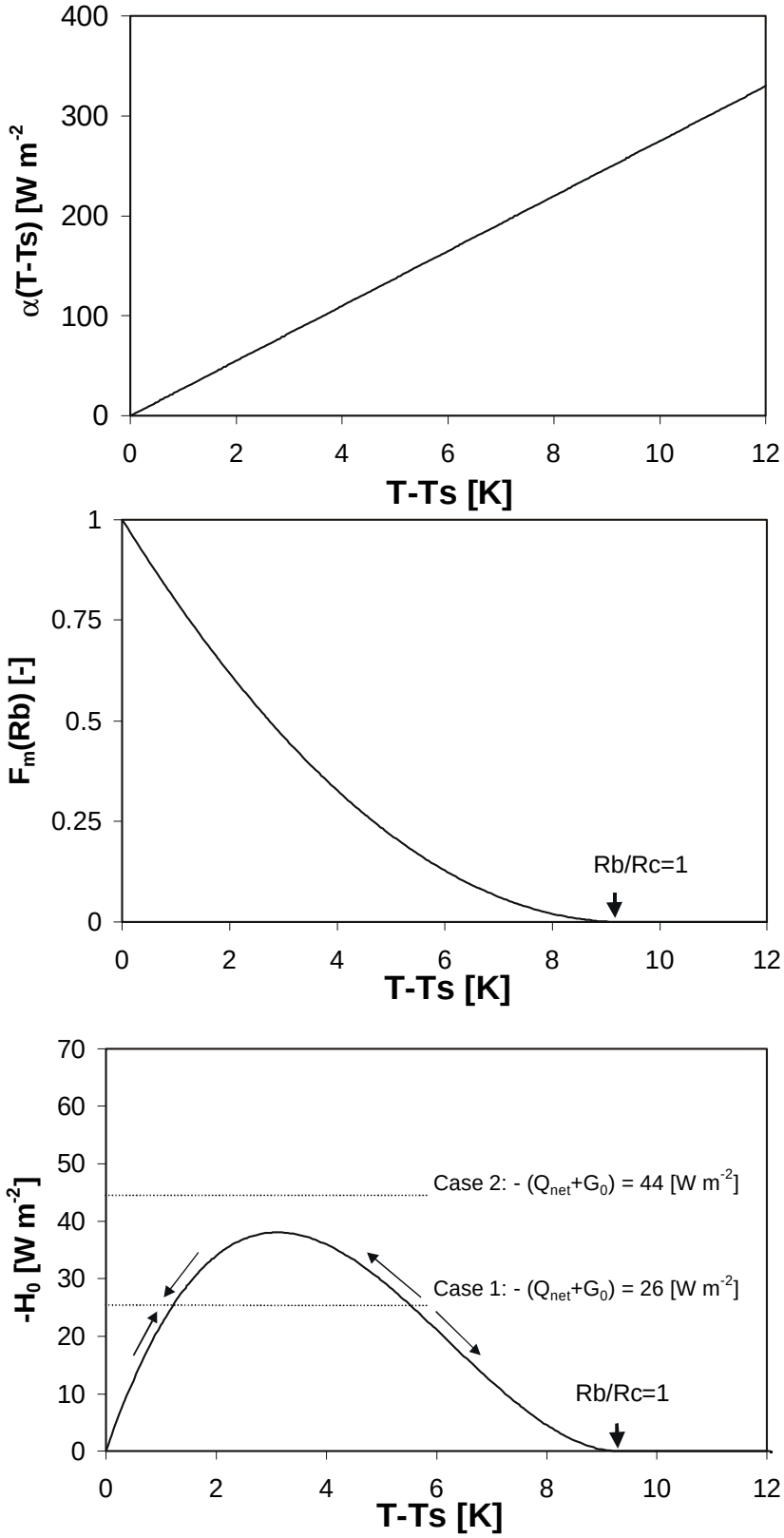

Figure 1. 6: the downward turbulent heat flux (1.6c) as a function of the temperature inversion in the lower atmosphere, under conditions of fixed shear. The two main factors contributing to this flux are given as a function of temperature inversion in 1.6a, the 'temperature gradient part', and 1.6b, the stability function part. In Fig. 1.6c two different values of imposed surface cooling are plotted, corresponding to two case studies discussed in the main text

The 'temperature gradient' part linearly increases with an increasing temperature difference (as with linear diffusion). The stability function however *decreases* with an increasing temperature difference, which, as before, reflects the decreasing mixing efficiency at higher stabilities.

The combined effect of both parts is given by the downward heat flux graph (1.6c), which, as a consequence, shows a clear maximum (De Bruin 1982, personal communication). It can be shown that this maximum occurs at $R_b / R_c = \frac{1}{3}$ and that its value is proportional to $|\mathbf{U}|^3$, R_c being the critical value of the bulk Richardson number (chapter 2). This graph is used to illustrate possible SBL dynamics by discussing two cases:
-case 1 with relative weak cooling: $-(Q_{net} + G_0) \approx 26$ [W m^{-2}]
-case 2,with relative strong cooling: $-(Q_{net} + G_0) \approx 44$ [W m^{-2}].

Case 1
In this case, H_0 equals $(Q_{net} + G_0)$ at two values of $T - T_S$ (notably at $T - T_S \approx 1.3$ [K] and $T - T_S \approx 5.6$ [K]). Thus, Eq. (8) has two equilibrium solutions (A and B). Point A is a (mathematically) stable equilibrium point attracting solutions: starting from a neutral situation (i.e. $T - T_S$ =0) the tendency in Eq. (8) will be negative ($\partial T_S / \partial t$ <0) causing an inversion to develop and strengthen, until H_0 equals $(Q_{net} + G_0)$. Also, an initial point just right from A will have a positive tendency ($\partial T_S / \partial t$ >0), causing the initial inversion $T - T_S$ to decrease until point A is reached. Point B, however, is an (locally) unstable equilibrium point. For example: an initial point just to the right of B will have a negative tendency ($\partial T_S / \partial t$ <0), because $|H_0| < |Q_{net} + G_0|$. This negative tendency however, will only increase $T - T_S$ causing the tendency to become even more negative. If there were no other compensating mechanisms, then the solutions would run away causing $T - T_S$ to increase infinitely, which would lead to a definite atmospheric decoupling from the surface (In the same way an initial point just left from B would end up in A). In reality, however, this 'run-away' behaviour of $T - T_S$ is opposed by negative feed-backs from the momentum budget and negative feed-backs though Q_{net} and G, which both depend on surface temperature.

Case 2
It is observed that there are no intersection points were H_0 equals $(Q_{net} + G_0)$. Because $|H_0|$ is smaller than $|Q_{net} + G_0|$ for all $T - T_S$, the tendency $\partial T_S / \partial t$ will always be negative, resulting in an infinite surface cooling. In this case, eventually all turbulent activity vanishes, resulting in a totally decoupled SBL. But, as before, in reality, feed-back mechanisms in Q_{net}, in G_0 and in the momentum budget may prevent such extreme surface cooling.

Discussion

The example above shows that even a very simple non-linear energy budget equation can respond very differently in situations with different external cooling rates. Even for a single cooling rate the system may have more than one solution (case 1). The fact that different initial conditions showed a different model response could even have implications for the predictability of stable boundary layers (McNider et al. 1995), although these predictability problems were not encountered in the present work.

Even though the introductionary example above is too simplistic (neglection of important feed-backs) to draw definite conclusions about SBL behaviour, it clearly demonstrates the possible vividness of SBL dynamics due to the non-linear interactions in the governing equations. Moreover it demonstrates that sudden regime transitions may be an inherent part of the SBL nature.

1.5 Research questions and contents

In the previous sections the non-linear character of the governing equations was discussed in relation to the decoupling/intermittency problems, as its consequences for the current numerical weather prediction practice. At this point the following question comes up naturally:

-how would SBL dynamics in a weather-prediction-type of model look like if we permitted decoupling and intermittency to occur?

Although, this question is still not answered, in the past some studies gave a hint of what might happen. An example (by Lin (1990) as referred to in McNider et al. (1995)) is shown in Figs. 1.7a,b,c. The results are from a typical mesoscale model run in a one-dimensional mode for the nocturnal boundary layer. The model (described by McNider and Pielke (1981)) contains local Richardson number closure, such as described in the previous sections and solves surface energy physics typical of today's generation of mesoscale and regional models.

The figures show predicted temperatures at 4 m for three different imposed geostrophic wind speeds. As a low geostrophic wind speed is applied the temperature evolution shows the characteristics of a decoupled atmosphere with extreme cooling near the surface. At high geostrophic wind speed a much warmer solution occurs. In between, at moderate geostrophic wind speed, the temperature shows an oscillatory type of behaviour. This type of behaviour results from a discontinuous/intermittent behaviour of the turbulent fluxes, and it leads to moderately low temperatures. Thus, it is observed that the model shows different regimes responding to different external forcings. The presence of different regimes in both observations (chapter 4) and modeling is a fascinating feature, which partly motivated the present work.

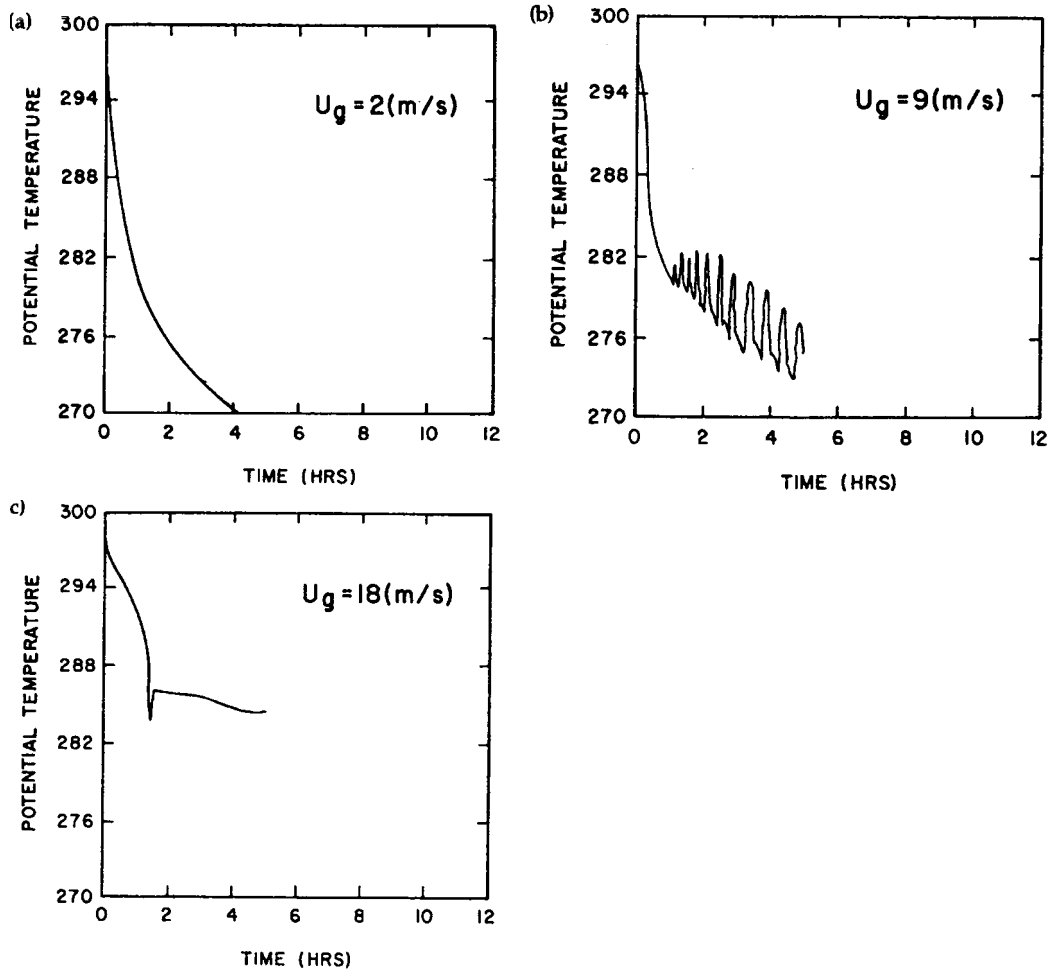

Figure 1. 7a,b,c: Time dependent solutions for temperature from a mesoscale boundary layer model for different imposed geostrophic wind speeds: **(a)** 2, **(b)** 9, **(c)** 18 [m s^{-1}] (Fig. from: McNider et al. 1995).

Research questions

In the present work the following questions are addressed:

I) - What is the physical essence of the behaviour showed by the examples above?
- Is it possible to simulate both intermittent and non-intermittent regimes with a simple model?

II) - What external forcing parameters control the transitions between these regimes?
- Can we predict the occurrence of intermittent and non-intermittent regimes?

III) – Which regimes are actually observed in the field and under what conditions do they occur?

The present work consists of three parts: the first part is a numerical study (chapter 2), the second part an analytical study (chapter 3) and the third part is an observational study (chapter 4).

-The numerical study in chapter 2 addresses the first research questions: the governing equations are truncated into a simple bulk model, which mimics the behaviour of Figs. 1.7a,b,c ,showing intermittent and non-intermittent regimes. Also the sensitivity of the

model behaviour to different surface characteristics and stability functions is investigated.

-The analytical study addresses the second research questions: the results of chapter 2 are generalized by studying the model equations using system dynamics techniques. As such a new classification is proposed that predicts the occurrence of different SBL regimes as a function of external forcing parameters and local surface properties.

-The observational study addresses the third research questions: surface layer observations are classified in different regimes and this classification is compared to the theoretical predictions of the numerical and analytical studies.

The chapters are published (Chapters 2 and 3), or accepted for publication (Chapter 4) as separate papers in the international Journal of Atmospheric Sciences, almost exactly in the form as they are presented in this thesis. As such, some minor repetition in the introductions of the chapters could not be avoided.

Chapter 2

Intermittent Turbulence and Oscillations in the Stable Boundary Layer over Land:

Part I: A bulk model

This chapter is based on:

Van de Wiel, B. J. H., R. J. Ronda, A. F. Moene, H. A. R. De Bruin, and A. A. M. Holtslag, 2002: Intermittent turbulence and oscillations in the stable boundary layer over land.
Part I: A bulk model. *J. Atmos. Sci.*, **59**, 942-958.

2.1 Introduction

On clear nights with weak winds, a frequently observed phenomenon is the weak and intermittent character of turbulence. Intermittent turbulence is characterised by brief episodes of turbulence with intervening periods of relatively weak or unmeasurable small fluctuations (Mahrt 1999). In this study we indicate intermittency by so-called 'global intermittency" in a sense that in the periods of weak turbulence eddies on *all* scales are missing of suppressed. This type of intermittency differs from the so-called 'fine-scale intermittency', sometimes found in turbulence literature, where fine scale structures occur intermittently within larger eddies (Mahrt, 1989).

An example of this 'global intermittency' is given in Fig. 2.1. Fig. 2.1 shows the development of the turbulent heat flux near the surface during a clear night with relatively weak winds. The measurements were obtained from sonic measurements (5 min. averages) of the Wageningen Meteorology and Air Quality group during the CASES99 field campaign (for a general description of this experiment see: Poulos et al. 2000).

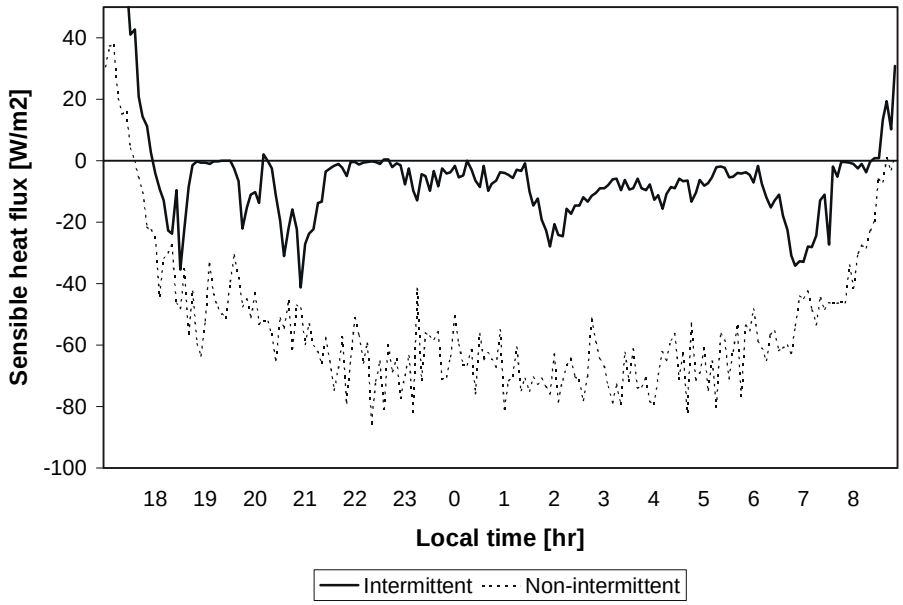

Figure 2. 1: Observed turbulent heat fluxes in two clear nights of 14/15th and 17/18th of october 1999, during the CASES99 field experiment, Kansas. The thick line represents a case with discontinuous turbulence (i.e. globally intermittent), observed in conditions with light surface winds. The dashed line represents a case with continuous turbulence (i.e. not globally intermittent), observed in conditions with strong surface winds.

The example shows a clear alternation between strongly turbulent periods with large negative heat fluxes and more quiet periods with hardly any heat flux. The discontinuous, intermittent turbulence causes changes in the mean evolution of the near surface temperature and wind speed. In case the period of the intermittent turbulence is regular this may result in oscillatory behaviour of the mean quantities. Therefore, in this text both "oscillatory behaviour" and "intermittency" refer to the same phenomenon.

For comparison, the results of a clear night with strong winds are shown, obtained during the same campaign. A totally different behaviour is visible with continuous turbulence resulting in an almost constant turbulent heat flux during the night. This type of weakly stratified cases is often found during nights with strong winds and/or during nights with cloudy conditions.

The knowledge of the physical mechanism(s) behind the intermittent behaviour of turbulence in the stable boundary layer (SBL) is still very limited, partly because of difficulties in measuring fluxes in weak, intermittent turbulence. It is unclear whether intermittency is generated by local shear effects, by instability on the scale of the entire surface inversion layer or by turbulence generated aloft diffusing to the surface (see: review on SBL issues by Mahrt 1999). Also, locally produced waves formed by Kelvin-Helmholtz instabilities could play a role in triggering turbulence bursts (e.g. Nappo 1991; also recently observed during CASES99 by Blumen (pers. communication)) as could the transverse eddies produced by the inflection point mechanism (Thorpe and Guymer 1977).

In this study we focus on an intermittency mechanism which results from a delicate interplay between radiative cooling and turbulent mixing in presence of a pressure gradient. This mechanism can be described as follows (cf. Businger 1973):
On clear nights thermal stability may increase fast, compared to the existing wind shear, due to the strong cooling of the surface. As a consequence the gradient Richardson number increases considerably and therefore turbulence is suppressed and, eventually, collapses. This results in a decoupling of the air from the surface. At this point, due to the very little friction acting on the air, the omnipresent pressure force starts to accelerate the air mass. Thus, shear increases until $Ri < Ri_{crit}$, eventually regenerating turbulence. As a result of this turbulence both stratification and shear are reduced quickly. Due to the strong surface radiation the stratification soon intensifies, causing Ri to increase so that turbulence is suppressed again. Now the whole process starts over again. Several cycles of the behaviour sketched above results in an intermittent character of turbulence in the stable boundary layer and oscillations in the near surface wind speed and temperature.

At presence, it is not clear whether this mechanism generates intermittent turbulence aloft, for example near the low-level jet (Vukelic and Cuxart, 2000), or that it generates intermittent turbulence near the surface via a direct surface-atmosphere interaction (Revelle 1993). In this study we confine ourselves to the direct interaction of the lower stratified atmosphere (first tens of meters) with the surface, without considering interaction with the atmosphere aloft. The intermitteny caused by this interaction is referred to in the following as: Atmosphere-Surface Intermittency (ASI).

Following the results of Blackader (1979), Revelle (1993) carried out a numerical study of SBL behaviour using a 1-dimensional multi-layer model. His model uses a simple first- order turbulence closure for the air layers with diffusion coefficients depending on the local gradient Richardson number. The surface energy balance at the soil surface is solved for dry conditions. Even with this simple model, the SBL shows intermittent turbulent behaviour near the surface for a certain range of geostrophic wind speeds. Also the intermittent, near surface dynamics does not show interaction with the developing low level jet aloft. The period of the intermittent turbulence

calculated by the model varies between half an hour to four hours depending on the actual environmental circumstances. The modelled periods are within the range of experimental results obtained by others as reported in Revelle (1993). Using a fog prediction model with comparable turbulence parameterization, Welch et al. (1986) clearly showed oscillatory behaviour in radiation fog, resulting in a series of fog dissipation and redevelopment episodes. The same study also shows oscillatory behaviour of fog development in field observations. Note that, an alternative explanation for oscillatory behaviour in a particular fog event at Cabauw was given by Duynkerke (1991) in terms of gravity wave theory.

McNider et al. (1995) carried out a theoretical study on SBL dynamics. Although they did not explain the oscillatory behaviour of the models mentioned above, their approach using bifurcation techniques applied to a simplified model largely inspired the present work and its companion paper.

An understanding of the physics behind intermittent turbulence and oscillations is of great practical importance for parameterization of the very stable boundary layer for numerical weather prediction (NWP) purposes. It is, for example, easy to understand why the commonly used average flux-profile relationships will be violated in intermittent flows: under these conditions the mean fluxes are largely determined by the (relatively short) bursting period, whereas the mean gradients are largely determined by the longer quiet periods with large gradients. This implies that no universal relationship can be found between the time-averaged profiles and the mean flux. In practice, however, the effect of intermittent turbulence is often parameterized by empirical corrections to the surface layer similarity functions for conditions of strong stability (Holtslag and De Bruin 1988, Beljaars and Holtslag 1991). Furthermore, for very stable situations this empirical corrections are needed to prevent a decoupling of the atmosphere in NWP leading to too low surface temperatures (Louis (1979), Beljaars and Viterbo (1998)). The decoupling phenomenon is closely related to intermittency, because of the fact that this decoupled system can become recoupled again by the influence of increased shear forced by the pressure gradient, leading to intermittent turbulence at the surface (Derbyshire 1999). Later in this text, we will discuss the effect of such empirical corrections on SBL model behaviour with respect to the intermittency phenomenon.

The purpose of this paper is to show that the main mechanism behind ASI can be described with a simple, non-linear bulk model, consisting of a coupled system of three non-linear differential equations. This model mimics oscillatory SBL behaviour triggered by the interaction between the bulk of the SBL and the underlying surface. Turbulence interactions with the overlying atmosphere are ignored. The bulk model appears to describe the main features of the oscillatory SBL. The main advantage of this approach is that it allows analytic solutions, which: a) give more insight in the influence of external (synoptic) forcings on the SBL development and b) give more insight in the internal system dynamics of the complex interactions between the radiation and turbulent processes.
The results of our approach are described in two papers: in Part I (this chapter), the model is described and several numerical solutions are presented, showing different regimes of behaviour. In a companion paper (hereafter denoted as Part II, chapter 3) analytic solutions will be presented. Herein, it will be shown that the numerical results

can be generalised in such a way that the occurrence of intermittent turbulence can be predicted from the evaluation of external parameters such as pressure gradient, cloud cover, and surface roughness (an extended abstract based on both papers is given in: Van de Wiel et al. 2000).

In section 2.2 the model equations are given. In section 2.3 typical examples of the model dynamics are given. The effect of different turbulence parametrizations on the model outcome is discussed in section 2.4. Section 2.5 deals with the comparison of our results with earlier studies. Finally, conclusions of this work are presented in section 2.6.

2.2 Model setup

2.2.1 General description

Points of departure for the current model of the physics in the SBL are the conservation equations for momentum and heat. In the derivation of the model equations it is aim to reduce the complexity of the physical system to a minimum while preserving those physical processes which, according to the authors, are the most relevant to study the present mechanism. In connection with this aspect Derbyshire (1999) argues that even the simplest analysis needs to couple explicitly the wind profile, temperature profile and surface heat budget. As shown below, our model design is in concordance with this statement. Furthermore, in section 2.3.1, we will show that the model behaviour of this simplified model resembles the behaviour of more detailed models.

We designed our atmosphere-surface bulk model with the following features:
1) It describes the interaction between the “bulk” of the SBL and the underlying surface.
2) The surface is covered with a low vegetation layer.
3) There is no interaction (except for radiation) between the turbulent SBL and the ‘free’ atmosphere above: at the top of the SBL the fluxes of momentum and sensible heat are zero
4) The depth of the SBL is taken constant (see: 2.2.5).
5) The SBL is “dry”, i.e. phase changes of water variables are ignored and there is no surface evaporation.
6) It is a bulk model, i.e. only the time evolution of the depth averaged temperature and wind speed is considered.
7) A simple radiation scheme is used based on a quasi grey body approach for the longwave radiation emitted of absorbed by the SBL, the surface and the overlying ‘free’ atmosphere and clouds.
8) In the momentum equation the Coriolis force is neglected.

Assumption 3) and 8) are is discussed in more detail because they limit the applicability of the model results:
Several observational studies (e.g. Caughey et al. 1979, Mahrt et al.1979, Nieuwstadt 1984) of the SBL show a decrease of the turbulent fluxes with height. In those cases, the height at which the fluxes vanish is referred to as the boundary layer depth h. The

present study is applicable in this type of conditions where there is no turbulent transport between the turbulent SBL and the 'free' atmosphere above. Basically, the restriction to these special cases was made in order to limit the complexity of the model (see: part II, chapter 3). This restriction means that the present model can *not* be applied in situations where the turbulence intensity increases with height. This kind of stable 'boundary layers' are also commonly observed (e.g. Smedman (1988); for a review on this so called 'top-down boundary layers', see: Mahrt (1999)). Obviously, this kind of top-down transport may influence SBL dynamics (McNider et al. 1995, Vukelic et Cuxart (2000); see discussion in section 2.5.1). Therefore, in the future, the present analysis could be generalised by including this type of interaction.

Assumption 8) considers the fact that the Coriolis force acts on the SBL with a time scale of a few hours (e.g. 3 hrs. at 45 degree lat. ; Blackadar (1957)), whereas the dynamics of the intermittent turbulent boundary layer have a typical time scale in the order of one hour (Revelle 1993). Furthermore, comparison of the present model with the results of Revelle (1993), who included Coriolis effects, learns that Coriolis effects are not essential for the intermittency mechanism to occur. The consequence of this assumption is, that in the present study our pressure gradient term in fact is the ageostrophic (of effective) pressure gradient term, or, in other terms, the pressure gradient in the direction of the mean flow. This, has to be kept in mind when interpreting the results.

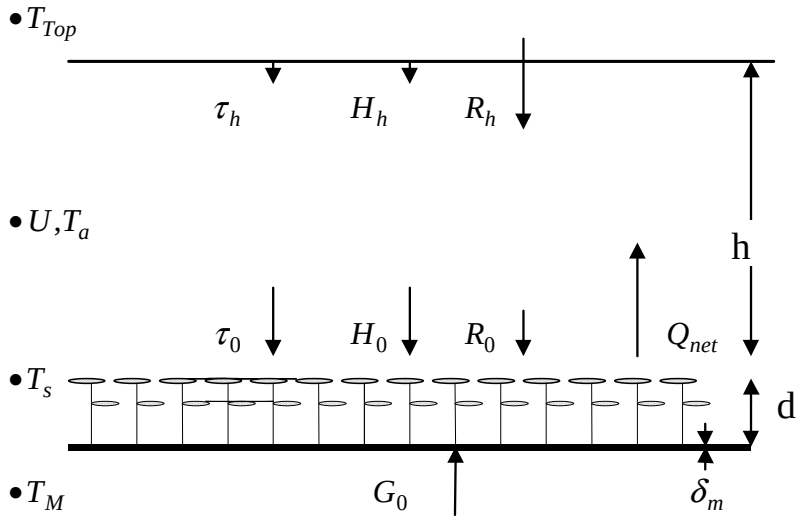

Figure 2. 2: The model system: state variables, fluxes, and model domain (see: App. 2A, for symbols).

Our physical model, sketched in Fig. 2.2, consists of four layers:
-the (deep) soil which is kept at a constant temperature; $-\infty < z < 0$
-the vegetation layer with depth d; $0 \le z \le d$
Within this layer, at the bottom of the vegetation layer, a thin mulch layer with thickness δ_m is present, which is regarded as a resistance, not as a separate layer (see 2.2.5).
-the air layer which has a constant depth h (the actual SBL); $d < z \le h$
-the 'free' atmosphere above the SBL; the longwave radiation emitted by the 'free'atmosphere does not vary in time; $h < z < \infty$

For this system, the basic equations for the layered averaged wind speed $\langle U \rangle$, air temperature $\langle T_a \rangle$ and vegetation temperature $\langle T_s \rangle$ are given by (see: list of symbols, App. 2A):

$$\int_d^h \frac{\partial U}{\partial t} dz = h \frac{\partial \langle U \rangle}{\partial t} = -\frac{h}{\rho} \frac{\partial P}{\partial s} + \frac{1}{\rho} \left[\tau_h - \tau_0 \right] \qquad (1)$$

$$\int_d^h \frac{\partial T_a}{\partial t} dz = h \frac{\partial \langle T_a \rangle}{\partial t} = \frac{1}{\rho c_p} \left[R_h - R_0 \right] - \frac{1}{\rho c_p} \left[H_h - H_0 \right] \qquad (2)$$

$$\int_0^d \frac{\partial T_S}{\partial t} dz = d \frac{\partial \langle T_S \rangle}{\partial t} = -\frac{1}{\rho_v c_v} \left[G_d - G_0 \right] \qquad (3)$$

For a formal discussion on the underlying governing equations used to derive the equations above, we refer to Appendix A of this thesis. Equation (1) represents the conservation of momentum for the depth integrated SBL. The first term represents the pressure gradient, an external variable determined by large-scale atmospheric processes. As before, this term represents the pressure gradient in the direction of the mean wind (the effective pressure gradient). The second term is the friction at the top and the bottom of the SBL. The second and the third expressions are the energy conservation equations for SBL and the vegetation layer. Herein H stands for the turbulent heat flux and R for the net longwave radiation for the *air layer* at the top and the bottom of the SBL. G_d and G_0 represent the energy flux at the vegetation top and the soil heat flux respectively. Note that $G_d = -Q_{net} + H_0$, with Q_{net} the net longwave radiation at the vegetation top (Q_{net} pos. downward, G_d, H_0 pos. upward). In the next sections a more detailed description of the various process parametrizations are given. The detailed set of model equations is summarised in App. 2B.

2.2.2 Parameterization of turbulent fluxes

To solve Eqs. (1)-(3) the turbulent fluxes at the boundaries of the atmospheric layer z=0 and z=h are required. In our model we assume the turbulent fluxes to vanish at z=h, which means $\tau_h = 0$ and $H_h = 0$. The turbulent fluxes at the boundaries are parameterized in terms of bulk properties of the SBL, i.e. a drag law formulation is applied. Although, in literature, a variety of drag law formulations are available (Csanady (1967), Blackadar and Tennekes (1968), Yamada (1976), Louis (1979)), the universality of drag laws is still under question (Stull, 1990). Especially at high stabilities when fluxes are not constant with height and non-stationary effects are present, those kind of flux parameterizations can be debatable (Delage (1997)). Nevertheless, in our opinion, it is useful to adopt a drag law formulation as a first order approximation to account for the basic feed back mechanisms between stratification, shear and turbulence. Therefore a drag law is chosen considering the following aspects:

-The drag law should possess the strong feed-back mechanism of stability on turbulent mixing efficiency (i.e. dependent on some form of Ri-number).

-The drag law should match with the integrated surface layer profiles resulting from similarity theory.

Also, for the purpose of our analytical analysis (Part II), the drag law formulation should be as simple as possible. As a matching case, the similarity functions of Businger et al. (1971), based on extensive surface layer measurements, are chosen. This results in a drag coefficient (or turbulent exchange function) which is quadratically dependent on the bulk Richardson number, assuming a critical value of the latter of 0.2 (see: 2.3.3; McNider et al. (1995), Derbyshire (1999)). The surface layer fluxes thus are calculated as:

$$\tau_0 = \rho u_*^2 = \rho \langle U \rangle^2 \cdot \frac{\kappa^2}{\left[\ln\left(\frac{\tilde{h}}{z_0} \right) \right]^2} \cdot f(R_b) \qquad (4)$$

$$H_0 = -\rho c_p \cdot |\langle U \rangle| \cdot \Delta T \cdot \frac{\kappa^2}{\left[\ln\left(\frac{\tilde{h}}{z_0} \right) \right]^2} \cdot f(R_b) \qquad (5)$$

with: $\Delta T = \langle T_a \rangle - \langle T_S \rangle$, $R_b = \left(\tilde{h} - z_0 \right) \cdot \frac{g}{T_{\mathrm{Re}f}} \cdot \frac{\left(\langle T_a \rangle - \langle T_S \rangle \right)}{\langle U \rangle^2}$

$$f(R_b) = \left(1 - \frac{R_b}{R_c} \right)^2 \quad ; 0 \le R_b \le R_c \qquad (6)$$

$$f(R_b) = 0 \quad ; R_b > R_c$$

A reference height $\tilde{h}$ has to be chosen, which is representative for the SBL profiles. In situations with intermittent turbulence and oscillating mean variables, SBL profiles will be time-dependent, causing the reference height to be a function of time. For simplicity, an effective reference height, representing the bulk of the SBL is defined, arbitrarily set at h/2. Furthermore, in the model we assumed that $z_{0m}=z_{0H}=z_0$. For notational convenience $\langle U \rangle, \langle T_a \rangle$ and $\langle T_s \rangle$ will be replaced in the following by U, T_a and T_s.

2.2.3 Parameterization of long wave radiation

In the model a so-called “emissivity approach” is adopted to describe the radiative characteristics of the atmosphere. It is well-known that the lower atmosphere does not emit nor absorb longwave radiation in the frequency range 8-14μm, known as the atmospheric window (Paltridge and Platt, 1976), and that it is almost opaque outside this region. Therefore an apparent emissivity is assigned to the lower atmosphere with a value in the range 0.7-0.9. Also clouds play an important role in the nocturnal surface radiation budget, because they emit long wave radiation both outside and inside the atmospheric window range. This extra amount of radiation is not absorbed by the air, but (almost) totally absorbed by the surface. Although this extra radiative forcing, strictly speaking, depends on the cloud cover, type and height of the clouds, a first order approximation only depending on cloud cover was adapted to simulate this effect: $cloud^{\downarrow} = N \cdot 60\,[\mathrm{W\ m^{-2}}]$(low level clouds at mid latitudes; Paltridge and Platt, 1976).

For the vegetation surface the radiative budget reads (Fig. 2.3):

$$Q_{net} = \varepsilon_a \sigma T_a^4 + N \cdot 60 - \varepsilon_s \sigma T_S^4 \quad (7)$$

From the amount of long wave radiation emitted by the surface only a part $\varepsilon_a \sigma T_S^4$ [W m^{-2}] is absorbed by the overlying air layer. The remaining part of the surface radiation (i.e. the part emitted in the window range) leaves the system.

Thus, the radiative budget for the air layer reads:

$$R_h - R_0 = \left(\varepsilon_a \sigma T_{Top}^4 - \varepsilon_a \sigma T_a^4\right) - \left(\varepsilon_a \sigma T_a^4 - \varepsilon_a \sigma T_s^4\right) \quad (8)$$

assuming the same emissivity for the air layer and the overlying air.

Next, for simplicity and for the purpose of our analytical analysis of the system equations (see: Part II) these equations will be linearized near a reference temperature by applying a Taylor series expansion, which leads to radiation terms linear in T_a and T_s.

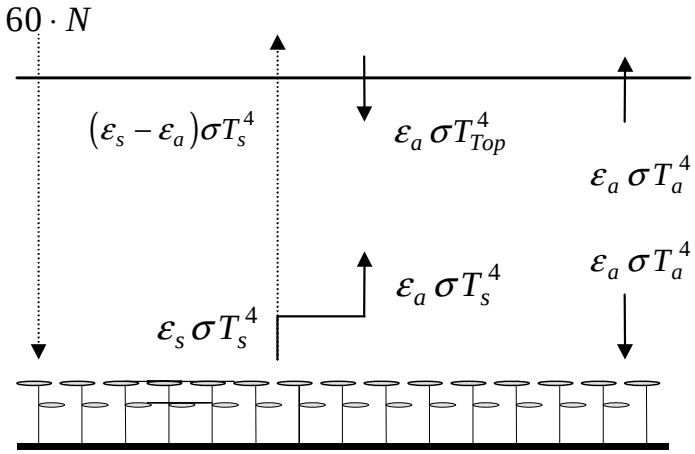

Figure 2. 3: Overview longwave radiation components

The linearized radiative budget for the air layer reads:

$$R_h - R_0 = 4\varepsilon_a \sigma T_{\mathrm{Re}f}^3 \left(T_s + T_{Top} - 2T_a\right) \quad (9)$$

The linearized radiative budget for the vegetation surface reads:

$$Q_{net} = \left\{-\sigma\left(\varepsilon_s - \varepsilon_a\right)T_{ref}^4 + N \cdot 60\right\} + 4\varepsilon_a \sigma T_{ref}^3 \left(T_a - T_s\right) - 4\varepsilon_a \sigma T_{ref}^3 \left(\frac{\varepsilon_s}{\varepsilon_a} - 1\right) \cdot \left(T_s - T_{ref}\right) \quad (10)$$

The first term on the right side will be defined as the isothermal net radiation:

$$Q_i \equiv -\sigma\left(\varepsilon_s - \varepsilon_a\right)T_{ref}^4 + N \cdot 60 \quad (11)$$

This isothermal net radiation is defined as the net radiation that would occur under isothermal conditions. It depends on the radiative properties ε_s, ε_a and N of the atmosphere and the vegetation cover, and determines the maximum radiative forcing on the system. It is comparable with the isothermal net radiation as defined by Monteith (1981) and by Holtslag and De Bruin (1988). For example: under cloudless conditions with ε_a equal to 0.8 and ε_s equal to 1.0 this would result in a Q_i of -75 [W m^{-2}], which is a typical value of the isothermal net radiation under those conditions.

2.2.4 Parametrization of surface temperature dynamics

In our model the surface temperature dynamics are described by a simple soil-vegetation scheme. It is well known that the existence of a small (isolating) vegetation

layer has a large impact on the development of the nocturnal surface temperature (Duynkerke, 1999). In case vegetation is present, the direct influence of the soil heat flux on the energy balance of the vegetation top is limited. This effect results in much lower surface temperatures for grassland than for bare soils, or road surfaces (Best, 1998). Also, because of this limited interaction and because of the *small thermal inertia* of the vegetation layer, the vegetation temperature is able to respond to quickly varying external forcings (Acevedo et al., 2000). This rapid reaction of the surface temperature has a direct impact on the stability of the lower atmosphere, which, in turn, has important consequences for the near surface atmosphere dynamics. Of course, this is particularly valid for situations with intermittent turbulence. However, the influence of this sensitivity of the vegetation temperature is not always considered in modelling studies, because often the (slow) diurnal cycle is studied.

Our soil-vegetation system consists of a thin vegetation layer with a small heat capacity. At the bottom of this vegetation layer there is a thin, loose organic mulch layer formed from dead plant material. Further we assume that:
-The soil layer has a constant temperature (i.e. the resistance of the mulch layer with non-turbulent air is large compared to the resistance to heat transport in the soil).
-Heat within the small canopy is distributed instantaneously within the canopy, so that the vegetation temperature is approximately equal to the vegetation surface temperature.
Thus the heat budget of the vegetation layer is (cf. Duynkerke, 1999):

$$\frac{\partial T_S}{\partial t} = \frac{1}{C_v}\left(Q_{net} - H_0 - \frac{\lambda_m}{\delta_m}\left(T_S - T_M\right)\right) \qquad (12)$$

With T_S the vegetation temperature, T_M the soil temperature and δ_m and λ_m the thickness and conductivity of the mulch layer. It is noted that value of the bulk conductance (defined as λ_m/δ_m) of the mulch/air layer in the vegetation (2.5 W m^{-2} K; table 2.1) is comparable with the value reported by Duynkerke (3 W m^{-2} K; 1999), estimated from Cabauw measurements over short grass. C_v stands for the heat capacity of the vegetation per unit of area [J K^{-1} m^{-2}] ($C_v = \rho_v c_v d$; see symbol list).

Note that the mathematical structure of (12) is such, that, by using different parameters, it exactly describes the surface temperature dynamics of a homogeneous (bare) soil, according to the well-known force-restore method (Deardorff, 1978). In section 2.3.5 this bare-soil interpretation of the problem will be addressed.

2.2.5 Model equations and solving

The final model consists of the set of equations which is given in appendix B. This set, derived in the previous sections, describes the development of the air temperature, the surface temperature and the wind speed in time. The equations are integrated in time using a fourth-order Runge-Kutta technique with a time step of ten seconds. The time integrations proved to be numerically stable for all runs. It is noted that, except for the example in section 2.3.1, only *stationary situations* are considered. This was done to enable a direct comparison between the present numerical results and the analytical analysis (part II) which is valid for the equilibrium situation. In average stationarity is reached within 15 hours, depending on the initial conditions and the thermal properties of the atmosphere and of the surface. To be sure about stationarity, runs after 30 hrs.

are shown. In advance, it is noted that, in general, the dynamic model behaviour (the intermittency) does not differ much between the transient period and the stationary period, enabling a possible extension of the stationary results to more realistic (i.e. transient) cases (see: section 2.5).

The model variables T_a, T_s and U are referred to as *internal variables*, because they are time dependent and consequently obtain a range of values for one run in time. It is noted that the bulk-Richardson number, which is directly related to T_a, T_s and U, is also a time dependent internal variable. On the other hand we will denote surface roughness, surface and air emissivity, cloud cover and pressure gradient as *external parameters.* These parameters, *which are constant* in time for each run, determine the development of the internal variables. So the physical behaviour simulated by the model will depend on the actual values of the external parameters. In table 2.1 the values of the parameters and constants used in the model runs are given. Unless stated otherwise, the results shown have been obtained with these values.

Symbol	Description	Type	(reference) value	Units
U	wind speed	int. variable	variable	[m s^{-1}]
T_a	air temperature	int. variable	variable	[K]
T_s	surface temperature	int. variable	variable	[K]
$\frac{1}{\rho}\frac{\partial P}{\partial s}$	effective pressure force (per mass);	ext. parameter	$2.0*10^{-4}$	[m s^{-2}]
N	cloud fraction;	ext. parameter	0.0	[-]
z_0	roughness length	ext. parameter	0.05	[m]
ε_a	air emissivity	ext. parameter	0.78	[-]
ε_s	surface emissivity	ext. parameter	1.0	[-]
C_v	heat capacity (per m^2) of low vegetated surface	ext. parameter	2000	[J m^{-2} K^{-1}]
λ_m/δ_m	bulk conductance of mulch/stagnant air layer	ext. parameter	2.5	[W m^{-2} K^{-1}]
T_{ref}	reference temperature	ext. parameter	285	[K]
H	boundary layer height	'int/ext.' par. see: 2.2.5	80	[m]
$\tilde{h}$	reference height (h/2)	'int/ext.' par. see: 2.2.5	40	[m]
C_p	heat capacity of dry air (at const. Press.)	phys. Constant	1005	[J kg^{-1} K^{-1}]
ρ	density of dry air	phys. Constant	1.2	[kg m^{-3}]
R_c	critical bulk Richardson number	phys.'constant' see: 2.3.3	0.2	[-]
g	gravity constant	phys. Constant	9.81	[m s^{-2}]
κ	Von karman constant	phys. Constant	0.4	[-]
σ	Boltzmann's constant	phys. Constant	$5.67*10^{-8}$	[J K^{-4} s^{-1}]

Table 2. 1: Overview of model parameters and physical constants. The values given are used in the model runs, unless stated otherwise. (Int. and ext. refer to internal and external variables/parameters respectively; phy. is for physical.

In table 2.1 the boundary layer height *h* is referred to as an external variable, because in our bulk model a fixed a priori value was assigned to the boundary layer height. This in order to avoid model complexity for our analytical analysis. In a real SBL this parameter is part of the system itself, and thus a dependent internal variable. As a model extension, one might think of parametrizing this height as a relaxation process in terms of external variables such as pressure force and radiative forcing (cf. Nieuwstadt et al. 1981).

2.3 Model results

2.3.1 Transient behaviour

An example of a 10 hour transient run is shown in Fig. 2.4, which is compared qualitatively with the results of an earlier study (not shown in Fig. 2.4) by Revelle (1993). Revelle uses a one-dimensional model with the same type of turbulence closure as in the present model. The model differs from the present model by the fact that it consists of a multi-level discretization, instead of a single level discretization and that it incorporates Coriolis effects, whereas in the present study these effects are neglected. In figure 2.4 a general decrease in surface temperature is seen as is generally observed in nocturnal conditions. Also after some time a sudden increase in temperature is visible, which after a short time drops back to the general trend.

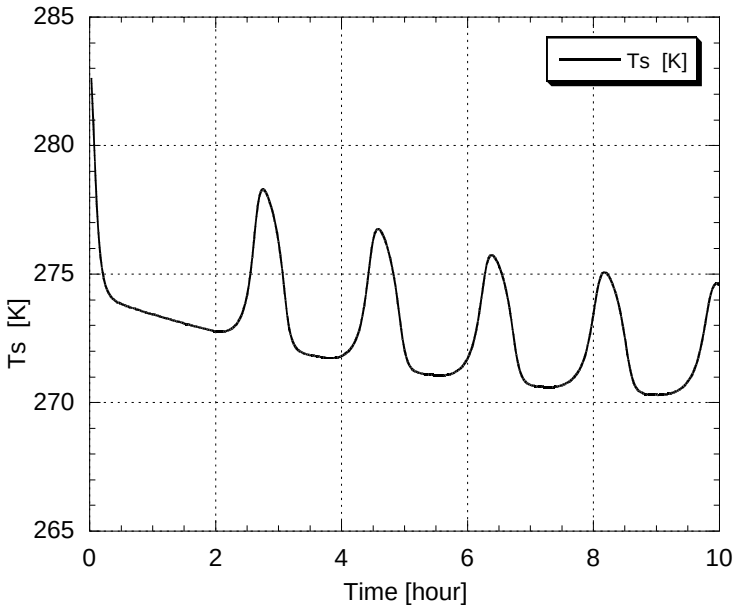

Figure 2. 4: Transient run showing the time evolution of the surface temperature during 10 hours as calculated by the model.

The occurrence of such temperature peaks confirms the results of Revelle, who showed that these peaks were related to intermittent bursts of turbulence. The period of the temperature peaks of about 1½-2 hours is comparable with the periods of temperature peaks reported by Revelle (i.e. 30-240 min.). The peak height of 4-5 K agrees with the peak height of the near surface temperature of about 5 K as in Revelle (see his Fig. 3). Thus, the truncated model presented here essentially shows the same type of behaviour as the more complex model. It is noted that temperature peaks of the surface temperature with a magnitude of several degrees are quite commonly observed.

Coulter et al. (2000) for example observed a decrease and increase of surface temperature of about 4 K within two hours during the CASES 99 experiment. Acevedo (2000) reported a temporal increase (+3 K) in near surface temperature and humidity during intermittent turbulence bursts.
Thus, the example in figure 2.4 shows that, the intermittency mechanism described qualitatively in the introduction, can be captured by a system of three coupled non-linear differential equations. Therefore, more insight in the atmosphere-surface intermittency (ASI) can be gained by studying the dynamics of this simplified system. In the next sections and in the companion paper (part II, chapter 3) the behaviour of the system will be studied in more detail.

2.3.2 Flow regimes

In this section different model regimes are studied as a function of the imposed effective pressure gradient. The pressure gradient is of importance in the SBL because it provides mechanical energy favouring turbulent mixing. Together with the amount of radiative surface cooling this turbulent mixing determines the strength of the nocturnal inversion (e.g. André and Mahrt, 1982). In the following it will be shown that not only the inversion strength (mean state) of the SBL, but also the *dynamic behaviour* is strongly influenced by this pressure gradient. In Fig. 2.5 the equilibrium value of the surface temperature is shown for three cases with different pressure gradients.

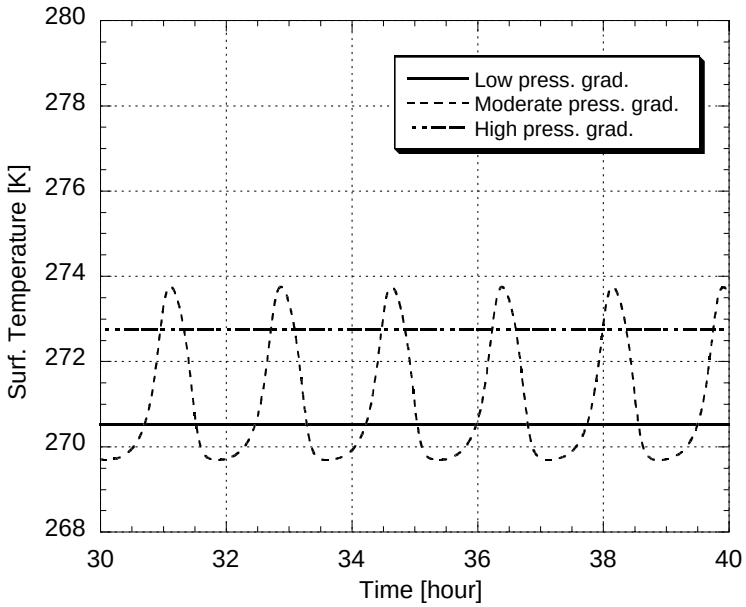

Figure 2. 5: Variation of surface temperature T_s after 30 hours (equilibrium situation) for different values of the pressure gradient $-(1/\rho \cdot \partial P/\partial s)$.

Clearly, three different regimes are visible:
a) Weak pressure force: turbulent fluxes are weak, resulting in the lowest surface temperature corresponding to the strongest inversion. The solution has a non-oscillatory character.
b) Strong pressure force: turbulent fluxes are strong, resulting in the highest surface temperature corresponding to the weakest inversion. Again, the solution has a non-oscillatory character.

c) Moderate pressure force: turbulent fluxes are alternately weak and strong, resulting in intermediate, but strongly oscillating surface temperatures (for a qualitative physical interpretation: see introduction).

The existence of three different regimes agrees with the results of more complex models reported by Lin (1990) and Revelle (1993). The three regimes are a result of a strong interplay between various coupled physical processes:
-wind speed is a function of the surface roughness, the pressure force and the stratification strength.
-the strength of the stratification is a function the emissivities of the atmosphere (incl. clouds) and the land surface and of the turbulent heat flux which, in turn, is an implicit function of wind speed.
For a further discussion on the physical interpretation of the equilibrium system behaviour we refer to part II.

2.3.3 The oscillatory regime

In this section the oscillatory case of the previous section is studied in more detail. In Fig. 2.6a the temporal behaviour of the internal model variables U, T_a and T_S is shown. The pattern of T_S, showing strong oscillations is the same pattern as presented in figure 2.5. Contrary to T_S, this oscillatory behaviour has almost disappeared in the graph of T_a. This is not surprising, because of the fact that the integrated air layer has a relatively large heat capacity, so that the impact of the (relatively small) intermittent fluxes is damped out largely. The height averaged wind speed clearly shows oscillatory behaviour with amplitude of about 1 m s^{-1}. The wind speed increases during the quiet periods and decreases during the turbulence bursts conform the mechanism described in the introduction.

In the introduction it was argued that the oscillatory behaviour of the mean variables like temperature and wind speed can be generated by intermittent turbulence (in the sense of discontinuous, but regular). This is illustrated by Fig. 2.6b, which corresponds to the same case as 2.6a. It is shown that the turbulent fluxes have a regular intermittent character leading to an oscillatory behaviour of the mean variables. Also, for the intermittent case, the transport of turbulent heat flux (peak values of –33 W m^{-2}) and momentum flux (peak values of 0.25 m s^{-1}) is well correlated, in contrary to transport by linear gravity waves (e.g. Kondo et al. 1978). This coupled transport of heat and momentum is controlled by the dynamics of the bulk Richardson number, which strongly influences the mixing efficiency of turbulence, via the turbulence exchange function $f(R_b/R_c)$ (see: Fig. 2.6c). In most cases the maximum value of (R_b/R_c) exceeded the value 1, resulting in periods with no turbulent transport, alternating with turbulent bursts. In some intermittent cases however, (R_b/R_c) did not cross the value of 1, which means that during intermittent turbulence the flow does not need to become completely laminar during calm periods, although it becomes very weakly turbulent. With respect to the discussion above it is noted that we adopted $(R_b/R_c)<1$ (with R_c equal to 0.2 for reasons in section 2.2.2) as a *sufficient* condition for the onset of turbulence, using an empirical bulk Richardson number rather than a

gradient Richardson number. Generally, the theoretical condition $(R_i/R_c)<1$ is only a *necessary* condition for the onset of turbulence (with R_c equal to 0.25, Miles (1961)).

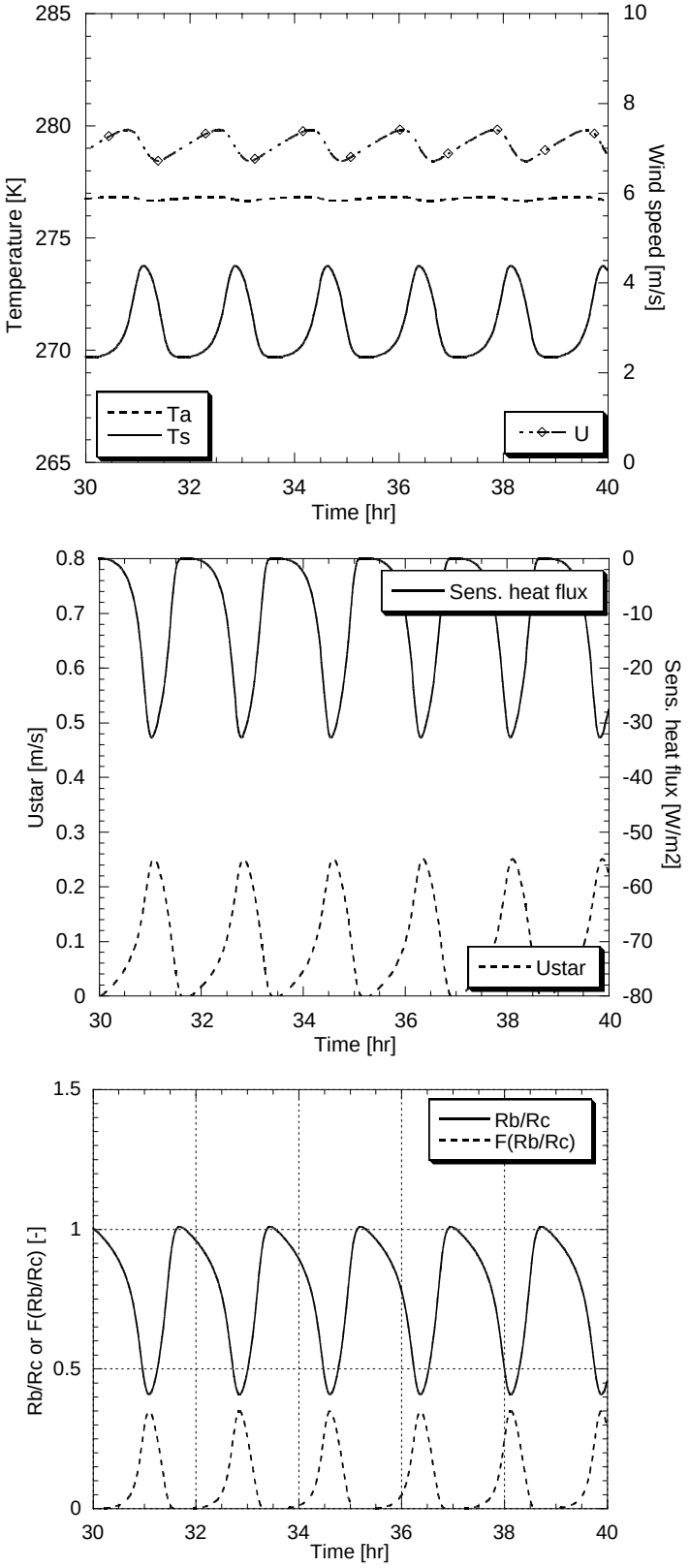

Figure 2. 6: (a) Behaviour of the surface temperature T_s, air temperature T_a and the wind speed U, **(b)** the sensible heat flux and the friction velocity and **(c)** the normalised bulk Richardson number R_b and the turbulent exchange function $f(R_b)$, in an equilibrium situation with intermittent turbulence.

2.3.4 Sensitivity to forcing parameters

In this section the sensitivity of the model to different atmospheric forcing parameters is investigated. In the companion paper (chapter 3) the results of section 2.3.4 and 2.3.5 are generalised by introducing a dimensionless parameter from which the model behaviour can be predicted.

In table 2.2a a few forcing parameters are varied compared to their reference value (only a single parameter is varied at a time). Also the amplitude of the equilibrium surface temperatures are given, with zero amplitude corresponding to the non-oscillating cases.

Parameter					
$-1/\rho \cdot \partial P/\partial s$ (x10^{-4}) [m s^{-2}]	0.5	1.0	**2.0**	4.0	8.0
Amplitude T_S [K]	0	3.1	4.1	3.3	0
N [-]	**0.00**	0.25	0.50	0.75	1.00
Amplitude T_S [K]	4.1	2.9	0.8	0	0
ε_a [-]	0.70	**0.78**	0.82	0.86	0.90
Amplitude T_S [K]	5.9	4.1	3.0	1.5	0

Table 2. 2a: Amplitude of surface temperature T_s as a function of external forcing parameters: $-(1/\rho \cdot \partial P/\partial s)$, N and ε_a . The bold numbers represent the reference values of Table 2.1.

In Fig. 2.5 it was shown that the value of the pressure gradient has a large influence on the different model regimes. This fact can also be found in table 2.2a, which shows no surface temperature amplitude at very low and high values of the pressure gradient, and large amplitudes at moderate pressure gradients. At the same time, it occurs that intermittent turbulence is more readily expected in situations with high radiative forcing, i.e. low values of cloud cover and atmospheric emissivity (table 2.2a). These facts follow the intuitive perception that no intermittency is expected under near neutral conditions. Thus, it is concluded that intermittent turbulence is expected to occur in nights with clear skies in the presence of a moderate to rather small pressure gradient.

2.3.5 sensitivity to local surface parameters

The relation between intermittency and land surface characteristics is studied by investigating the sensitivity of the model to local surface parameters (table 2.2b). From table 2.2b it occurs that both the heat capacity of the vegetation layer and the bulk conductance (here defined as: λ_m/δ_m) of the thin mulch/non-turbulent air layer are important parameters controlling the amplitude of the vegetation temperature: a vegetation layer with a small heat capacity and a low conductance to the upper soil, is able to respond quickly to changing external forcings allowing a rapid change of stability in the lower atmosphere.
Table 2.2b also shows that larger oscillations of surface temperature are expected over rough surfaces than over smooth surfaces. Thus, the results of table 2.2b clearly show that the intermittent surface-atmosphere dynamics is very sensitive to the surface characteristics. This means that for this type of intermittency modelling, a rather

detailed description of physical surface characterics is needed, to model the rapid surface temperature fluctuations, found in these circumstances.

Parameter					
Z_0 [m]	0.025	**0.050**	0.100	0.300	1.000
Amplitude T_S [K]	2.5	4.1	4.9	5.9	6.6
C_v [J m^{-2} K^{-1}]	10 000	5000	**2000**	1000	500
Amplitude T_S [K]	0	0	4.1	6.9	8.7
λ_m/δ_m [W m^{-2} K^{-1}]	10.0	5.00	**2.50**	1.25	0.625
Amplitude T_S [K]	0	0	4.1	6.6	8.3

Table 2.2b: Amplitude of surface temperature T_s as a function of local surface parameters: Z_0, C_v and λ_m/δ_m. The bold numbers represent the reference values of Table 2.1.

In this light it is interesting to know what would happen above a bare soil surface or over an ocean. To look at this aspect we first notice the following: mathematically Eq. (12), which describes the temperature development of a vegetation, is exactly equivalent to the well-known force-restore method. This method uses an analytical solution for a (single mode) sinusoidal forcing on a homogeneous soil to describe the temporal evolution of the surface temperature (e.g. Deardorff, 1978). According to this method, the equation for the surface temperature over a bare soil is given by:

$$\frac{\partial T_S}{\partial t} = \frac{2}{\rho_g c_g d_g}(Q_{net} - H_0) - \omega(T_S - T_M) \qquad (13)$$

with: ρ_g, the density [kg m^{-3}] and c_g [J kg^{-1} K^{-1}] the heat capacity of the soil, ω ($=2\pi/period$) [rad s^{-1}] the angular frequency of the external forcing and T_S [K] and T_M [K] the surface and the deep soil temperature. The so-called e-folding depth d_g [m] depends on both the thermal properties of the soil as well as on the frequency of the imposed forcings:

$$d_g = \sqrt{\frac{2\lambda_g}{\omega \rho_g c_g}} \qquad (14)$$

with λ_g [W m^{-1} K^{-1}], the conductivity of the soil. The force-restore method is often applied for modelling the diurnal cycle of the surface temperature for which the period is known. This contrary to the present intermittent case, where this a priori choice is not evident. Based on our earlier results (2.3.1) and on the results of Revelle (1993) periods of 30 min. 1½ hour and 4 hours are used as a test case (in principle it is also possible to find the period in an iterative way). Model simulations were performed for three different soil types (Oke, 1978):

-dry sand (λ_g=0.30 [W m^{-1} K^{-1}], ρ_g=1.6≅ 10^3 [kg m^{-3}], c_g=0.80≅10^3 [J kg^{-1} K^{-1}] and d_g=0.012-0.033[m]).

-wet sand (λ_g=2.2 [W m^{-1} K^{-1}], ρ_g=2.0≅ 10^3 [kg m^{-3}], c_g=1.48≅10^3 [J kg^{-1} K^{-1}] and d_g=0.021-0.058[m]).

-clay (λ_g=1.18 [W m^{-1} K^{-1}], ρ_g=1.8≅ 10^3 [kg m^{-3}], c_g=1.25≅10^3 [J kg^{-1} K^{-1}] and d_g=0.017-0.049[m]).

The model results showed to be the same for the different soil types: for none of the soil types the model shows intermittent behaviour. This is caused by the fact that the

soil heat capacity and its conductivity are large compared to the vegetated case, which prevents a rapid surface cooling. Keeping in mind the limitations of the force-restore method it is concluded that, according to the present model, intermittency is not easily found above a homogeneous bare soil. Of course, inhomogeneous (e.g. crusted or tilted) soils will behave differently. Also, intermittency having *another origin* than the present mechanism, may still occur. We may extend these bare soil conclusions to oceans: due to the extreme large heat capacity of water it is likely that the intermittent surface-atmosphere dynamics will not occur above a large water surface.

2.4 Impact of turbulence parameterization

2.4.1 Stability functions

In this section we will investigate the effect of the turbulence parameterization on the model outcome by comparing different types of stability functions. In figure 2.7 a few examples of such stability functions are given as a function of the bulk Richardson number.

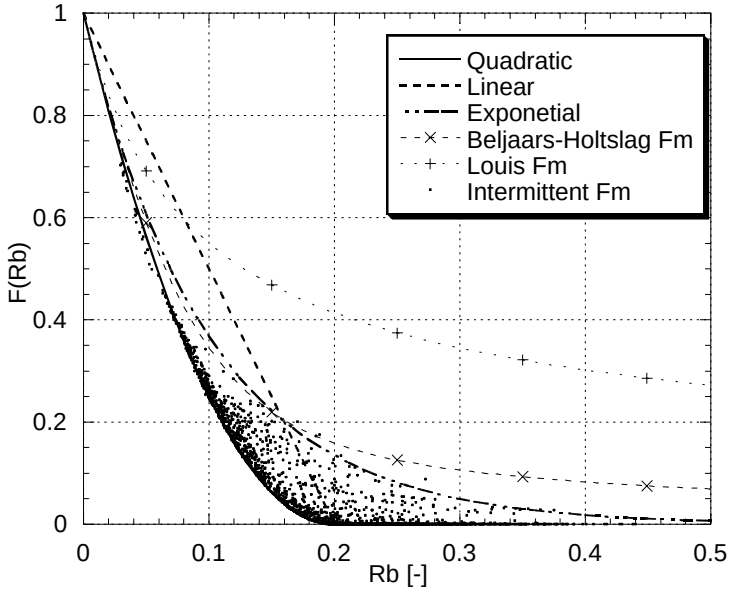

Figure 2. 7: Various stability functions for turbulent exchange as a function of the bulk Richardson number. The dots correspond to the *time-averaged* (30 min.) values of the stability function during an intermittent run with the original quadratic stability function used in each time-step.

The rationale behind these functions differs from one to another, reflected in the different shapes of the stability functions. The quadratic and the linear stability functions, for example, assume the existence of a critical (bulk) Richardson number, beyond which no turbulent transport is possible. This clearly results in a sharp cut-off of the stability function at this critical value of the bulk Richardson number. On the other hand, some of the other functions assume no critical bulk Richardson number resulting in a “broad tail” of the stability function. For example, the formulation of Beljaars and Holtslag (1991) allows some turbulence transport even at high Richardson numbers to account for non-stationary effects such as the occurrence of intermittent turbulence. The well known Louis functions (Louis,1979) show “broad tails” resulting in relatively high values of the stability function at large Rb numbers. Although the Louis functions are not based on observational material, they are of great practical use in operational weather forecast models. They produce higher and more

realistic surface temperatures in conditions of strong stratification, resulting in a better model performance than with the more observationally based stability functions (Beljaars and Viterbo 1998). This is related to the fact that modelling with the observationally based stability functions easily causes a decoupling of the atmosphere with the surface due to the small turbulent exchange at high stability (Beljaars and Holtslag 1991, Derbyshire 1999).
Finally, we mention the formulation of Mahrt (1987), that accounts for sub grid fluxes due to terrain heterogeneity. In this study only homogeneous situations are considered, which means that the Mahrt formulation does not apply. Nevertheless, considering the very broad tail of this stability function, it is likely that the results of Mahrt's functions would have been comparable with those of the Louis-functions.

2.4.2 Modelled stability functions for the intermittent case

A novel and interesting result in figure 2.7 is given by the dots: the dots represent the time averaged values of the stability function during a transient run with oscillations (like in Fig. 2.4), with the original quadratic stability function used instantaneously during each model time step. During the first 8 hours of a transient run, half-hour averages of wind speed, temperature and turbulent fluxes were calculated as is common practice in observational studies. From these half-hour fluxes and gradients the mean Richardson number and stability functions f_m and f_h were calculated (only f_m is given in Fig. 2.7). We observe that the explicit modelling of the intermittent turbulence is reflected in the (small) tail behaviour of the stability function, although the original quadratic stability function shows no tail. This confirms the earlier statement that stability function with "broad tails" to some extent can be regarded as time-averaged parameterizations of intermittency and non-stationary effects. Also, due to the intermittent character of the turbulence, the uniqueness of the (averaged) flux profile relationship is gone. This is mainly due to the fact that the mean gradients are largely determined by the relatively long quiet period with little turbulence, while the fluxes are largely determined by the short bursting period. This means that a direct link between the flux and the gradient cannot exist.

By sampling at fixed times (as is common practice), extreme cases, such as 90% of the time interval with laminar flow and 10% turbulent flow, are easily included, causing large scatter in the time-averaged stability function (for reasons given above). This scatter can be reduced if one samples conditionally over a complete intermittent period (i.e. over both a laminar and a turbulent period), so that the time-average profiles and fluxes are more representative for the sampling period. In Fig. 2.8 stability function are compared for the conditional and the non-conditional sampling case, calculated for the same equilibrium run. From this figure it is concluded that, by using conditional sampling, a better estimate of the 'mean' gradients and fluxes during intermittent turbulence is made, resulting in a stability function which resembles more the original Businger-Dyer function. Of course, some scatter remains present, due to the 'non-uniqueness' of the flux-profile relationships in intermittent conditions.
It is noted that in Fig. 2.8, other than in Fig. 2.7, the (bulk) Richardson numbers are calculated by dividing the total buoyancy destruction ($\propto \sum(T_a - T_S)$) by the total shear production ($\propto \sum U^2$). This somewhat different averaging procedure is done because, strictly speaking: $\overline{U}^2 \neq \overline{U^2}$, for a non-stationary situation. The use of a different

averaging procedure for the Richardson number, however, had very little effect on the results.

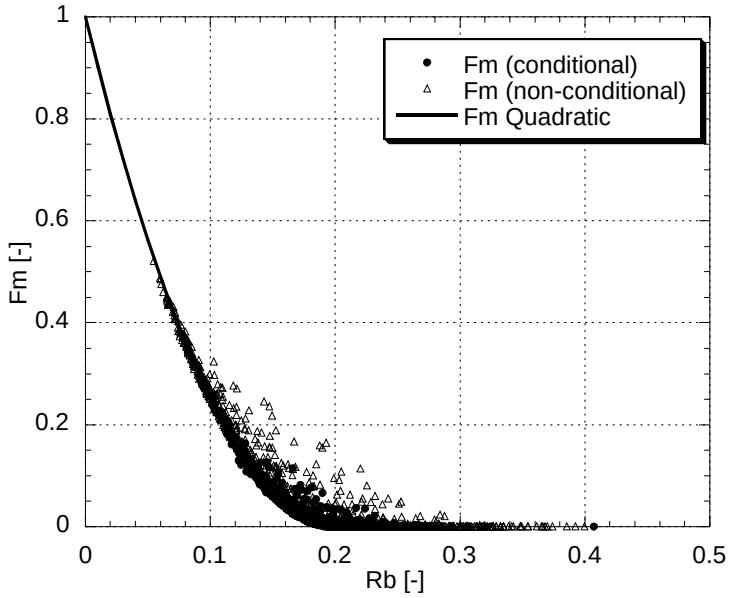

Figure 2. 8: Calculated stability functions $f_m(R_b)$ for oscillatory situations in the equilibrium, using conditional and non-conditional sampling. For comparison the original stability function used in the model, is given.

2.4.3 Transient runs for different stability functions

To investigate the effect of the shape of the stability functions on the SBL dynamics, in figure 2.9, ten-hour transient runs of the surface temperature are plotted, which correspond to the different stability functions showed in fig 2.7. For all runs the same set of parameters, given in table 2.1, is used.

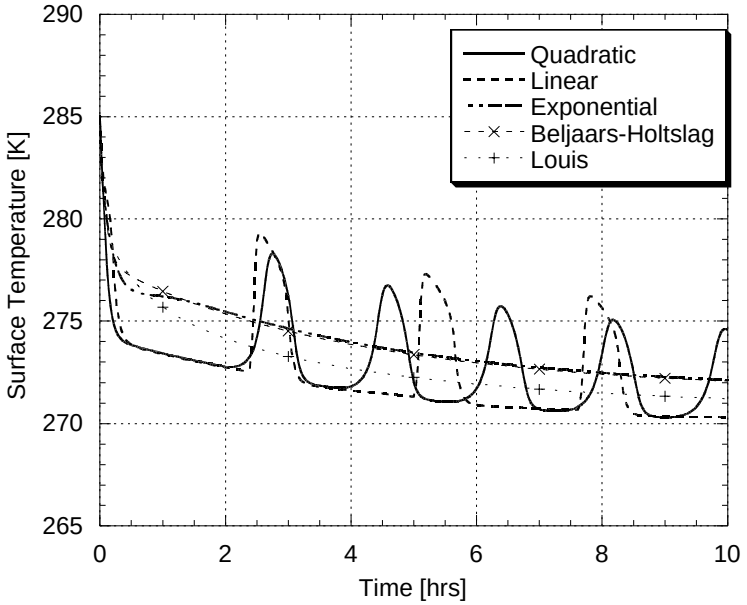

Figure 2. 9: Transient runs for different turbulent parametrisations $f_{m,h}(R_b)$, showing the time evolution of the surface temperature T_s during 10 hours as calculated by the model.

It occurs that the general decrease in surface temperature is comparable for the different parameterizations. On the other hand, for this particular set of parameters, oscillatory behaviour with intermittent turbulence occurs for two stability functions only. Both oscillatory runs correspond to stability functions with a sharp cut-off, i.e. stability functions which assume the existence of a critical Richardson number, beyond which no turbulent transport is possible. To investigate if the sharp cut-off in the stability function is responsible for the oscillatory behaviour, a number of additional runs with the non cut-off turbulent parameterizations was carried out. It turned out that also for these stability functions oscillatory solutions are possible. For example: a run with the exponential stability function using different values of C_v (500 J m^{-2} K^{-1}) and roughness length (0.5m), produces intermittent turbulence with oscillatory behaviour in the surface temperature with a period of about 1 hour. Using the same values and doubling the pressure gradient (8.0 $\cong$ 10^{-4} m s^{-2}), also the Beljaars-Holtslag functions produces oscillatory behaviour with a period of about half an hour. *Thus a sharp cut-off is not necessarily responsible for oscillatory behaviour*, which confirms the finding of Derbyshire (1999) stating that such cut-off in not a necessary condition for SBL decoupling. On the other hand, multiple runs show that a broad tail in the stability functions is able to suppress oscillatory behaviour, so that the set of physically realistic parameters causing oscillatory behaviour becomes smaller for these type of functions. Thus a non-oscillatory solution is *more likely* when the stability function attains a limited value at high Ri numbers. Especially, the Louis formulation (1979) has such a broad tail, that intermittency is not observed within the physically realistic parameter space. Thus, the use of broad-tail stability functions can be of practical use in numerical weather prediction, if one does not want to resolve oscillations.

2.5 Discussion

2.5.1 Comparison with previous work

The results from the numerical analysis with the 1-layer model generally shows agreement with the behaviour of the model results of Revelle (1993). Oscillating as well as non-oscillating regimes are encountered in both studies. It is worthwhile noting that, although a multi-layered model up to 1 km is used by Revelle, the oscillating dynamics only occurs in the lowest two model levels up to 10m. His results show that at 30m the atmosphere is decoupled from the surface and follows an inertial oscillation, as commonly observed in stable boundary layers (albeit mostly at higher levels). This is directly related to the fact that above 10m the Richardson number shows to be above critical. Revelle's use of two different values for the critical Richardson number for the surface layer (0.4) and the above surface layer (0.25) could have some influence, although it is noted by Revelle that a single Richardson criterion gives the same results for low geostrophic wind speeds (< 5 m s^{-1}), i.e. the range where the oscillatory behaviour occurs. The fact that the oscillation dynamics only occur below 30m in the example shown by Revelle, favours the use of a simple approach using a 1-layer model in the present study.

Recently, an interesting study with different turbulence parameterization was carried out by Vukelic and Cuxart (2000). In their analysis they use a SBL model with a simplified second order turbulence closure scheme (prognostic TKE) and apply

constant surface forcing by prescribing the turbulent heat flux at the ground level. They show that oscillatory behaviour (period of about 40 minutes) in the wind speed and the TKE production occurs in the upper part of the low level jet. Because constant surface forcings are applied, they can not reproduce the intermittency which was actually observed from measurements close to the ground. Instead, the model runs showed a ground level decoupled from the dynamics above.

Derbyshire (1999) reviews the decoupling phenomenon, which is defined as a cessation of turbulent transport between the surface and the atmosphere. In a situation with intermittent turbulence, also the surface layer itself temporarily becomes decoupled from the surface during quiet periods. So the decoupling process is closely related to the oscillatory behaviour of turbulence as discussed in this text. Derbyshire shows that several SBL schemes seem to allow decoupling. Furthermore his analytical analysis, on a simplified Couette flow with no pressure force and Coriolis effects, shows that decoupling can be interpreted as a process driven by positive feed backs between the surface temperature and the SBL parameterization, slowed down by soil thermal inertia. It is shown that the decoupling process is sensitive to the surface roughness and the soil thermal properties, which is confirmed by our results. Although in his article the possible recovery of the SBL (i.e. restored SBL-surface interaction) after a period of decoupling is not studied, Derbyshire mentions the importance of the large-scale pressure gradient on this SBL recovery (by acceleration leading to an increase of wind shear).

McNider et al. (1995) use a simplified, two-layer SBL model, with the same kind of parameterization as presented in this text, to study SBL dynamics. They report some oscillatory behaviour of the mean variables for certain parameter ranges, which confirms the results of this study. Contrary to our results however, they report double-valued equilibrium solutions for certain values of the external parameters. For example two values of U_{eq}, $T_{a,eq}$ and $T_{s,eq}$ are found for a particular combination of external parameters. The existence of multiple solutions could have strong implications for the predictability of the SBL in the sense that even slight changes in initial conditions would lead to quite different solutions for temperature and wind speed. The difference in model behaviour between both studies can be explained by the use of different boundary conditions. In our study at the upper model boundary the turbulent fluxes are assumed to be zero (prescribed fluxes). In the study of McNider et al. at the model boundary the potential temperature and the wind speed (geostropic) are prescribed, allowing turbulent interaction between the actual model and the higher levels. Imposing this kind of boundary condition, basically two type of equilibrium solutions are possible: 1) The overlying air is decoupled from the model layer. In this case the equilibrium solution of de model basically follows our results, where the momentum of the model layer is supplied by the pressure force. 2) The overlying air interacts with the model layer. In this situation extra momentum and heat from above are supplied to the model domain, resulting in an equilibrium solution different from the situation without this transport.

The numerical studies mentioned above show, that the basic intermittency mechanism, caused by the interaction between radiative cooling, pressure force and the effect of stratification on turbulent mixing, is a possible candidate to be responsible for the observed intermittent behaviour of the SBL. At the same time it is not clear, at what

level this intermittency is generated: are the turbulent bursts generated close to the jet and transported downwards, or are they generated near the ground caused by the atmosphere-surface interaction (this text). It is clear that there is a big need for experimental evidence (such as the CASES99 experiment, Poulos et al. 2000), which can provide more information about SBL dynamics improving our knowledge about stable boundary layers.

2.5.2 Practical/experimental issues

In this study a simple conceptual bulk model is developed to study SBL dynamics. Although such an approach has theoretical advantages, it requires special attention to practical/experimental issues. Due to the simplifications and assumptions details are lost and results must be interpreted carefully. Below, some practical aspects are addressed which show that direct comparison of the model results with measurements is not straightforward:
-Most of the results, like the sensitivity analysis (table 2a,b), were obtained for the equilibrium situation, which is reached, no earlier than after 10-15 hours, depending on the actual parameter values (section 2.2.5). It is clear that most of the nocturnal boundary layers are not in equilibrium at all (e.g. Nieuwstadt et al. 1981). Therefore, for several runs, we compared the equilibrium model behaviour with its transient behaviour with respect to the oscillations. It turned out that in most cases, the differences were only marginal, with slightly larger periods and amplitudes occurring in the transient period (e.g. compare figures 2.4 and 2.5).
-The assumption that the external parameters (e.g. pressure gradient and cloud cover) are constant during the night will be violated in practice (the same goes for the boundary layer height).
-Also, the assumption of horizontal homogeneity will be violated in practice. Not only synoptical parameters, but also surface characteristics vary in space. Without extending the present framework to 2-D or 3-D equivalents, the influence of inhomogeneity on intermittent surface atmosphere dynamics can not be assessed.
-Although, predictions about the oscillatory behaviour of the surface temperature can be easily verified, oscillations in the integrated values of mean variables will be more difficult to obtain: the values have small amplitudes and the height integrated signal will be blurred by uncertainties in the SBL height estimations.

In addition, some important processes in the SBL such as dew/fog formation, advection, drainage flow and wave activity processes, are neglected. So in case the above mentioned processes are important, the applicability of the model is limited. Nevertheless, in our opinion, this model could serve as a framework for future theoretical and experimental research on this intermittency mechanism.

2.6 Conclusions

This paper focuses on an intermittency generating mechanism which results from a *direct interaction between the lower atmosphere and the surface*. In this idealised case, interaction of the near-surface atmosphere with the low-level jet and/or elevated turbulence is not considered, despite their possible relevance to SBL dynamics. Also, the influence of other effects, often found in real SBL's like: advection, gravity waves,

drainage flows and dew formation is not considered. In future work, the present framework could be extended by incorporating these processes.

The main conclusion of this paper lies in the fact that this complex Atmospheric Surface Intermittency (ASI) can be captured by a coupled system of only three nonlinear differential equations. This reduced system possesses the most essential elements of the SBL: built up of stratification associated with a strong cooling of the surface by longwave radiation, supply of mechanical energy by the (ageostrophic) pressure gradient, and the limiting effect of stratification on turbulent mixing efficiency. It is also shown that both intermittent (oscillatory) and non-intermittent (non-oscillatory) regimes are found for different sets of external parameters. This result is confirmed by some others (e.g. Revelle (1993)) with more detailed model configurations.

The reduction of the process complexity to a simple bulk system makes it possible to study this system analytically. In a companion paper an analytical system analysis is made which leads to an explicit equilibrium solution of the system. By using analytical bifurcation theory the present numerical results are generalised such, that the occurrence of intermittent/oscillatory model behaviour can be predicted from evaluation of the external parameters (see: part II, chapter 3).

We found that intermittent turbulence is expected to occur in nights with clear skies in the presence of a moderate to rather small (ageostrophic component of the) pressure gradient. Furthermore, it is found that the presence of a vegetation layer largely influences SBL dynamics. Due to the low heat capacity of the vegetation in combination with its isolating properties (stagnant air in the lower part of the canopy), its surface temperature may change rapidly on changing turbulent heat fluxes. This change in surface temperature in turn has a direct effect on the radiation and turbulent heat budgets, causing an important feed-back mechanism, which may lead to instability (part II). According to the authors, any modelling of ASI should therefore include the possibility of a vegetation layer (or another isolating layer such as a snow layer). It was also found, that ASI is less likely to occur over bare soil surfaces, and unlikely to occur over large water surfaces, due to higher heat capacities and conductivity's preventing rapid changes of surface temperatures.

A comparison on turbulence parameterization shows that the general shape of the stability functions (i.e. the limiting effect of stratification on turbulent mixing) is an important feed-back mechanism in SBL modelling. In principle a broad class of stability functions allow oscillatory behaviour of SBL models. However, the shape of the tail of the stability functions plays an important role in suppressing this oscillatory behaviour. Furthermore, it was shown that, in practice, a stability function with a sharp cut-off at the critical Richardson number *effectively* shows tail behaviour when time-averages are used. This is a consequence of averaging oscillatory, non-linear processes, especially when non-conditional sampling is applied.

From the number of mechanisms which can cause an intermittent character of turbulence in the SBL, only one is considered in the present study. Currently, it is not clear if the different intermittency mechanisms are related to each other and where they occur in the SBL. For example, it is not clear whether turbulence bursts can be

generated near the ground, or if they are generated near the low-level jet and transported downward. Therefore extended experimental studies such as CASES99 (Poulos et al. 2000) are needed to clarify on this issue and improve our knowledge about the stable boundary layer.

Acknowledgements

The authors wish to thank Peter Duynkerke for reading the manuscript and providing useful suggestions. Also, we thank our colleague Oscar Hartogensis, for providing the data used for the examples in the introduction.

Appendix 2A: symbol list

c_p	heat capacity of air at constant pressure	[J kg^{-1} K^{-1}]
C_v	heat capacity of the surface vegetation per unit area	[J m^{-2} K^{-1}]
c_v	(specific) heat capacity of the vegetation	[J kg^{-1} K^{-1}]
d	depth of the vegetation layer	[m]
d_g	e-folding depth of the soil layer	[m]
δ_m	thickness of the mulch layer	[m]
ε_a	emissivity of the atmosphere	[-]
ε_s	emissivity of the surface	[-]
f	stability function (turb. exchange function)	[-]
f_m	stability function for the turbulent momentum flux	[-]
f_h	stability function for the turbulent heat flux	[-]
G_d	heat flux at the top of the vegetation layer	[W m^{-2}]
G_0	heat flux at the soil surface	[W m^{-2}]
h	depth of the turbulent layer (here: BL height)	[m]
$\tilde{h}$	reference height	[m]
H_h	sensible heat flux at the bound. layer top	[W m^{-2}]
H_0	sensible heat flux at the surface	[W m^{-2}]
κ	Von Kármán constant	[-]
λ_g	soil conductivity	[W K^{-1} m^{-1}]
λ_m	conductivity of the mulch layer	[W K^{-1} m^{-1}]
N	fraction of cloud cover	[-]
P	pressure	[Pa]
Q_{net}	net radiation budget of the surface	[W m^{-2}]
Q_i	isothermal net radiation	[W m^{-2}]
ρ	density of dry air	[kg m^{-3}]
ρ	(bulk) density of the vegetation layer	[kg m^{-3}]
ρ_g	density of the soil	[kg m^{-3}]
R_b	bulk Richardson number	[-]
R_c	critical bulk Richardson number	[-]
R_h	net longwave rad. of the BL at the bound. lay top	[W m^{-2}]
R_0	net longwave rad. of the BL near the surface	[W m^{-2}]
σ	Boltzmann constant	[W m^{-2} K^{-4}]
s	horizontal distance	[m]
τ_0	surface shear stress	[N m^{-2}]
τ_h	shear stress at the boundary layer top	[N m^{-2}]
t	time	[s]
ΔT	temperature difference $(T_a - T_s)$	[K]
T_a	(height averaged) air temperature	[K]
$\langle T_a \rangle$	height averaged air temperature	[K]
T_M	soil temperature	[K]

T_{ref}	reference temperature	[K]
T_s	vegetation (surface) temperature	[K]
$\langle T_s \rangle$	depth averaged vegetation temperature	[K]
T_{Top}	temp. of atm. above the turb. bound. layer	[K]
U	(height averaged) wind speed	[m s^{-1}]
$\langle U \rangle$	height averaged wind speed	[m s^{-1}]
u_*	friction velocity	[m s^{-1}]
ω	angular speed of intermittency period	[s^{-1}]
z	height coordinate	[m]
z_0	roughness length	[m]

Appendix 2B: full set of equations

Given our discussion in section 2.2, the full set of equations is summarised as:

$$\frac{\partial U}{\partial t} = -\frac{1}{\rho}\frac{\partial P}{\partial s} - \frac{1}{h}\cdot\frac{\kappa^2}{\left[\ln\left(\frac{h/2}{z_0}\right)\right]^2}\cdot U^2\cdot f(R_b)$$

$$\frac{\partial T_a}{\partial t} = \frac{4\varepsilon_a \sigma T_{ref}^3 \left(T_s + T_{Top} - 2T_a\right)}{\rho c_p h} - \frac{1}{h}\cdot\frac{\kappa^2}{\left[\ln\left(\frac{h/2}{z_0}\right)\right]^2}\cdot U\cdot(T_a - T_s)\cdot f(R_b)$$

$$\frac{\partial T_s}{\partial t} = \frac{-\sigma(\varepsilon_s - \varepsilon_a)T_{ref}^4 + 60\cdot N}{C_v} + \frac{4\varepsilon_a \sigma T_{ref}^3}{C_v}\cdot(T_a - T_s) + \frac{4\varepsilon_a \sigma T_{ref}^3}{C_v}\cdot\left(\frac{\varepsilon_s}{\varepsilon_a} - 1\right)\cdot(T_{ref} - T_s)$$
$$+ \frac{\rho c_p}{C_v}\cdot\frac{\kappa^2}{\left[\ln\left(\frac{h/2}{z_0}\right)\right]^2}\cdot U\cdot(T_a - T_s)\cdot f(R_b) - \frac{1}{C_v}\cdot\frac{\lambda_m}{\delta_m}\cdot(T_s - T_M)$$

with:

$$f(R_b) = \left(1 - \frac{R_b}{R_c}\right)^2 = \left(1 - \frac{1}{R_c}\cdot\frac{g(h/2 - z_0)}{T_{ref}}\cdot\frac{T_a - T_s}{U^2}\right)^2 \qquad ; 0 \le \frac{R_b}{R_c} \le 1$$

$$f(R_b) = 0 \qquad ; \frac{R_b}{R_c} > 1$$

Chapter 3

Intermittent Turbulence and Oscillations in the Stable Boundary Layer over Land:

Part II: A system dynamics approach

This chapter is based on:

Van de Wiel, B. J. H., A. F. Moene, R. J. Ronda, H. A. R. De Bruin, and A. A. M. Holtslag, 2002: Intermittent turbulence and oscillations in the stable boundary layer over land.
Part II: A system dynamics approach. *J. Atmos. Sci.*, **59**, 2567-2581**.**

3.1 Introduction

On clear nights with weak winds, a frequently observed phenomenon is the weak and intermittent character of turbulence. Intermittent turbulence is characterised by brief episodes of turbulence with intervening periods of relatively weak or unmeasurable small fluctuations (Mahrt 1999). In this study we indicate intermittency by so-called "global intermittency" in a sense that in the periods of weak turbulence eddies on *all* scales are missing of suppressed. An observational example of this 'global intermittency' is given in a companion paper by Van de Wiel et al. (2002; hereafter: part I or chapter 2). The discontinuous, intermittent turbulence causes changes in the mean evolution of the near surface temperature and wind speed. In case the period of the intermittent turbulence is regular this may result in oscillatory behaviour of the mean quantities. Therefore, in this text both "oscillatory behaviour" and "intermittency" refer to the same phenomenon.

Intermittent turbulence can be generated by several physical mechanisms (see: Part I). Traditionally, some of these mechanisms, like the formation and breaking of gravity waves, attained a lot of attention, both from a theoretical and observational point of view (e.g. Hunt et al. (1985), Nappo (1991), Duynkerke (1991)). In this paper we address another intermittency generating mechanism, which is generated by a direct atmosphere-surface interaction. This kind of intermittency is therefore referred to as Atmosphere-Surface Intermittency (ASI; see: Part I). The mechanism causing this ASI is a variation on the mechanism discussed qualitatively by Businger (1973) and Turner (1973). It is described as follows:
On clear nights thermal stability may increase fast due to the strong cooling of the surface. As a consequence the gradient Richardson number increases considerably and therefore turbulence will be suppressed and will eventually collapse. This results in a decoupling of the air from the surface. Because of the very little friction acting on the air the omnipresent pressure force will start to accelerate the air mass. Thus, shear increases until $Ri < Ri_{crit}$, eventually regenerating turbulence. As a result of this turbulence shear is reduced quickly and soon thermal stability dominates over shear, the Richardson number increases and turbulence is suppressed again. At this point the whole process will start over again. Several cycles of the behaviour sketched above will result in an intermittent character of the turbulence in the near-surface stable boundary layer and oscillations in the near surface wind speed and temperature.

The above shows that the intermittency mechanism is closely related to the decoupling phenomenon (e.g. Derbyshire 1999), with the exception that in the intermittency case the SBL turbulence is able to 'recover' by an increase of wind shear. An understanding of both phenomena is of great importance for numerical weather predicting modelling, because decoupling in SBL models results in surface temperatures which are too low, compared to measured surface temperatures (Derbyshire 1999). In practice this problem is circumvented by application of empirical formulations parameterising surface fluxes at high stabilities (e.g. Louis (1979), Holtslag and De Bruin (1988) and Part I). However these formulations are based on model performance rather than on surface layer based observation (Beljaars, 1998). Therefore, prediction of decoupling and intermittency could be useful in future improvements of physically based surface-layer parameterization in NWP models.

At presence it is not clear whether the intermittency mechanism described above generates intermittent turbulence aloft, for example near the nocturnal jet (as studied by: Vukelic and Cuxart (2000) and Ha and Mahrt (2001), or that it generates intermittency near the surface via a direct atmosphere-surface interaction (e.g. Revelle (1993)). In this study we confine ourselves to the direct atmosphere-surface interaction (first tens of meters), without considering interaction with the atmosphere aloft.

In Part I the results of numerical SBL modelling by several authors are discussed. The models use first order turbulence closure schemes (Blackadar (1979), Welch et al. (1986), Lin (1990), Revelle (1993), McNider et al. (1995)). All these models show intermittent behaviour of surface layer turbulence for some parameter ranges, resulting in oscillating mean variables such as wind speed, temperature and moisture. At present, however, a (quantitative) theoretical basis for this intermittency mechanism is still lacking. Thus, a better insight into this intermittency-mechanism is needed. To this end, in part I, the physical essentials of the models mentioned above were extracted, which results in a system of only three coupled non-linear differential equations. The simplified model essentially shows the same behaviour as the more complex models, resulting in intermittent and non-intermittent regimes for different parameter ranges.

The use of this simplified model enables us to study the complex interactions between the turbulent and radiative processes *analytically*, using a system dynamics approach. Our system dynamics approach is largely inspired by the work of McNider et al. (1995) who used numerical bifurcation techniques applied to a simplified model to study SBL dynamics. However the latter authors did not explain the oscillatory behaviour of the models mentioned above.

The two main goals of this paper are:
1) Provide a *quantitative* theoretical basis for the results of the numerical studies mentioned above. An exact stability criterion for intermittency will be given as a function of external forcing parameters. This gives the possibility to classify different SBL regimes into intermittent and non-intermittent cases.
2) Provide a further understanding of the instability *mechanism* causing intermittent behaviour.

In section 3.2 the model equations derived in Part I are presented in their scaled form. In section 3.3 equilibrium solutions of the model are given and the formal stability criterion is derived. In section 3.4 a classification based on the criterion is introduced and compared with other classifications. For practical use, a simplified stability criterion and its physical interpretation are given in section 3.5. Discussion and conclusions are given in section 3.6 and 3.7.

3.2 The system equations

In this text, point of departure is the set of equations given in App. 3B, which is derived in detail in the companion paper (Part I). For the symbol list we refer to App. 3A. This set of equations describes the time-evolution of wind speed, air temperature and surface temperature for a simple system consisting of four layers (Fig 3.1):

-the soil, which is kept at a constant temperature T_M ; $-\infty < z < 0$
-the vegetation layer with depth d and surface temp. T_S (at canopy top); $0 \le z \le d$
Within this layer, at the bottom of the vegetation layer, a thin mulch layer with thickness δ_m is present, which has a negligible heat capacity but relatively low heat conductivity.
-the air layer which has a constant depth h (the actual SBL); $d < z \le h$
-the 'free' atmosphere above the SBL, with constant temperature; $h < z < \infty$

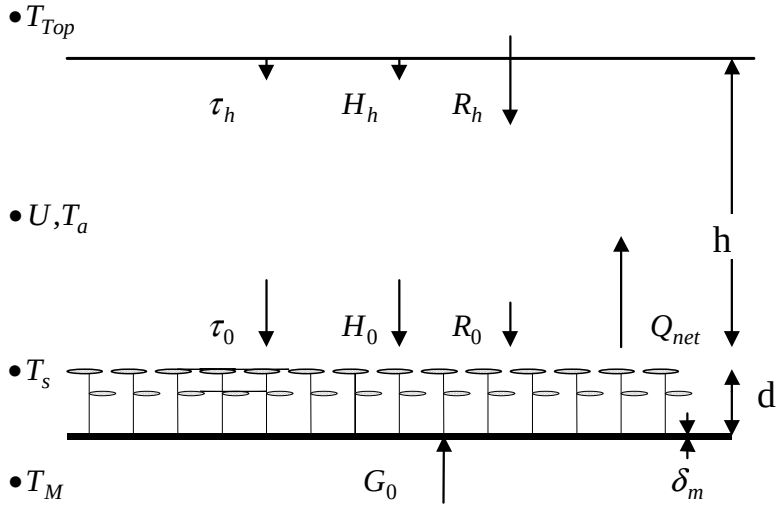

Figure 3. 1: An overview of the model system: state variables, fluxes and model domain. The symbols are explained in App. 3A. A detailed system description is given in Part I.

As in Part I, this paper focuses on an intermittency generating mechanism which results from a *direct interaction of the lower atmosphere and the (vegetated) surface*. In this idealised case, interaction with the low level jet and/or elevated turbulence (see review by Mahrt, 1999) is not considered. A discussion about the consequences of such idealisation is given in Part I. Some other model characteristics are:
-First order closure of turbulence, with an exchange function depending on a bulk Richardson number.
-Constant effective pressure force (i.e. component in the direction of the mean wind) imposed; Coriolis effects are neglected.
-Constant boundary layer depth.
-Long wave radiation processes are modelled using an emissivity approach.

For notational convenience, the equations given in App. 3B will be scaled resulting in a compact set of equations. In our scaling analysis a few characteristic scales are needed: a time scale, a length scale and a temperature scale. The boundary layer depth is taken as a characteristic length scale. The pressure force is used to define a velocity scale, because it drives the system. Note that, in our simplified system, the pressure

gradient balances with the momentum flux divergence across the SBL, in stationary conditions.
With the help of the characteristic length scale the velocity scale can be converted in a typical time scale. So we arrive at:

-length scale (h): h; velocity scale (U_k): $\left(-\frac{1}{\rho}\frac{\partial P}{\partial s}\cdot h\right)^{\frac{1}{2}}$;

-time scale (τ_{bl}): $\left(h\Big/-\frac{1}{\rho}\frac{\partial P}{\partial s}\right)^{\frac{1}{2}}$;

Next a characteristic temperature scale will be defined. The temperature difference between T_a and T_s will be driven mainly by the radiative cooling of the vegetation surface. In Part I it was shown that the isothermal net radiation, Q_i (Holtslag and De Bruin, 1988), is a measure of the maximum cooling strength of the vegetation surface given the prescribed radiative conditions (ε_a, ε_s and N). This Q_i will act upon the vegetation surface on a time scale τ_{bl}. For a vegetation layer with a total heat capacity per unit area of C_v [J m^{-2} K^{-1}] this will result in a typical temperature drop. Thus, a temperature scale is defined as:

-temperature scale (T_k): $\frac{|Q_i|\,\tau_{bl}}{C_v}$;

The above mentioned scaling parameters will be used to rewrite the equations of App. 3B in their dimensionless equivalent. To this end we define the dimensionless wind speed $\hat{U}$, the dimensionless air $\hat{T}_a$ and soil $\hat{T}_s$ temperatures and time $\hat{t}$ by noting:

$$\hat{U}=\frac{U}{U_k}\quad;\ \hat{T}_a=\frac{T_a}{T_k}\quad;\hat{T}_s=\frac{T_s}{T_k}\quad;\hat{t}=\frac{t}{\tau_{bl}}$$

Also, for notational convenience we define a radiative 'exchange coefficient' as:

$$a=4\varepsilon_a\sigma T_{ref}^3$$

and a neutral drag coefficient as:

$$c_{Dn}=\kappa^2\cdot\left[\ln\left(\frac{h/2}{z_0}\right)\right]^{-2}.$$

Substitution of the scaling variables $\hat{U}$,$\hat{T}_a$, $\hat{T}_s$ and $\hat{t}$ in the original set in App. 3B, gives:

$$\frac{\partial\hat{U}}{\partial\hat{t}}=1-c_{Dn}\cdot\hat{U}^2\cdot f\left(\hat{R}_b\right) \qquad (1)$$

$$\frac{\partial\hat{T}_a}{\partial\hat{t}}=\frac{a\tau_{bl}}{C_a}\left(\hat{T}_s+\hat{T}_{Top}-2\hat{T}_a\right)-c_{Dn}\cdot U\cdot\left(\hat{T}_a-\hat{T}_s\right)\cdot f\left(\hat{R}_b\right) \qquad (2)$$

$$\frac{\partial\hat{T}_s}{\partial\hat{t}}=-1+\frac{a\tau_{bl}}{C_v}\cdot\left(\hat{T}_a-\hat{T}_s\right)+\frac{a\tau_{bl}}{C_v}\cdot\left(\frac{\varepsilon_s}{\varepsilon_a}-1\right)\cdot\left(\hat{T}_{ref}-\hat{T}_s\right)$$
$$+\frac{C_a}{C_v}\cdot c_{Dn}\cdot\hat{U}\cdot\left(\hat{T}_a-\hat{T}_s\right)\cdot f\left(\hat{R}_b\right)-\frac{\lambda_m}{\delta_m}\cdot\frac{\tau_{bl}}{C_v}\cdot\left(\hat{T}_s-\hat{T}_m\right) \qquad (3)$$

Also the wind speed and the temperatures in $f(R_b)$ are scaled:

$$f\left(\hat{R}_b\right) = \left(1 - \frac{\hat{R}_b}{\hat{R}_c}\right)^2 \qquad ; 0 \le \frac{\hat{R}_b}{\hat{R}_c} \le 1$$

$$f\left(\hat{R}_b\right) = 0 \qquad ; \frac{\hat{R}_b}{\hat{R}_c} > 1 \qquad (4)$$

with:

$\hat{R}_b = \frac{\hat{T}_a - \hat{T}_s}{\hat{U}^2}$ and $\hat{R}_c = R_c \cdot \frac{T_{ref}}{g\left(h/2 - z_0\right)} \cdot \frac{U_k^2}{T_k}$

This set of equations, describing the atmosphere-land interactions, is used in the analytical stability analysis.

3.3 Stability analysis of the equilibrium solution and derivation of the intermittency parameter

3.3.1 The equilibrium solution and its mathematical stability

Equations (1)-(3) contain three unknown variables $\hat{U}$, $\hat{T}_a$ and $\hat{T}_s$. These non-linear differential equations have no general explicit solution. It is, however, possible to analyse the equilibrium solution of this system by setting the time derivatives to zero. A rather complex set of three non-linear algebraic equations remains. This set of equations, however, can be solved using some algebraic substitution techniques. The equilibrium solution of the system $\hat{U}_{eq}$, $\hat{T}_{a,eq}$ and $\hat{T}_{s,eq}$, as a function of the external parameters, is given in Appendix 3C.

The model runs in Part I revealed that, in an equilibrium situation, the system is able to respond in two ways:
-the system reaches a stable solution (in a mathematical sense), in which the values of $\hat{U}$, $\hat{T}_a$ and $\hat{T}_s$ reach their equilibrium values $\hat{U}_{eq}$, $\hat{T}_{a,eq}$ and $\hat{T}_{s,eq}$, as calculated in App. 3C.
-the system reaches an unstable solution, where the values of $\hat{U}$, $\hat{T}_a$ and $\hat{T}_s$ *oscillate* around their equilibrium values $\hat{U}_{eq}$, $\hat{T}_{a,eq}$ and $\hat{T}_{s,eq}$.

In this section the stability of the equilibrium solution is investigated with the help of so called bifurcation techniques. For those not familiar with this type of stability analysis we give a short outline in Appendix B of the thesis, based on the excellent introductionary book on bifurcations by Seydel (1988). For a more rigorous treatment on Hopf-bifurcations we refer to Hopf (1942) and Marsden and McCracken (1976). Readers not interested in the mathematical details may proceed to the example of section 3.3.3.

In our analysis, the point of departure is the equilibrium solution of the system. The (local) stability of the system is investigated by applying a Taylor series expansion to the equations near this equilibrium point. This leads to a linear system of equations describing the behaviour of $\hat{U}$, $\hat{T}_a$ and $\hat{T}_s$ near the equilibrium point. Information about the stability of the solution is obtained by evaluating the eigenvalues of the system. Positive eigenvalues correspond to solutions which are unstable in time. In the same

way negative eigenvalues correspond to stable behaviour and imaginary eigenvalues to cyclic/periodic behaviour near the equilibrium point. The values of the eigenvalues depend on the actual values of the external parameters. One could for example analyse the model behaviour while varying a certain parameter λ (e.g. pressure gradient). When λ passes some critical value λ_{crit} a positive eigenvalue may change sign and the stable equilibrium point may turn into an unstable point. This qualitative change of the equilibrium solution when passing λ_{crit} is called branching or *bifurcation*. The type of bifurcation that connects a *stable* equilibrium with a *periodic* motion is called a *Hopf-bifurcation.* The linearized system evaluated at the Hopf bifurcation point has a pair of purely imaginary eigenvalues $\pm i\beta$ which denotes the beginning of a cycle.

Because cyclic behaviour for certain parameter ranges was found, it is assumed that in our system a Hopf-bifurcation (HB) occurs. In this case two imaginary eigenvalues must exist for a certain combination of external variables. Reversing this argument: by setting this constraint on the eigenvalues the combination of external parameters can be found for which a transition in model behaviour will occur. From that point it is possible to define a dimensionless number (denoted with Π) consisting of *all external parameters*, which defines, and thus predicts, the equilibrium behaviour of the model. In section 3.3.3 it will be shown that the assumption about the existence of a Hopf-bifurcation is valid.

3.3.2 Application of the Hopf-bifurcation technique: derivation of the intermittency parameter

In this section the Hopf-bifurcation technique is applied to the SBL system described by Eqs. (1)-(3). The resulting dimensionless number is given explicitly in App. 3D. The derivation of this number consists of the following steps:

-Starting point is a system consisting of three coupled non-linear ordinary differential equations containing three unknown variables: $\hat{U}$, $\hat{T}_a$ and $\hat{T}_s$.

-The equilibrium situation for the system ($\partial\hat{U}/\partial\hat{t} = \partial\hat{T}_a/\partial\hat{t} = \partial\hat{T}_s/\partial\hat{t} = 0$) is solved. This gives the equilibrium values of the variables $\hat{U}_{eq}$, $\hat{T}_{a,eq}$ and $\hat{T}_{s,eq}$, as a function of the external parameters (App. 3C).

-The system is linearized by making a Taylor expansion around the equilibrium situation. To this end the Jacobian of the system is calculated. Element A_{ij} of the Jacobian is defined by:

$$A_{ij} = \frac{\partial F_i(x_1, x_2, x_3)}{\partial x_j} \qquad i = 1,2,3 \quad j = 1,2,3 \qquad (5)$$

with F_i is the right hand side of the ith equation (either (1),(2) , or (3)), and $x_1 = \hat{U}$, $x_2 = \hat{T}_a$ and $x_3 = \hat{T}_s$. For example A_{12} is the element consisting of the right hand side of the equation for $\partial\hat{U}/\partial\hat{t}$ differentiated with respect to $\hat{T}_a$.

-The Jacobian is evaluated at the equilibrium point, so the equilibrium values $\hat{U}_{eq}$, $\hat{T}_{a,eq}$ and $\hat{T}_{s,eq}$ are substituted in the elements A_{ij}.

-In order to calculate the eigenvalues μ of the linearized system the characteristic polynomial of the Jacobian is calculated:

$$-\mu^3 - f_1 \cdot \mu^2 - f_2 \cdot \mu - f_3 = 0 \qquad (6)$$

were f_1, f_2 f_3 are the coefficients of the characteristic polynomial, which in turn are functions of the Jacobian elements A_{ij}.

The numerical results revealed a transition between stable and oscillatory behaviour for a certain combination of external parameters. This leads to a crucial step in our derivation: we *assume* that this transition is a Hopf-bifurcation (the assumption is verified below). Then, since at the Hopf-bifurcation point the system should have two imaginary eigenvalues $\mu = \pm i\beta$, the characteristic polynomial *must* have the following form:

$$\pm\left(\mu^2 + \beta^2\right)(\mu + \alpha) = 0 \qquad (7)$$

or, rewritten:

$$\pm(-\mu^3 - \alpha \cdot \mu^2 - \beta^2 \cdot \mu - \alpha\beta^2) = 0 \qquad (8)$$

Equating (6) and (8) (thus, noting $f_1 = \alpha$, $f_2 = \beta^2$ and $f_3 = \alpha\beta^2$) leads to a relation between the coefficients f_1 , f_2 and f_3 at the HB point:

$$\frac{f_1 \cdot f_2}{f_3} = 1 \qquad (9)$$

The left hand side is a dimensionless group consisting of (all) external parameters which reaches a critical value of 1 at the HB point.

Formally, Eq. (9) is only valid *at* the HB point. Now, as a working hypothesis, we *extend* the findings of (9), by defining the left hand side of (9) as a relevant dimensionless group characterising the system behaviour. Thus a classification parameter is proposed by (again, for the explicit form, see: App. 3D).:

$$\Pi = \frac{f_1 \cdot f_2}{f_3} \qquad (10)$$

By definition $\Pi = 1$ at the HB point. Furthermore, it can be shown, by differentiating Π with respect to the eigenvalues, that, near the HB point, an unstable equilibrium corresponds to $\Pi < 1$ and a stable equilibrium to $\Pi \geq 1$. It is noted that the analysis above is done for the linearized system near the equilibrium. This means that, strictly speaking, no general statements can be made for the entire parameter space.
However, from several thousands runs, referring to a wide range a meteorological conditions, not a single example showed behaviour which differed from the results of the local analysis presented above.
Thus, keeping in mind the restrictions of the analytical analysis, we generalise our results such that: $\Pi < 1$ corresponds to periodic limit behaviour and $\Pi \geq 1$ corresponds to stable limit behaviour of the model.

3.3.3 An example

In this section the results of the analytical analysis above are compared with the results of the time dependent solutions of the numerical model (i.e. Eqs. (1)-(3) of App. 3B) to show that the predictions of the analytical analysis are supported by the numerical

results. For details of these runs we refer to chapter 2 (Part I). In figure 3.2 the value of the intermittency parameter Π is plotted as a function of the pressure gradient term. All other external parameters are kept constant (values given in table 2.1, Part I). Our analytical analysis in the previous section showed that a transition in flow behaviour is expected at $\Pi = 1$. In the case Fig. 3.2 refers to, Π equals 1 for two different values of $-1/\rho \cdot \partial P/\partial s$, notably at $-1/\rho \cdot \partial P/\partial s = 0.652 \cdot 10^{-4}$ and $-1/\rho \cdot \partial P/\partial s = 4.460 \cdot 10^{-4}$ [m s^{-2}]. This means that if the pressure gradient is gradually increased from low to high values, two transitions in flow behaviour are expected. To test this prediction, in figure 3.2 five points are selected in such a way that there is a point on each side of the flow transition. Besides, an additional point in the middle of the pressure gradient axis is selected. The five points are denoted with the letters A to E, corresponding with runs A to E depicted in figure 3.3a and 3.3b.

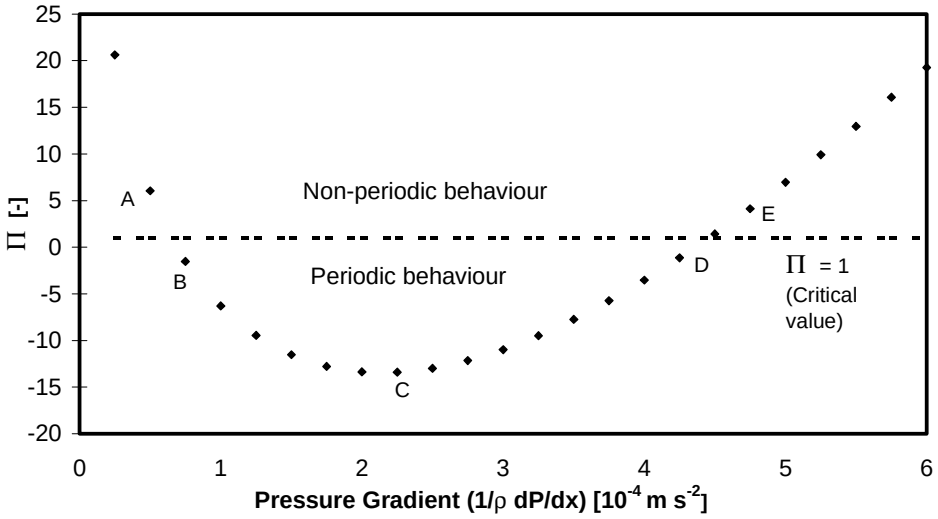

Figure 3. 2 : The dimensionless intermittency parameter Π as a function of the pressure gradient. The critical level $\Pi = 1$, which separates two different types of system behaviour, is given in the small dotted line.

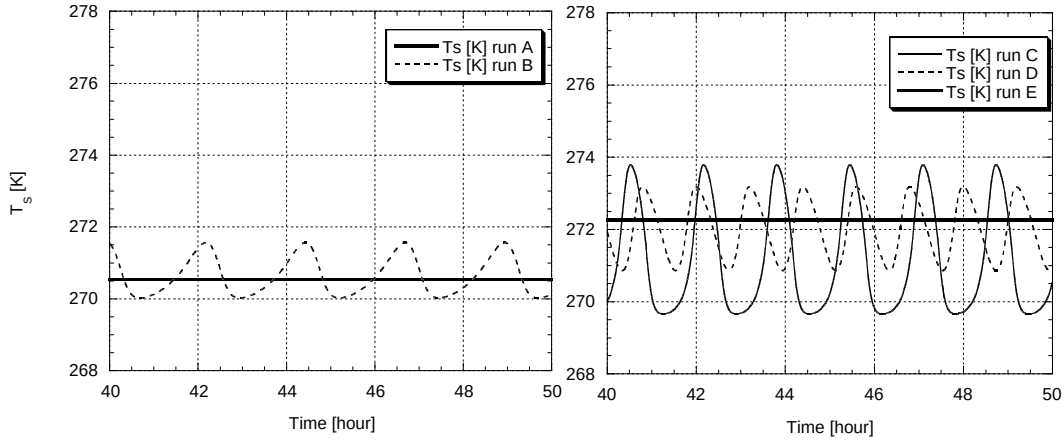

Figure 3. 3a,b: Equilibrium behaviour of the surface temperature calculated by the numerical model, for five different values of the pressure gradient. Run A and B **(3.3a)** correspond to case A and B presented in figure 3.2. Similarly, run C,D, and E **(3.3b)** correspond to cases C, D, and E.

These runs are done with identical parameters (cf. Table 2.1, Part I) except for the imposed pressure gradient, which is varied as in Fig. 3.2. It is noted that only

equilibrium situations are considered, because the analytical solution is, strictly speaking (see discussion Part I), only valid for the equilibrium situation. To assure equilibrium, results after 40 hours of model time are shown.

A comparison of figures 3.3a and 3.3b with figure 3.2 shows that a transition in flow behaviour appears to occur when Π crosses the critical value $\Pi = 1$, as predicted independently by the analytical model. Furthermore, the numerical runs show oscillating behaviour in those cases where the dimensionless Π parameter is smaller than 1 and non-oscillating behaviour for $\Pi \geq 1$. This is in agreement with the analytical predictions made by the local, analysis near the Hopf-bifurcation. The example in Fig. 3.2 is confined to runs where the pressure gradient was varied as external parameter. Several thousands of additional runs were carried out for a wide range of external parameters. For all cases this again resulted in oscillating behaviour for $\Pi < 1$ and non-oscillating behaviour for $\Pi \geq 1$. Therefore strong evidence is found that, in the physically realistic parameter space, our local analysis of the non-linear system can be generalised.

3.4 Flow regimes in the SBL: a classification based on dynamics

3.4.1 Classification based on SBL dynamics

We propose to use the dimensionless Π parameter as a classification parameter dividing equilibrium behaviour in: oscillatory behaviour ($\Pi < 1$) and non-oscillatory behaviour ($\Pi \geq 1$). Two important external parameters determining the equilibrium model behaviour are the pressure gradient and the isothermal net radiation, because they control both the kinetic energy being supplied and the amount of negative buoyancy flux. Not only the equilibrium values of $\hat{U}$, $\hat{T}_a$ and $\hat{T}_s$, but also the *stability* of the equilibrium (in a mathematical sense) will be influenced by these parameters. As an illustration, the dependence of Π on the isothermal net radiation and the (effective) pressure gradient is given in a contour plot in Fig. 3.4. All points within the contour line of $\Pi = 1$ have values of Π lower than 1 and thus correspond to the oscillatory case. In the same way, points outside the line $\Pi = 1$ correspond to the non-oscillatory case. In figure 3.4 it is seen that skies with little or no clouds, i.e. situations with strong isothermal net radiation (-45 to -80 W m^{-2}), three regimes exist cf. section 3.3.3. In fact, for such clear skies, the oscillating regime appears to split a single regime of non-periodic flow (see part I).

When, in Fig. 3.4 the absolute value of the isothermal net radiation is decreased, a point is reached (about -45W m^{-2}) where the oscillating regime does not exist whatever pressure gradient is imposed. In this situation the increased cloud cover reduces the loss of energy from the surface. This means that the instability mechanism sketched in the introduction (see also section 3.5) is less likely to occur and a non-oscillatory equilibrium situation will emerge. So in cases with moderate to large cloud cover only one regime with continuous turbulence exists. Note that this fact also agrees with the common observation that intermittent turbulence of the SBL occurs mostly during clear nights over land.

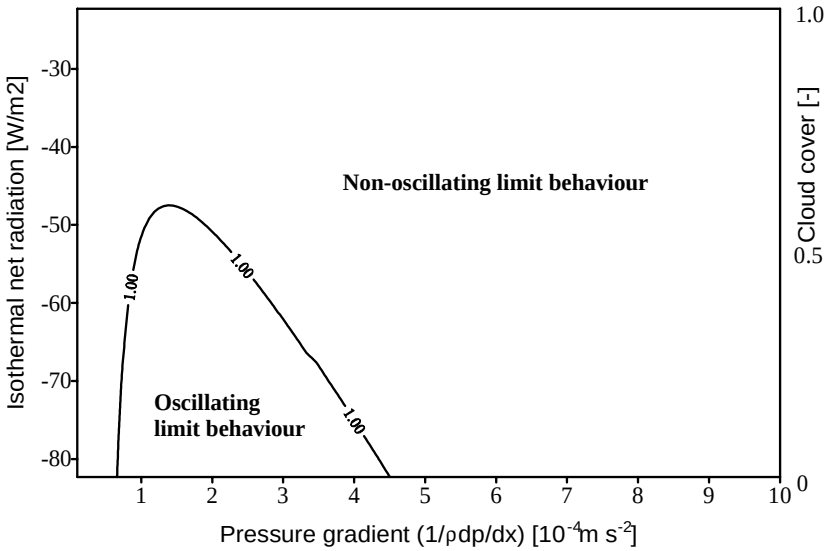

Figure 3. 4: Contourplot showing the dependence of the dimensionless intermittency parameter Π on the isothermal net radiation and on the (effective) pressure gradient. The critical level $\Pi = 1$,is given in a single contour line. For convenience, the cloud cover corresponding to the isothermal net radiation values, is given on the right axis.

3.4.2 Relation to other SBL classifications

In the past a number of SBL classifications have been proposed. At present no general picture of SBL classification seems to exist. Most of the classifications reported in literature are based on static considerations rather than on dynamics. Some of these static indicators, based on similarity theory (such as z/L) proved to be very useful in classifying surface layer measurements (Mahrt et al., 1998) and, more general, for classifying the SBL (Holtslag & Nieuwstadt, 1986). Others propose static classification based on some form of a bulk Richardson number (e.g. Stull 1983, Revelle 1993). The purpose of this section is to illustrate the fact that 'static' indicators, such as the bulk Richardson number, provide different information about the equilibrium state than 'dynamic' indicators, such as Π .

But first, we will show that a 'static' indicator based on *external* parameters provides useful information about the same indicator calculated from *internal* variables. The first 'static' indicator for our system is defined as an so-called external bulk Richardson number:

$$R_{b,ext} = \frac{g z_{sc}}{T_{ref}} \cdot \frac{\Delta T_{sc}}{U_{sc}^2} \qquad (11)$$

where z_{sc}, ΔT_{sc} and U_{sc} are the characteristic height scale, temperature scale and velocity scale respectively.

-Recall that the boundary layer height h is taken as a typical height scale $(z_{sc} = h)$.

-As a typical velocity scale we use $U_k / \sqrt{c_{Dn}}$. The division factor $\sqrt{c_{Dn}}$ is introduced to convert the velocity scale U_k (section 3.2) with a magnitude of order u_* to a velocity scale comparable with the logarithmic wind speed under neutral conditions.

-The temperature scale is defined as the temperature difference between T_a and T_s at radiative equilibrium of the soil surface. It can be derived from the long wave radiation budget by setting Q_{net} to zero and applying Taylor expansion around T_a . Thus

a temperature scale ΔT_{sc} is found: $\Delta T_{sc} = \frac{1}{4} \cdot \left(\varepsilon_s - \varepsilon_a^*\right) \cdot T_{ref}$ (see: Holtslag and De Bruin, 1988). Note that the temperature scale of section 3.2 (T_k) is not used, because of the fact that C_v is not a relevant parameter in the non-oscillating case.

Inserting the expressions for z_{sc}, ΔT_{sc} and U_{sc} in (11) gives a simple estimate:

$$R_{b,ext} = \frac{\left(\varepsilon_s - \varepsilon_a^*\right)}{-1/\rho \cdot \partial P/\partial s} \cdot \frac{g c_{Dn}}{4} \qquad ; \qquad \varepsilon_a^* = \varepsilon_a + \frac{60 \cdot N}{\sigma T_{ref}^4} \qquad (12)$$

where, ε_a^* is the so called apparent emissivity for the atmosphere. Next, $R_{b,ext}$ may be compared with the so-called internal bulk Richardson number $R_{b,\mathrm{int}}$ calculated from the 'true' equilibrium values of U, T_a and T_s, under the same circumstances. $R_{b,\mathrm{int}}$ is defined as:

$$R_{b,\mathrm{int}} = \frac{g h}{T_{ref}} \cdot \frac{T_{a,eq} - T_{s,eq}}{U_{eq}^2} \qquad (13)$$

In figure 3.5 $R_{b,\mathrm{int}}$ is plotted against $R_{b,ext}$. Figure 3.5 shows that there is a strong relationship between $R_{b,\mathrm{int}}$ and $R_{b,ext}$, although at high values $R_{b,ext}$ becomes independent of $R_{b,\mathrm{int}}$. This is the case because there is no limit on the value of $R_{b,ext}$, whereas $R_{b,\mathrm{int}}$ has to stay below its critical value in order to keep a finite value of the surface friction to oppose the (small) pressure force.

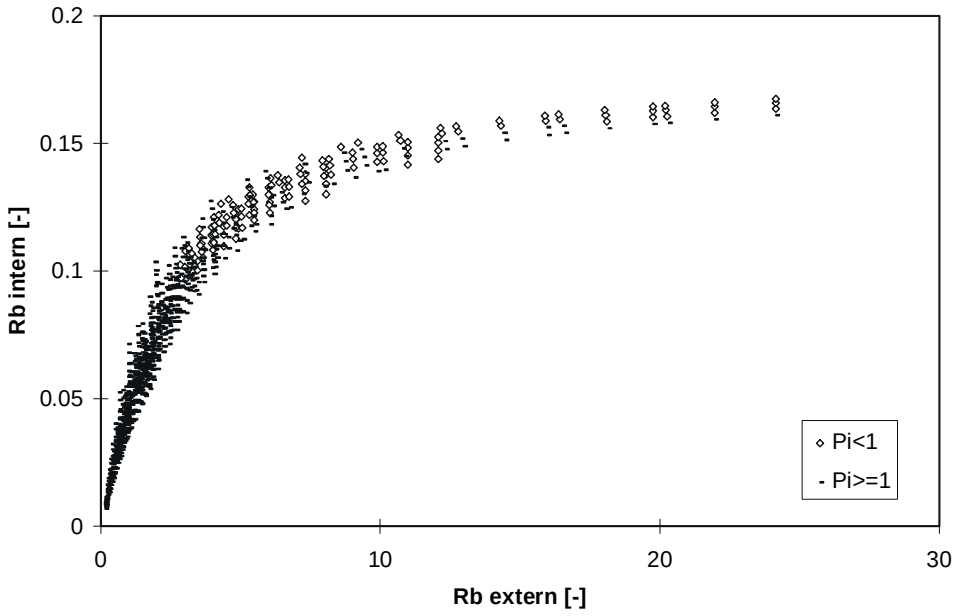

Figure 3. 5: Internal bulk Richardson number, calculated from the equilibrium values of U, T_a and T_s, plotted against the external bulk Richardson number, calculated from external parameters. Oscillatory cases ($\Pi < 1$) and non-oscillatory cases ($\Pi \geq 1$) are denoted with different symbols.

In Fig. 3.5 different symbols are used for oscillatory and non-oscillatory equilibrium cases. It is observed that *both* oscillatory and non-oscillatory situations occur simultaneously for a broad range of $R_{b,ext}$ and $R_{b,\mathrm{int}}$. This means that knowledge about a single bulk Richardson number only does not provide enough information about the

(mathematical) stability of the system. Information about this stability can be gained by evaluation of Π (or, alternatively, by using additional information about another dimensionless number K, together with information about the bulk Richardson number see: section 3.5). Nevertheless, it is noted that, roughly speaking, most oscillatory cases tend to occur in situations with high bulk Richardson numbers, and most non-oscillatory cases in situations with low bulk Richardson numbers. This result is in agreement with the observations of Kondo et al. (1978). They show that, with increasing Ri-numbers, a transition in flow behaviour from non-intermittent to intermittent flow is expected. The transition between these flow regimes occurs for a rather broad range of Ri-numbers, as indicated in Fig. 3.5.

3.5 A simplified criterion for instability

3.5.1 Introduction

In section 3.3 the instability criterion (i.e. $\Pi = 1$) for the SBL system given by Eq.(1)-(3) was derived formally. Although application of this formal criterion gives an exact prediction of the actual stability of the system, it does not provide insight in the physical background of the instability mechanism, due to the complex form of Π. Therefore, in this section, a less exact but simpler stability criterion is given, which does allow a physical interpretation.

The simplified criterion for instability is derived by application of a Fixed Shear Criterion for Instability (FSCI; Derbyshire, 1999). To this end the unscaled temperature equations for T_a and T_s of App. B. are combined into a single equation, describing the time evolution of the temperature gradient $(T_a - T_s)$. We consider near-equilibrium situations with no net flux to the combined atmosphere-surface system. As such $a\left(T_{Top} - T_a\right) = -(Q_i + G)$) and we assume T_{ref} to be close to T_s. In that case the combined equation reads:

$$\frac{d(T_a - T_s)}{dt} = m\left[-\left(Q_i - \lambda_m/\delta_m \cdot (T_s - T_M)\right) - a(T_a - T_s) - \rho c_p c_{Dn} \cdot (T_a - T_s) \cdot U \cdot f(R_b)\right] \qquad (14)$$

with, $m = 1/C_v + 1/C_a$.

This equation (14), together with the momentum equation (Eq. 1 App. 3B) forms our new simplified system. As an approximation, the stability of this system is investigated by studying the response of Eq. (14) to an initial disturbance in $(T_a - T_s)$, keeping U fixed at its equilibrium value (FSCI). In this way, we find that the system is *unstable* when:

$$\left\{\frac{\partial}{\partial(T_a - T_s)}\left[\frac{d(T_a - T_s)}{dt}\right]\right\}_{eq} > 0 \qquad (15)$$

Thus, the r.h.s. of (14) is differentiated to $(T_a - T_s)$: a positive value refers to a positive feed-back namely that any disturbance in $(T_a - T_s)$ is enhanced, leading to instability. Obviously, in the same manner, a negative value indicates a negative feed-back stabilising the system.

A physical interpretation of (15) is possible in terms of the surface energy balance, represented by the r.h.s. of (14). For example, a sudden cooling of the surface (by a little disturbance from the equilibrium), results in an increase of the stratification $(T_a - T_s)$. The decrease in T_s causes a compensating temporal increase in the soil heat flux, in the radiative heat flux (outside the atm. window, i.e. $a(T_a - T_s)$) and in the downward turbulent heat flux. These compensating fluxes counteract the sudden cooling, forming a negative feed-back, which stabilises the system (mathematically speaking).
In conditions of strong stratificaton (high Ri-numbers), however, the turbulent heat flux may *decrease* in spite of an increasing temperature gradient, due to the limiting effect of stratification on mixing efficiency (see also: De Bruin (1994) and Malhi (1995)). If this effect is large compared to the compensating effects by the soil heat flux and the radiative heat flux, this will cause an increase in the energy loss at the surface. This leads to an *amplification* of the disturbance in $(T_a - T_s)$ from the equilibrium, causing instability.

Before we derive the fixed shear criterion for instability it is noted that we confine ourselves to cases with $C_v << C_a$, also assuming a small heat capacity of the vegetation compared to the thick soil layer, so that the amplitude in T_s is large compared to the amplitudes in T_a and T_M (see: Part I). This means that $d(T_s - T_M) \approx -d(T_a - T_s)$. Now, criterion (15) is applied to (14), keeping the wind speed at its equilibrium value. The equilibrium wind speed can be found from Eq. 1 of App. 3B so that the results can be expressed in terms of Rb. Thus it is found that the system is unstable (oscillating) if:

$$\left\{\frac{R_b}{R_c}\right\}_{eq} > \frac{(K+1)}{3} \qquad (16)$$

with:

$$K = \frac{a + \lambda_m/\delta_m}{\rho c_p \sqrt{c_{Dn}} \cdot \sqrt{P_g h}} \quad \text{and} \quad P_g = -1/\rho \cdot \partial P/\partial s \text{ (for brevity).}$$

It is observed that the criterion for instability (16) depends on *two dimensionless groups*:

1) The normalised equilibrium bulk Richardson number: $(R_b/R_c)_{eq}$
2) The partitioning parameter: K

Both groups can easily be calculated from the external variables. In appendix 3E the expression of the first group $(R_b/R_c)_{eq}$ is given in terms of the radiative forcings and of the (ageostrophic) pressure gradient.

The second dimensionless group K, which we will denote as the *Partitioning Parameter*, is physically interpreted as the ratio of the summed radiative and soil heat exchange coefficient compared to the exchange coefficient for turbulent heat transport (or, alternatively, the ratio of fluxes). As mentioned before, a large exchange coefficient for longwave radiation and for soil heat flux *counteracts* the effect of a decreasing exchange coefficient of the turbulent heat flux at high Ri-numbers. Contrary to the turbulent heat flux, radiative and soil heat flux increase monotonically with an increasing temperature gradient. Thus, as in many physical problems (e.g.

compare the Rayleigh number), a large 'diffusive' component prevents physical instability.

Note from (16) that application of the FSCI to turbulent heat flux *only* would result in $R_b/R_c \geq 1/3$ as a criterion for instability. However, taking the effects of soil heat flux and radiative heat flux into account, we observe that $R_b/R_c \geq 1/3$ is merely a necessary condition for instability, not a sufficient condition. This confirms the findings of section 3.4.2, namely that instability is more likely to occur at high Richardson numbers but also that the bulk Richardson number is not the only parameter determining the dynamic behaviour (stability) of the system.

3.5.2 Comparison of stability criteria

In this section the simplified stability criterion given by Eq. (16) is compared with the detailed Π criterion. To this end we define a parameter S as:

$$S = \left\{\frac{R_b}{R_c}\right\}_{eq} - \frac{K+1}{3}$$

Thus, positive values of S indicate instability. In figure 3.6 the value of S is plotted against $-(\Pi - 1)$, for a large number of different parameter sets. The transformation $-(\Pi - 1)$ is chosen instead of Π, to assure that negative values of $-(\Pi - 1)$ correspond to stable cases and positive values with unstable cases, as is the case with S. If there were an exact agreement between both stability indicators, the 'butterfly' of figure 3.6 should exactly be located in the first and the third quadrant, with a crossing through the origin. Thus, it is observed that the agreement between the two stability criteria is rather good. Only for the points near the origin (i.e. the weakly intermittent cases with small amplitudes) a slight disagreement between the criteria is present due to the approximations in the derivation of S (especially, the assumption of a fixed shear, whereas in reality disturbances in stratification strength affect U_{eq}, see also Derbyshire (1999)). Thus, it is concluded that the simplified criterion given by (16) is good approximation for the detailed Π criterion.

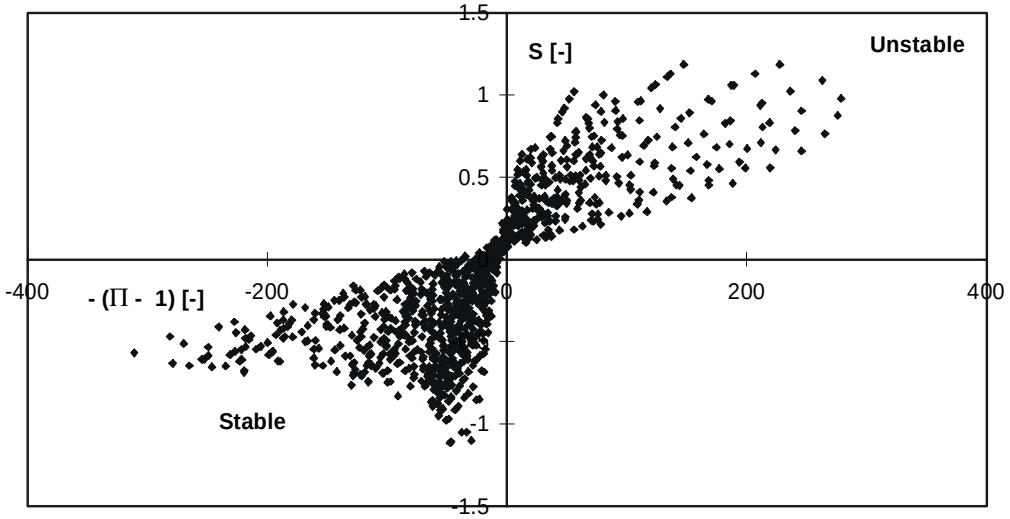

Figure 3. 6: Comparison of the approximate stability criterion S versus the exact stability criterion $-(\Pi - 1)$.

3.6 Discussion

3.6.1 Intermittency versus decoupling

The present study has some parallel with the recent study of Derbyshire (1999) who studied the so-called decoupling phenomenon of the SBL over cold surfaces. He defines the decoupling as a cessation of turbulent transport between the surface and the atmosphere due to high stability. Decoupling of the SBL is strongly related to intermittent SBL behaviour, with the exception that in the latter case the SBL recovers after decoupling due to an acceleration of the air by the pressure gradient, ultimately causing a turbulence burst. Actually, an example shown by Derbyshire (1999; his Fig. 9), shows a recovery from a very small heat flux twice. Generally, the present study agrees with the results of Derbyshire. Both studies reveal a strong sensitivity of the (dynamic) stability of the SBL to the radiative forcing, the pressure gradient, the thermal properties of the (vegetated) surface and its roughness (see: part I). Also the importance of the shape of the stability functions ($f(R_b)$) on the dynamic stability is recognised in both studies.

Derbyshire (1999) addresses the possibility of a positive feedback in the cooling of the surface: in the presence of a strong stratification, an increase in stratification causes a decrease in turbulent heat exchange so that the surface cooling is enhanced even further. In both the present study and in the study of Derbyshire the possibility of this feed-back phenomenon is studied in approximation by investigation of a so-called fixed shear criterion for instability (FSCI). The main difference between the FSCI in both studies lies in the fact that Derbyshire (1999) concentrates on the instability criterion in terms of the *turbulent heat flux,* whereas in the present study the FSCI is interpreted in terms of the so-called *energy supply*, which, in addition to the turbulent heat flux, includes the effect of the radiative and soil heat exchange.
With the help of this 'energy supply' concept, the SBL classification of Fig. 3.6 is interpreted as follows: for *every* possible combination of the pressure gradient and the isothermal net radiation an equilibrium solution can be found (ranging from a 'near-neutral' equilibrium with high turbulent fluxes to a radiative equilibrium with no turbulent fluxes). However, for a fixed value of the pressure gradient, there is a certain maximum value of the isothermal radiation which can be supplied by a stationary energy supply. In case a higher value of the isothermal radiation is imposed on the system, the system will compensate this with an oscillatory energy supply, reflected by intermittent turbulence.

3.6.2 Impact of the boundary conditions

McNider et al. (1995) used a simplified, two-layer SBL model, with the same kind of parameterization as presented in this text, to study SBL dynamics. In order to study SBL dynamics, they used numerical bifurcation techniques (unlike our analytical approach). They report some oscillatory behavior of the mean variables for certain parameter ranges, which confirms the results of this study. Contrary to our results however, they report double-valued equilibrium solutions for certain values of the external parameters. For example two values of U_{eq}, $T_{a,eq}$ and $T_{s,eq}$ are found for a particular combination of external parameters. The existence of multiple solutions

could have strong implications for the predictability of the SBL in the sense that even slight changes in initial conditions would lead to quite different solutions for temperature and wind speed.

The difference in model behavior between both studies can be explained by the use of *different boundary conditions*. In our study at the upper model boundary the turbulent fluxes are assumed to be zero (prescribed fluxes). In the study of McNider et al. at the model boundary the potential temperature and the wind speed (geostropic) are prescribed, allowing turbulent interaction between the actual model and the higher levels. Imposing this kind of boundary condition, basically two type of equilibrium solutions are possible: 1) The overlying air is decoupled from the model layer. In this case the equilibrium solution of de model basically follows our results, where the momentum of the model layer is supplied by the pressure force. 2) The overlying air interacts with the model layer. In this situation extra momentum and heat from above are supplied to the model domain, resulting in an equilibrium solution different from the situation without this transport.

The comparison between the present study and the study of McNider et al. shows that a possible interaction between the upper air and the near-surface air allows a larger number of dynamical cases, than the specific cases discussed in this paper. Therefore, from both a modelling and observational point of view (see: below), there is a need for studying the possibility of an interaction between the high level shear and the atmosphere surface intermittency (ASI), as presented here.

3.6.3 Practical issues

The classification proposed in the previous sections can be used as a framework to study observations of different SBL-regimes. In the previous section we already emphasised that the present analysis is valid for a special class of SBL's. We assumed fluxes to decrease with height, and assumed no interaction of the near surface layer with elevated shear layers Also, due to the idealised structure of the bulk model, a comparison with observational data is not straightforward. Below a few examples are given:

a) The boundary layer height is a prescribed (external) variable, whereas in reality this height is a dependent (internal) system variable.

b) Coriolis effects are neglected, which means that the imposed pressure gradient in fact represents an effective pressure gradient in the (non-fixed) direction of the mean wind speed.

c) The analytical derivation of Π is, strictly speaking, only valid for an equilibrium situation. In reality however, the nocturnal boundary layer keeps on cooling all night, so that a real equilibrium is not reached (e.g. Nieuwstadt and Tennekes (1981)). Nevertheless, the results may be extended to quasi-steady situations (see: Part I).

d) Bulk approaches are used to calculate fluxes. This means that model results have to be compared with measured bulk variables, rather than with local profiles. This will smooth out a lot of detail.

It is challenging to release some of these (strict) assumptions in future theoretical work. At the same time, it is challenging to investigate the relation between the atmosphere-surface intermittency (ASI) and other mechanisms that can generate oscillations and intermittent turbulence, such as gravity waves and shear flow instabilities near the level of the wind maximum.

3.7 Conclusions

In the stable boundary layer discontinuous, intermittent turbulence can be generated by a direct atmosphere surface interaction without interaction with the air aloft. This intermittency mechanism is associated with the most essential elements of the SBL: the built up of stratification by strong surface cooling, the supply of mechanical energy by the synoptic pressure gradient and the limiting effect of stratification on mixing efficiency. In a companion paper (Part I), model simulations show that the essence of this intermittent behaviour can be captured by simplifying the SBL to a system of three coupled nonlinear differential equations describing the time-evolution of wind speed, air temperature and surface temperature. In the present study the same system is studied analytically in order to get more insight in the physical mechanism of this intermittent SBL behaviour. The analysis resulted in the conclusions mentioned below

The system dynamic analysis shows that, from a mathematical point of view, the transition from a continuous turbulent regime to a discontinuous, intermittent regime, can be explained as a Hopf-bifurcation connecting a non-oscillatory and an oscillatory state of the system. This property is used in the derivation of a dimensionless intermittency parameter (Π), from which the equilibrium behaviour of the system (i.e. oscillatory or non-oscillatory) can be predicted exactly. As for the equilibrium solution, the intermittency parameter can directly be evaluated from the values of the external parameters. As such, this parameter is used to classify SBL behaviour. It is also shown that this classification based on dynamic SBL behaviour, differs from classifications based on ‘static’ stability parameters such as z/L or on a single Richardson number.

In the present study, a physical explanation for the instability mechanism which leads to intermittent SBL behaviour was given in terms of a Fixed Shear Criterion for Instability (FSCI, Derbyshire (1999)). The analysis shows that in most cases SBL instability is caused by the following positive feed-back:
In case a strong stratification is present, the magnitude of the turbulent heat flux *decreases* with increasing stratification, due to the fact that under strong stratification the limiting effect of stratification on turbulent heat transport becomes more important than the increase in temperature gradient. This means that a positive disturbance on the stratification, causes a smaller heat flux, which means that less energy is supplied to the surface, enhancing the stratification and thus enhancing the disturbance.

In addition, it was shown that high values of the exchange coefficient for radiative transport and for the soil/vegetation heat flux have a stabilising effect on the system because they prevent a rapid change of the surface temperature. This confirms the results of Part I, showing the importance of vegetation thermal characteristics on the intermittency dynamics.

For the system described in part I an explicit equilibrium solution is found. The solution gives the equilibrium values of the internal parameters (wind speed, air temperature and surface temperature) and of the fluxes (turbulent heat flux, net radiation and soil heat flux) as a function of the external forcing parameters. Therefore, this equilibrium solution may provide a useful starting point for future flux parameterisations in terms of external parameters.

A critical remark is made regarding the generality of the present results. Although the intermittency mechanism arising from a positive feedback between stratification and mixing efficiency in shear flow is an important candidate explaining the observed intermittency in SBL's, it is presently not clear whether this intermittency is caused by a direct surface-atmosphere interaction (present work), if the intermittency is formed in shear layers higher up (Vukelic and Cuxart, 2000, Ha and Mahrt, 2001), or by a combination of both. The present work only provides a framework for the first case. It would be challenging to extend the present framework to the more general case, allowing both atmosphere-surface interaction and interaction with higher shear layers.

Finally, there is a strong need for experimental research on the occurrence of intermittency in stable boundary layers. Extensive measurement campaigns such as CASES99 (Poulos et al. 2000) may help improving our knowledge about the generation of these intermittent events. Also, the observations might answer the question about how the intermittency mechanism decribed in this work is related to other intermittency generating mechanisms such as wave induced turbulence and high level shear instabilities. Finally, in order to understand under what circumstances an intermittent character of turbulence near the surface is to be expected, a *classification based on observations* of different SBL regimes under different synoptic conditions, would be of great value.

Acknowledgements

The authors wish to thank Richard McNider and Peter Duynkerke for reading the manuscript and providing useful suggestions.

Appendix 3A: Symbol List

Apart from the convention notation (e.g. for $g, z_0, \varepsilon_a, \kappa, \sigma$, see Part I) the following symbols are used:

α	real eigenvalue of Jacobian	[-]
a	long wave radiation exchange coefficient	[-]
A_{ij}	element of the Jacobian	[-]
β	imaginary eigenvalue of Jacobian	[-]
c_{Dn}	neutral drag coefficient	[-]
C_a	heat capacity of the air column per unit area	[$Jm^{-2}K^{-1}$]
C_v	heat capacity of the veg. layer per unit area	[$Jm^{-2}K^{-1}$]
δ_m	thickness of the thin mulch layer	[m]
d	height of the vegetation layer	[m]
G_0	soil heat flux	[Wm^{-2}]
h	depth of the turbulent boundary layer	[m]
H	sensible heat flux	[Wm^{-2}]
K	Partitioning Parameter	[-]
λ	bifurcation parameter	[units]
λ_m	conductivity of the thin mulch layer	[$WK^{-1}m^{-1}$]
m	inverse weighted heat capacity	[$K\ m^2\ J^{-1}$]
μ	dummy element of characteristic polynomial	[-]
N	fraction of cloud cover	[-]
Π	intermittency parameter	[-]
P_g	(acceleration due to) pressure gradient	[$m\ s^{-2}$]
Q_{net}	net radiation	[Wm^{-2}]
Q_i	isothermal (or maximum) net radiation	[Wm^{-2}]
R	longwave radiative component	[Wm^{-2}]
R_b	bulk Richardson number	[-]
$\hat{R}_b$	scaled bulk Richardson number	[-]
R_c	critical bulk Richardson number	[-]
$\hat{R}_c$	modified critical bulk Richardson number	[-]
S	simplified stability parameter (FSCI)	[-]
s	distance	[m]
τ	shear stress	[Nm^{-2}]
τ_{bl}	boundary layer time scale	[s]
$\hat{t}$	scaled time	[-]
T_a	(height averaged) air temperature	[K]
$\hat{T}_a$	scaled air temperature	[-]
T_k	temperature scale	[K]
T_{ref}	reference temperature	[K]
T_s	surface temperature	[K]
$\hat{T}_s$	scaled surface temperature	[-]
T_{Top}	temp. of atm. above the turb. bound. layer	[K]

U	(height averaged) wind speed	[ms^{-1}]
U_k	velocity scale	[ms^{-1}]
$\hat{U}$	scaled wind speed	[-]

Appendix 3B: The Unscaled System Equations

Our simplified system derived in Part I is based on three coupled nonlinear differential equations for U, T_a and T_S. They read as:

$$\frac{\partial U}{\partial t} = -\frac{1}{\rho}\frac{\partial P}{\partial s} - \frac{1}{h}\cdot\frac{\kappa^2}{\left[\ln\left(\frac{h/2}{z_0}\right)\right]^2}\cdot U^2\cdot f(R_b) \tag{1}$$

$$\frac{\partial T_a}{\partial t} = \frac{4\varepsilon_a\sigma T_{ref}^3\left(T_s + T_{Top} - 2T_a\right)}{C_a} - \frac{\rho c_p}{C_a}\cdot\frac{\kappa^2}{\left[\ln\left(\frac{h/2}{z_0}\right)\right]^2}\cdot U\cdot(T_a - T_s)\cdot f(R_b) \tag{2}$$

$$\begin{aligned}\frac{\partial T_s}{\partial t} = {} & \frac{-\sigma(\varepsilon_s - \varepsilon_a)T_{ref}^4 + 60\cdot N}{C_v} + \frac{4\varepsilon_a\sigma T_{ref}^3}{C_v}\cdot(T_a - T_s) + \frac{4\varepsilon_a\sigma T_{ref}^3}{C_v}\cdot\left(\frac{\varepsilon_s}{\varepsilon_a} - 1\right)\cdot(T_{ref} - T_s) \\ & + \frac{\rho c_p}{C_v}\cdot\frac{\kappa^2}{\left[\ln\left(\frac{h/2}{z_0}\right)\right]^2}\cdot U\cdot(T_a - T_s)\cdot f(R_b) - \frac{1}{C_v}\cdot\frac{\lambda_m}{\delta_m}\cdot(T_s - T_M)\end{aligned} \tag{3}$$

with:

$$f(R_b) = \left(1 - \frac{R_b}{R_c}\right)^2 = \left(1 - \frac{1}{R_c}\cdot\frac{g(h/2 - z_0)}{T_{ref}}\cdot\frac{T_a - T_s}{U^2}\right)^2 \qquad ; 0 \le \frac{R_b}{R_c} \le 1$$

$$f(R_b) = 0 \qquad ; \frac{R_b}{R_c} > 1 \tag{4}$$

Appendix 3C: The Equilibrium Solution

The equilibrium solution of the system (Eq. (1)-(3), App. 3B) is given below. Note that the equilibrium values of all the fluxes (e.g. H_{eq}, $u_{*,eq}$) can be calculated directly from $\hat{U}_{eq}$, $\hat{T}_{a,eq}$ and $\hat{T}_{s,eq}$.

$$\hat{U}_{eq} = -\frac{b}{2} + \frac{1}{2}\sqrt{b^2 - 4c}$$

$$\hat{T}_{a,eq} = -\left(\hat{U} - \delta\right) \cdot \left(\frac{C_a \hat{R}_c}{a\tau_{bl}}\right) \cdot \frac{\alpha}{1+2\alpha} + \gamma$$

$$\hat{T}_{s,eq} = \left(\hat{U} - \delta\right) \cdot \left(\frac{C_a \hat{R}_c}{a\tau_{bl}}\right) \cdot \frac{1}{1+2\alpha}$$

in which:

$$b = \left(\frac{C_a}{a\tau_{bl}}\right) \cdot \frac{\alpha+1}{2\alpha+1} - \sqrt{c_{Dn}} \qquad c = -\delta \cdot \left(\frac{C_a}{a\tau_{bl}}\right) \cdot \frac{\alpha+1}{2\alpha+1} - \frac{\gamma}{\hat{R}_c}$$

$$\alpha = \left(\frac{\varepsilon_s}{\varepsilon_a} - 1\right) + \left(\frac{\lambda_m/\delta_m}{a}\right) \qquad \delta = \left(\frac{a\tau_{bl}}{C_a}\right) \cdot \frac{1}{\hat{R}_c} \cdot \left(T_{Top} - 2\gamma\right) + \sqrt{c_{Dn}}$$

$$\gamma = -1 \cdot \left(\frac{C_v}{a\tau_{bl}}\right) + \hat{T}_{Top} + \hat{T}_{ref}\left(\frac{\varepsilon_s}{\varepsilon_a} - 1\right) + \hat{T}_M \cdot \left(\frac{\lambda_m/\delta_m}{a}\right)$$

Appendix 3D: Explicit Form Pi-parameter

Following the derivation of section 3.3, Π is given by:

$\Pi = \frac{f_1 \cdot f_2}{f_3}$, with:

$$f_1 = -A_{11} - A_{22} - A_{33}$$

$$f_2 = A_{11}A_{22} + A_{22}A_{33} + A_{11}A_{33} - A_{32}A_{23} - A_{31}A_{13} - A_{21}A_{12}$$

$$f_3 = -A_{11}A_{22}A_{33} + A_{32}A_{23}A_{11} + A_{21}A_{12}A_{33} - A_{21}A_{32}A_{13} - A_{31}A_{12}A_{23} + A_{31}A_{22}A_{13}$$

Next the matrix elements of the Jacobian are given. In order to keep the matrix elements compact, equation (1) of App. 3B is substituted when possible.

$$A_{11} = -\frac{2}{\hat{U}} - 4\frac{\sqrt{c_{Dn}}}{\hat{R}_c} \cdot \frac{\hat{T}_a - \hat{T}_s}{\hat{U}^2} \qquad A_{21} = -\frac{\hat{T}_a - \hat{T}_s}{\hat{U}^2} - 4\frac{\sqrt{c_{Dn}}}{\hat{R}_c} \cdot \frac{\left(\hat{T}_a - \hat{T}_s\right)^2}{\hat{U}^3}$$

$$A_{12} = 2\frac{\sqrt{c_{Dn}}}{\hat{R}_c} \cdot \frac{1}{\hat{U}} \qquad A_{22} = -2\frac{a\tau_{bl}}{C_a} - \frac{1}{\hat{U}} + 2\frac{\sqrt{c_{Dn}}}{\hat{R}_c} \cdot \frac{\hat{T}_a - \hat{T}_s}{\hat{U}^2}$$

$$A_{13} = -2\frac{\sqrt{c_{Dn}}}{\hat{R}_c} \cdot \frac{1}{\hat{U}} \qquad A_{23} = \frac{a\tau_{bl}}{C_a} + \frac{1}{\hat{U}} - 2\frac{\sqrt{c_{Dn}}}{\hat{R}_c} \cdot \frac{\hat{T}_a - \hat{T}_s}{\hat{U}^2}$$

$$A_{31} = \frac{C_a}{C_v} \cdot \frac{\hat{T}_a - \hat{T}_s}{\hat{U}^2} + 4\frac{C_a}{C_v} \cdot \frac{\sqrt{c_{Dn}}}{\hat{R}_c} \cdot \frac{\left(\hat{T}_a - \hat{T}_s\right)^2}{\hat{U}^3}$$

$$A_{32} = \frac{a\tau_{bl}}{C_v} + \frac{C_a}{C_v} \cdot \frac{1}{\hat{U}} - 2\frac{C_a}{C_v} \cdot \frac{\sqrt{c_{Dn}}}{\hat{R}_c} \cdot \frac{\hat{T}_a - \hat{T}_s}{\hat{U}^2}$$

$$A_{33} = -\frac{a\tau_{bl}}{C_v} - \frac{a\tau_{bl}}{C_v} \cdot \left(\frac{\varepsilon_s}{\varepsilon_a} - 1\right) - \frac{C_a}{C_v} \cdot \frac{1}{\hat{U}} + 2\frac{C_a}{C_v} \cdot \frac{\sqrt{c_{Dn}}}{\hat{R}_c} \frac{\hat{T}_a - \hat{T}_s}{\hat{U}^2} - \frac{\lambda_m}{\delta_m} \frac{\tau_{bl}}{C_v}$$

The values of $\hat{U}, \hat{T}_a$ and $\hat{T}_s$ at the equilibrium point are given by $\hat{U}_{eq}$, $\hat{T}_{a,eq}$ and $\hat{T}_{s,eq}$ as presented in appendix 3C.

Appendix 3E: The Equilibrium Bulk Richardson Number

In order to evaluate the stability criterion of section 3.5 an expression for the normalised bulk Richardson number is needed. The equilibrium value of R_b/R_c as a function of 'external' variables can be derived from equation (14) in combination with the unscaled momentum equation (Eq. 1 App. 3B):

$$\left(\frac{R_b}{R_c}\right)_{eq} = 1 + \frac{(\sigma^* - 1) - \sqrt{(\sigma^* - 1)^2 + 4\sigma^*(\delta^* + 1)}}{2(\delta^* + 1)}$$

with:

$$\delta^* = \frac{-(Q_i + G)}{\rho c_p} \cdot \frac{1}{P_g h} \cdot \frac{\sqrt{c_{Dn}}}{\sqrt{P_g h}} \cdot \frac{1}{R_c} \quad \text{and} \quad \sigma^* = \frac{a}{\rho c_p \sqrt{c_{Dn}} \cdot \sqrt{P_g \cdot h}}$$

δ^* can be interpreted as the maximum normalised bulk Richardson number, determined by the available amount of energy ($Q_i + G$). This amount is divided into 1) turbulent heat flux and 2) radiative heat flux (outside the window region).
σ^* can be interpreted as the ratio between the exchange coefficient for radiation and the exchange coefficient for turbulent heat flux.
It is noted that G is not a real external parameter, in a sense that it can be determined beforehand. However, additional analysis showed, that in our model system it could easily be parameterised in terms of Q_i by: $G \approx \alpha \cdot Q_i$, with $\alpha = (\lambda_m/\delta_m)/((\lambda_m/\delta_m) + a)$.

Chapter 4

Intermittent Turbulence and Oscillations in the Stable Boundary Layer over Land:

Part III: A classification for observations during CASES99

This chapter is based on:

Van de Wiel, B. J. H., A. F. Moene, O. K. Hartogensis, H. A. R. De Bruin, and A. A. M. Holtslag, 2002: Intermittent turbulence and oscillations in the stable boundary layer over land.
Part III: A classification for observations during CASES99. *J. Atmos. Sci., (accepted, pending minor revisions).*

4.1 Introduction

On clear nights with weak winds, a frequently observed phenomenon is the weak and intermittent character of turbulence in the atmospheric boundary layer. Intermittent turbulence is characterized by brief episodes of turbulence with intervening periods of relatively weak or unmeasurable small fluctuations (Mahrt, 1999). Despite of its common nature, relatively little is known about the physical mechanisms behind the intermittent turbulence in the stable boundary layer. Intermittency can be generated by several physical mechanisms (see: Van de Wiel et al. 2002a, chapter2): by local shear effects (Ha and Mahrt, 2001), by instability on the scale of the entire surface inversion layer, or by turbulence generated aloft diffusing to the surface [see review on SBL issues by Mahrt (1999))]. Also, locally produced waves formed by Kelvin-Helmholtz instabilities could play a role in triggering turbulence bursts [e.g., Coulter, 1990; Nappo, 1991; also recently observed during CASES99 (Poulos et al., 2002)].

In the present work and in the companion papers of Van de Wiel et al. (chapters 2&3), hereafter VdW(a,b), we focus on an intermittency mechanism which results from a direct interaction between the lower atmosphere and the surface, in presence of a pressure gradient. According to this mechanism, described in detail in VdW(a,b), intermittency is generated by an alternating sequence of SBL collapse (cessation of turbulence) as a consequence of strong surface cooling, followed by a recovery of the SBL (generation of turbulence). The recovery is induced by acceleration of the air by the pressure gradient during the collapse period (period of reduced friction). This increases the shear until $Ri < R_c$, eventually providing the condition for turbulent mixing (Businger, 1973; Turner, 1973). It is noted that in VdW(a,b) interaction with higher shear levels (as in Ha and Mahrt (2001)) was not considered, thus limiting the generality of the present results.

In VdW(a) the physical essentials of the mechanism described above were extracted, which resulted in a model system of three coupled nonlinear differential equations. As such it was shown that this truncated model was able to mimic the observed intermittent turbulence. Also, the model simulated *both* an intermittent and two non-intermittent regimes for different parameter ranges, resulting in three different regimes for clear sky conditions. Furthermore the simplified model essentially showed the same behaviour as more complex models (e.g. Blackadar (1979), Lin(1990), Revelle(1993); McNider et al. (1995)).

In a second paper, VdW(b), the model equations were studied analytically following a system dynamics approach. This resulted in a dimensionless parameter (denoted as: Π) which showed to be a predictor of the equilibrium behavior (e.g. intermittent or non-intermittent) of the simplified system. This critical parameter Π is merely a function of *external 'forcings/parameters'* such as the pressure gradient and the radiative forcing and of local properties such as surface roughness and surface heat capacity. As such, this parameter was proposed as a classification tool to predict intermittent and non-intermittent SBL regimes. It was shown that $\Pi < 1$ corresponds to intermittent situations and $\Pi \geq 1$ corresponds to non-intermittent cases.

For a specific location with fixed local properties the dependence of Π on external forcings can be drawn in a *classification diagram*, valid for that location. An example is given in Fig. 4.1 showing the critical level $\Pi = 1$ as a contour-line for different

values of the effective pressure gradient and of the isothermal net radiation Q_i, the latter being a measure of the radiative forcing (the upper part of Fig. 4.1, indicates cloudy conditions, see: section 4.2). According to this Π-concept, all cases within the contour-line, $\Pi < 1$, correspond to SBL's with intermittent turbulence and all cases outside the contour-line, $\Pi > 1$, correspond to non-intermittent cases. It is observed that under clear sky conditions three regimes are predicted when increasing the effective pressure gradient, confirming VdW(a). For cloudy cases only a single non-intermittent (i.e. continous turbulent) regime is predicted.

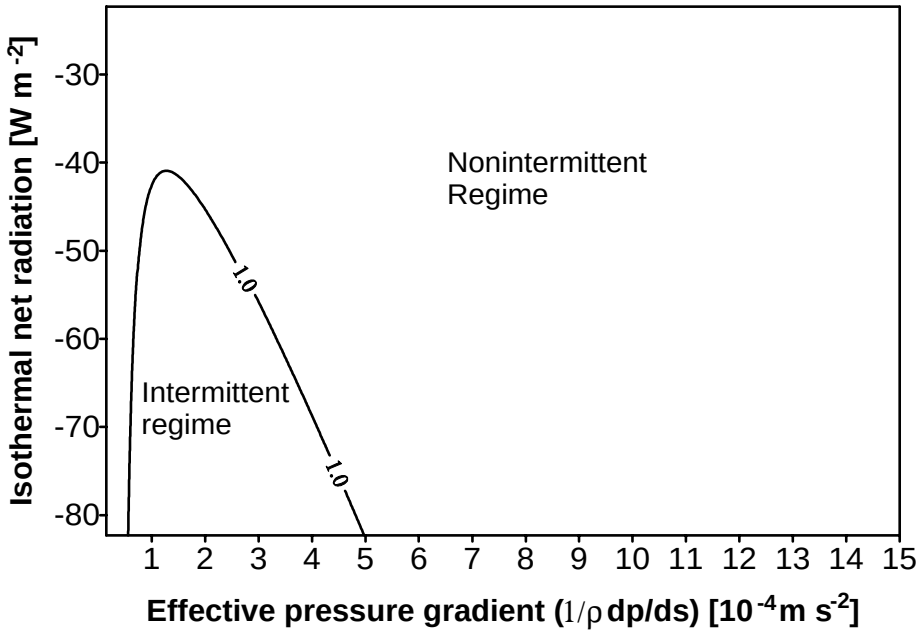

Figure 4. 1: Classification of SBL regimes in terms of external parameters. The figure represents a contour plot of Π -values. Only one contour-line is drawn, viz. that of the critical level $\Pi = 1$. Within this line ($\Pi < 1$) intermittent cases are expected, and non-intermittent cases are expected outside this line($\Pi > 1$).

The main goal of the present paper is to:

a) Classify the different nights of the CASES99 field experiment into subregimes (section 4.3), based on flux time-series. Key question: are three different regimes observed?

b) Determine the value of Π for each night (section 4.4). Key question: where would the CASES99 nights be located in terms of Fig. 4.1?

c) Compare the classification based on 'external' parameters using Π with the results of the classification based on flux time-series (i.e. internal variables)(section 4.5).

The extensive cooperative field experiment CASES99 (Cooperative Atmospheric Surface-Exchange Study) was carried out by various groups from the U.S. and Europe in Kansas, October 1999 (see: this issue and Poulos et al. ,2002). The experiment lasted for a whole month, under *various meteorological conditions*, which makes the experiment very suitable to study the different SBL regimes in relation to the external forcings.

The paper is organized as follows: in section 4.2 a short data description is given. Section 4.3, 4.4 and 4.5 address objectives a), b) and c) respectively. Discussion and conclusions follow in sections 4.6 and 4.7.

4.2 Data description

The CASES99 stable boundary layer experiment took place during October 1999, 50 km east of Wichita, Kansas, USA. The experimental area, covered with dry, open prairie-grass (0-0.25m high), was relatively flat with some minor slopes in the order of 0.5 degrees. A vast array of instruments was deployed. For a general description of the experiment we refer to Poulos et al. (2002) and to the official CASES99 internet site: http://www.colorado-research.com/cases/CASES-99.html, (data freely available).

The Meteorology Group of Wageningen University provided observations at one point (N37'38.611' W096'44.233') in a nested network of flux stations around the central 55-m flux tower of NCAR. An eddy covariance system was set-up at a height of 2.65m and operated at 20Hz. It consisted of a CSAT3 sonic anenometer and a KH2O Krypton hygrometer, from Campbell Sci. Inc. Raw data were stored on a laptop and processed as described in Hartogensis et al. (2002).

In order to get detailed information about the temporal variation of the fluxes (section 4.3) a rather short averaging period of 5 min. was chosen. Comparison with 30 min. averaged fluxes (not shown) gave little systematic difference, favoring the use of a short averaging period.

Short-wave radiation components were measured with an CM14 albedometer and longwave components by a CG2 pyrgeometer (both Kipp and Zn), mounted on a tripod at 1.5m. From these radiation components the net radiation was calculated. Two soil heat flux plates were employed (at -0.054m; TNO, REBS-HFT3) together with two Pt-100 soil thermometers (at –0.028m and –0.080m;Wageningen University). Both radiation and soil measurements were sampled at 5s and averaged and stored every 10min.(Campbell 21x). For a more detailed description of all the measurements by the Wageningen Group, we refer to the web-site above.

Boundary layer heights were inferred from Sodar measurements at Beaumont, Whitewater and Oxford as part of the ABLE program infrastructure (Argonne National Laboratory Boundary Layer Experiment; see: Poulos et al. 2002).

4.3 Observed flow regimes during CASES99

4.3.1 *Method*

In this section a classification based on observations of flux time-series is made, which will be compared with the theoretical framework in section 4.5. The different nights are divided into classes according to the typical characteristics of their turbulent heat flux time-series. The turbulent heat flux near the surface is chosen as indicator, because the turbulent heat flux is directly influenced by two external key-parameters: the synoptic pressure gradient and the isothermal net radiation (section

4.4). From numerical simulations by VdW(a) and the analytical work by VdW(b) it became clear that three typical time traces of the turbulent heat flux are to be expected: 1) a regime with high turbulent transport and non-intermittent fluxes, 2) a regime with intermittent fluxes, 3) a regime with very low turbulent transport and non-intermittent fluxes. These theoretically predicted traces are used as a guideline for the classification introduced below. It will be shown that the time-series could easily be evaluated by eye because the different regimes show very different behavior. In order to avoid subjectivity, only clear examples were classified (a priori) as such (see below).

4.3.2 *Results: a classification of SBL regimes using observation of flux time-series*

Using time series of the surface fluxes (H and u_*) it is found that the CASES99 nights (indeed) can be subdivided in the following regimes:

a) Continuous turbulent regime
b) Intermittent regime
c) Radiative regime

To illustrate the main features of each class, typical examples are given below:

Continuous turbulent nights

In figure 4.2 the turbulent heat flux is shown during a clear night with continuous turbulence (Oct.14/15). The sensible heat flux reaches a large value of about –45 [W m^{-2}], due to strong radiative surface cooling ($Q_{net} \approx$ -75 [W m^{-2}]) in combination with strong turbulent mixing ($u_* \approx$ 0.5 [m s^{-1}]).

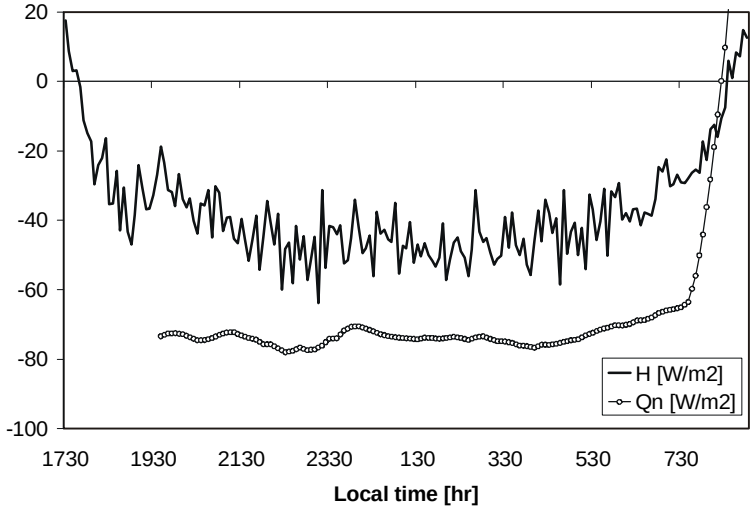

Figure 4. 2: typical example of a time-series of the turbulent heat flux and net radiation in a continuous turbulent night (Oct.14/15).

Intermittent nights

In Figs. 4.3a,b two typical examples of intermittent nights are given. These examples give an impression about the typical time-scales and amplitudes of the turbulent events and the quiet periods. It is observed that they are rather irregular. Some turbulent periods have very small amplitudes of 5 [W m^{-2}] and time-scales of less than ten minutes, others amplitudes of 25 [W m^{-2}] and a duration of 4 hrs. The quiet periods may, but need not, result in a total decay of the flux, and the time-scales also ranges from tens of minutes to a few hours.

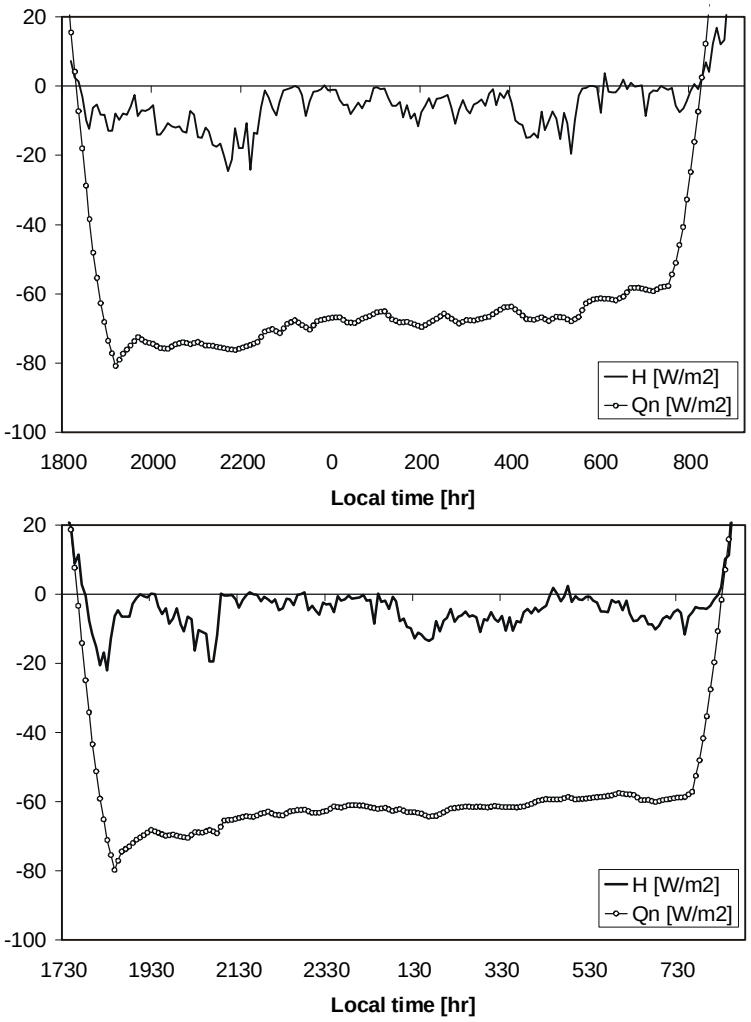

Figure 4. 3a,b: typical examples of turbulent heat flux and net radiation in two nights with intermittent turbulence (Oct. 4/5; fig. 4.3a), and (Oct. 23/24; fig. 4.3b).

An interesting result is given by the net radiation graphs of Figs. 4.3a and b, showing small deviations superimposed on a smooth decreasing trend (absolute value). The smooth trend results from a strong surface cooling during the night. The small deviations are caused by the turbulent bursts, leading to alterations of the surface temperature which immediately affects the net radiation (chapter 2).

Radiative nights

In contrast to the well-mixed case of Figs. 4.2 a night with hardly any turbulent heat flux is shown in Figs. 4.4. Because the transport of energy through the atmosphere by turbulence is so small we indicate these nights simply as ‘radiative nights’.

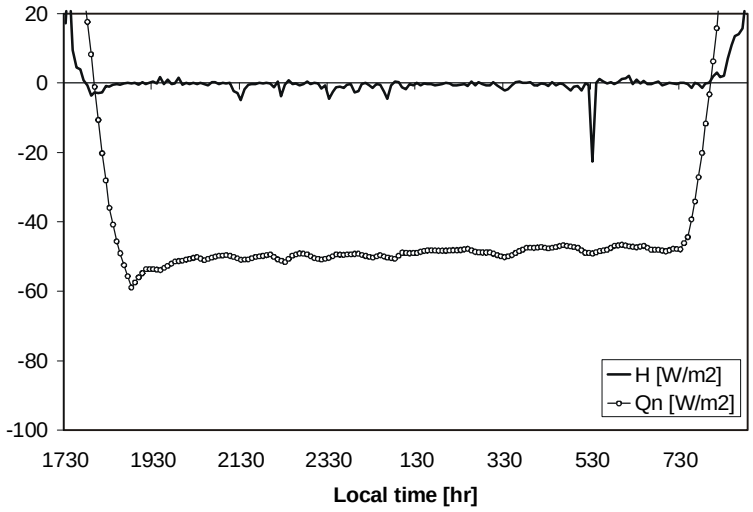

Figure 4. 4: typical example of a time-series of the turbulent heat flux and net radiation in a radiative night (Oct. 9/10).

A cloudy case

Contrary to the previous clear-sky examples, in Fig. 4.5 (Oct.16-17) a night with variable cloud cover is shown

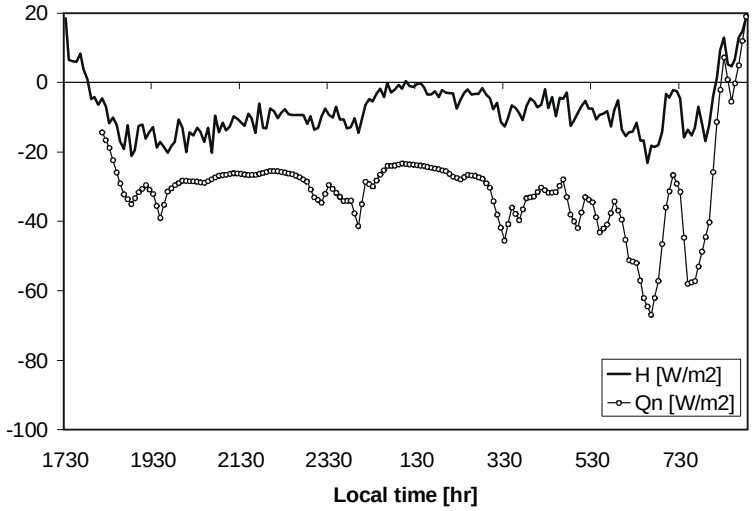

Figure 4. 5: Heat flux and net radiation in a night with time-varying cloud cover (Oct.16/17).

.

In this case the turbulent heat flux demonstrates alternating higher and lower values. From this heat flux graph only, it looks as if this could be a night with intermittent turbulence. On the contrary, however, *it is a night with continuous turbulence*, as will be shown below. In the following, Fig. 4.5 is compared with Fig. 4.3a (Oct. 4-5). Comparing the net radiation graphs of both figures, it is observed that the magnitude

of the net radiation during Oct. 16/17 is much smaller and more variable than during 4/5 Oct, indicating the presence of clouds in the first place. The contrast between the two nights becomes more evident in the friction velocity graphs (Fig. 4.6).

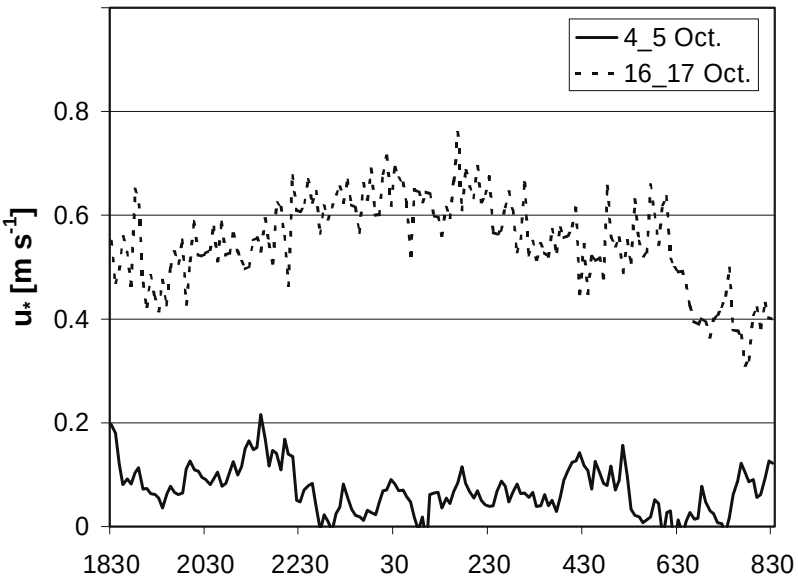

Figure 4. 6: Examples of friction velocity during an intermittent and a non-intermittent night

In the intermittent situation (Oct. 4/5) the values of u_* are very low and correlated with H . In the continuous turbulent case (Oct. 16/17), the values of u_* are high and not correlated with H . These examples show that in the cloudy night the radiative factors are limiting for the turbulent heat flux, whereas in the clear night the mixing efficiency is the limiting factor for the turbulent heat flux. In terms of K-theory: in the cloudy case the (small) temperature gradient is limiting, whereas in the clear and intermittent case the (small) turbulent diffusivity is limiting (De Bruin, 1994; Derbyshire,1999; VdW(b)).

A transient or 'non' case

In the previous examples the behavior of near surface turbulence was classified into three different regimes. It is realized that any SBL classification is only a simplification of real SBL complexity (Mahrt et al., 1998). This fact is illustrated by a 'pathological' example given in Fig. 4.7.

In the beginning of the night, the figure seems a perfect example of a night with continuous turbulence. After 2 hr LST however, it is observed that the heat flux H rapidly decreases from about –40 [W m^{-2}] to almost zero. This collapse of turbulence was also clearly visible in u_* (not shown) decreasing from about 0.35 [m s^{-1}] around 0 hr to 0.05 [m s^{-1}] around 6 hr LST. Apart from some influence of high level clouds, the net radiation remains rather large. Around 7 LST (40 min. before sunrise) a sudden recovery of H and u_* (increasing from 0.02-0.22 m s^{-1}, within 5 min) occurs. It seems that rapidly changing synoptic conditions strongly influenced the mechanical budget of the SBL. Several of these kind and other transitional cases were observed during CASES99. In this study these cases are not classified explicitly, but are indicated as *'non'(-classified) cases*.

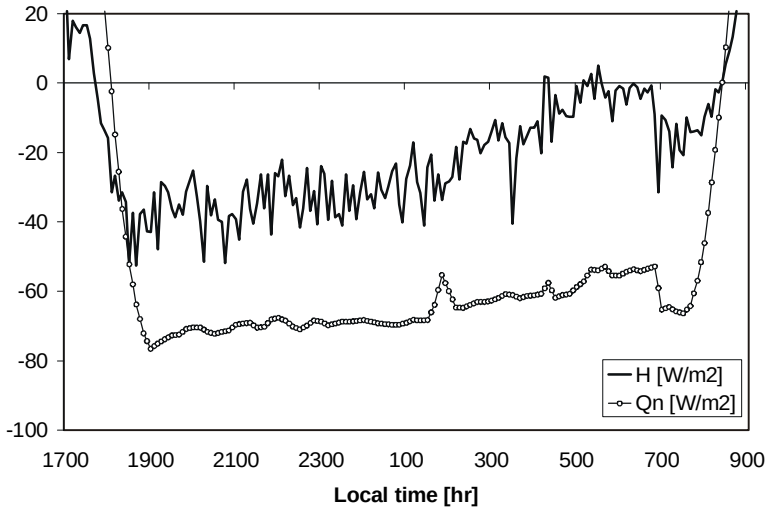

Figure 4. 7: Turbulent heat flux and net radiation during a night with transient behavior (Oct. 12/13).

4.3.3 Classification applied to the whole CASES99 dataset

The classification of the previous section was applied to the whole CASES99 data period. The results of this classification are summarized in table 4.1. Also in table 4.1 the mean values of some basic micrometeorological variables are given to indicate typical values occurring at different conditions/regimes. The averages were calculated over 0-6 hr LST. This period is chosen because it is often the most stationary period of the night (contrary to the period after sunset), although a purely stationary period (as assumed in VdW(b)), in its strict sense that the variables do not change in time, is not reached

From table 4.1 it occurs that 20 out of 28 nights were classified. From these 20 classified night 8 nights (40%) showed continuous turbulence during the 6 hrs. period, 8 nights (40%) showed intermittent turbulence, and 4 nights (20%) behaved as a radiative nights. From this frequency statistics the number of intermittent and radiative nights may seem rather high compared to the number of turbulent nights. This can be explained by the large number of clear nights during the CASES99 field campaign. (Poulos et al. 2002). It is well-known that clear sky conditions favor moderately to strongly stable SBL's that may lead to radiative or intermittent nights. In more cloudy conditions the number of intermittent/radiative nights will be less.

Although a detailed discussion about the micrometeorological characteristics of each night is beyond the scope of this paper, some general characteristics are outlined:
-As expected, turbulent nights mostly occur in situations with strong winds and weak inversions. In the same way intermittent and radiative nights tend to occur in low wind conditions with stronger temperature inversions.
-Most of the nights show large net radiation indicating clear nights.
-From the mechanical point of view, a large range in u_* values (0.02-0.59 m s^{-1}) is observed, leading to a broad range of stability conditions.
-Mostly, the latent heat flux is small.

-Generally speaking, the magnitude of the soil heat flux (SHF) is large compared to the other terms in the energy balance, showing the importance of this process. Therefore, a detailed description of the SHF-measurements and its analysis is given in appendix 4A, together with some innovative results. Because the complete set of SHF instruments by Wageningen University was only available at the end of the experiment, only this part of the measurements is given.

DOY [-]	Date [-]	Time LST[hr]	Class [-]	u_* ms^{-1}	Q_{net} Wm^{-2}	H Wm^{-2}	LvE Wm^{-2}	G Wm^{-2}	U_10 ms^{-1}	T_10 [K]	T_s [K]
274	1-Oct.	0 - 6	**Non**	0.150	-65.8	-23.4	4.5	-	3.42	285.27	282.57
275	2-Oct.	0 - 6	**Non**	0.267	-35.2	-15.9	16.4	-	4.68	286.65	285.70
276	3-Oct.	0 - 6	**Turb.**	0.295	-6.2	7.0	18.8	-	4.46	281.30	282.44
277	4-Oct.	0 - 6	**Non**	0.213	-49.3	-2.9	2.3	-	3.76	276.99	277.36
278	5-Oct.	0 - 6	**Int.**	0.061	-66.8	-5.9	-0.5	-	3.29	279.97	277.08
279	6-Oct.	0 - 6	**Int.**	0.075	-61.7	-6.9	-2.2	-	2.82	285.16	281.41
280	7-Oct.	0 - 6	**Turb.**	0.438	-71.2	-48.4	14.8	-	6.40	288.80	286.57
281	8-Oct.	0 - 6	**Int.**	0.139	-48.3	-10.1	-5.6	-	3.15	287.49	285.82
282	9-Oct.	0 - 6	**Int.**	-	-	-	-	-	-	-	-
283	10-Oct.	0 - 6	**Rad.**	0.022	-48.6	-1.2	-0.6	-	2.03	288.62	284.45
284	11-Oct.	0 - 6	**Turb.**	0.360	-65.8	-32.7	10.0	-	5.59	288.94	287.20
285	12-Oct.	0 - 6	**Turb.**	0.217	-64.3	-20.4	-2.1	-	4.05	290.38	287.91
286	13-Oct.	0 - 6	**Non**	0.199	-62.5	-17.5	-1.8	-	3.67	290.38	288.10
287	14-Oct.	0 - 6	**Rad.**	0.031	-62.8	-1.4	-0.3	-	2.26	281.50	278.71
288	15-Oct.	0 - 6	**Turb.**	0.494	-73.9	-45.6	5.7	-	7.21	292.79	290.41
289	16-Oct.	0 - 6	**Turb.**	0.451	-58.9	-13.8	9.2	-	7.45	285.44	285.24
290	17-Oct.	0 - 6	**Turb.**	0.594	-31.2	-5.7	12.5	-24.0	9.30	282.63	283.04
291	18-Oct.	0 - 6	**Int.**	0.094	-55.6	-4.1	2.9	-39.7	2.97	277.02	275.01
292	19-Oct.	0 - 6	**Rad.**	0.033	-57.6	-1.1	0.4	-45.1	2.14	279.87	276.65
293	20-Oct.	0 - 6	**Int.**	0.070	-61.9	-5.7	0.1	-38.9	3.06	278.11	275.17
294	21-Oct.	0 - 6	**Non**	0.115	-63.2	-14.3	-0.2	-32.1	3.94	283.37	279.19
295	22-Oct.	0 - 6	**Non**	0.119	-60.7	-17.7	3.2	-30.9	4.50	286.16	280.68
296	23-Oct.	0 - 6	**Non**	0.172	-70.1	-19.3	3.1	-42.6	4.35	278.86	276.71
297	24-Oct.	0 - 6	**Int.**	0.067	-61.2	-4.8	0.5	-48.3	2.92	275.02	273.12
298	25-Oct.	0 - 6	**Turb.**	0.296	-69.6	-34.5	3.9	-29.5	6.28	282.11	279.45
299	26-Oct.	0 - 6	**Rad.**	0.018	-53.4	-1.7	-0.3	-39.6	2.02	285.29	277.64
300	27-Oct.	0 - 6	**Int.**	0.158	-65.4	-27.8	0.0	-28.9	3.81	288.12	283.35
301	28-Oct.	0 - 6	**Non**	0.230	-59.6	-28.9	0.3	-	4.19	287.97	285.28

Table 4. 1 Classification of CASES99 nights based on turbulent heat flux observations. Also, an overview of some basic micrometeorological variables (6 hr. averages), gathered by Wageningen University is given.

4.4 Application of Π: input parameters

4.4.1 Introduction

In this section the dimensionless Π-number (VdW(b)) is evaluated for each night to predict the particular SBL regime for that night. Thus, for each night, the input parameters have to be estimated from the data, which is not a trivial task, in view of the simplified character of the theoretical model. Therefore, we discuss the parameters in relation to the available data, which will result in an overview-table of input parameters and Π-numbers. Due to its extremely complex form, the explicit form of

the Π-parameter is not discussed here. For the exact analytical form of Π and its derivation we refer to VdW(b).

4.4.2 Estimation of external forcing parameters

The effective pressure gradient

VdW(a) showed that in the theoretical model, an *effective* value of the pressure gradient is used rather than the 'real' pressure gradient, due to the negligence of Coriolis effects. Here, the effective pressure gradient is defined as: the pressure gradient in the direction of the mean wind speed in the lower atmosphere. In practice it is not straightforward to estimate this effective value accurately:

-The mean wind direction close to the surface may vary in time, especially in conditions of intermittent turbulence, where changes in surface friction cause changes in the (cross-isobaric) flow direction up to tens of degrees. This affects the effective component of the pressure gradient.
-In the SBL the 'mean' wind may vary considerably with height (e.g. Nieuwstadt and Tennekes, 1981), which makes it difficult to choose a single 'representative' mean wind direction for the lower atmosphere.
-Often, from weather maps only limited time intervals with pressure data are available (e.g. each 6 hrs.), whereas the pressure gradient may vary during these intervals.

Therefore, a different approach is followed in order to obtain a measure for the effective pressure gradient. Point of departure is the momentum budget of the mean wind speed following the model of VdW(a,b):

$$\frac{\partial U}{\partial t} = -(\frac{1}{\rho}\frac{\partial P}{\partial s})_{effective} - \frac{u_*^2}{h} \qquad (1)$$

In this equation the influence of advection was neglected. Furthermore, a 'classical' boundary layer structure was assumed (as e.g. in Nieuwstadt, 1984) were the stress decreases gradually with height until it vanishes at the boundary layer top. If also the assumption of stationarity is adopted (as in the original derivation of Π) then the effective pressure gradient can be replaced by

$$-(\frac{1}{\rho}\frac{\partial P}{\partial s})_{effective} = \frac{u_*^2}{h} \qquad (2)$$

This substitution is applied to figure 4.1 (Fig. 4.8). Note that the shape of Fig. 4.8 is unchanged compared to Fig. 4.1. From now on axis as in Fig. 4.8 will be used.
Adopting the assumptions above, the effective pressure gradient is estimated from the data by using *6-hour* averaged values of u_* and boundary layer height (see 4.4.5).

It is however realized that many real SBL's do not show 'classical' behavior. For example, Mahrt and Vickers (2001) show a number of CASES99 nights were fluxes temporarily increase with height (upside down BL's) before they decrease higher up. Also, SBL are often non-stationary, by many causes, as with inertial oscillations. This means that Eq. (2) can at best only provide a crude approximation of the effective pressure gradient, limiting the generality of Fig. 4.8 (see discussion).

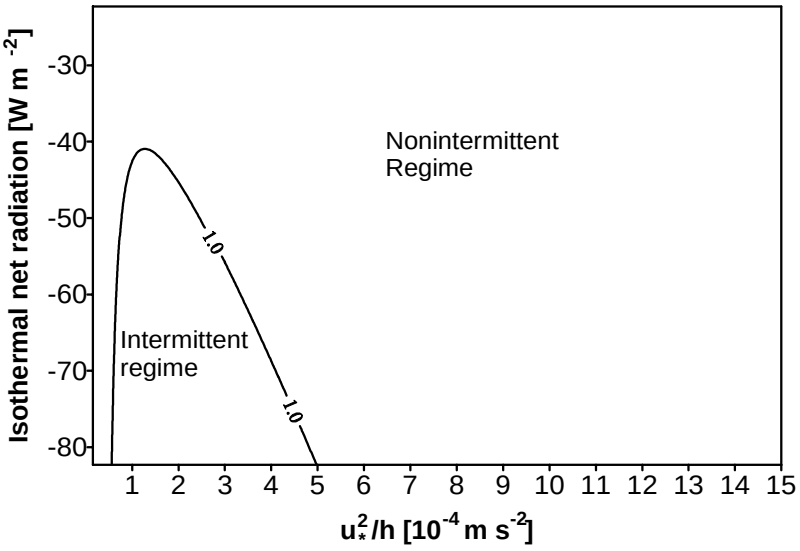

Figure 4. 8: As Fig. 1 but with the horizontal axis in terms of u_*^2/h instead of (effective) pressure gradient.

The isothermal net radiation

A second key parameter determining the radiative forcing on the SBL system as defined in VdW(a,b) is the so-called isothermal net radiation (Monteith, 1981; Holtslag and De Bruin 1988). The isothermal net radiation is defined as the net radiation that would occur if the near surface layer were isothermal. This definition becomes clear by noting the linearized longwave radiation budget for the surface in the model (a small correction term is neglected):

$$Q_{net} \approx [-\sigma(\varepsilon_s - \varepsilon_a)T_{ref}^4 + N \cdot 60] + 4\sigma T_{ref}^3 (T_a - T_S) \qquad (3)$$

This equation is derived by linearization of the original budget equation near a reference temperature, T_{ref} (see: VdW(a)):

$$Q_{net} = \varepsilon_a \sigma T_a^4 + N \cdot 60 - \varepsilon_s \sigma T_S^4 \qquad (4)$$

By writing the net radiation equation as Eq. (3), it is clear that it can be divided in two parts: a part containing independent external parameters ε_a, ε_s and cloud cover N (octa), and a part containing system variables T_a (air temperature) and T_S (surface temperature). The first part of (3) is defined as the isothermal net radiation Q_i, for it equals the net radiation Q_{net} if $T_a = T_S$. For our data set Q_i is estimated from: $Q_i = Q_{net} - 4\sigma T_{ref}^3 (T_a - T_S)$, with T_a measured at 10m, as in table 4.1.

4.4.3 Estimation of local system parameters

An important parameter determining the vegetation-soil interaction is the so-called bulk conductance of the mulch/stagnant air layer within the vegetation (VdW(a)). This bulk conductance is denoted with λ_m / δ_m [W m^{-2} K^{-1}], with: λ_m the conductance [W m^{-1} K^{-1}] and δ_m the thickness of the mulch/stagnant air layer [m]. It determines the heat flux through the vegetation layer, given a temperature difference between the vegetation top (radiation temperature T_S) and the soil surface (T_M):

$$G = \lambda_m / \delta_m \cdot (T_M - T_S) \qquad (5)$$

For dense vegetation the bulk conductance can be easily determined by measuring G in combination with the radiation temperature of the vegetation T_S and the top-soil temperature T_M. In CASES99 the surface was covered with dry, open prairie grass, so that bare soil was visible between the grass. Thus, the infrared camera (at 1.5m), measures a composite of the vegetation top temperature T_S and the top soil temperature T_M. If, for simplicity, we assume $\varepsilon_s = 1$ for both vegetation and bare soil, this gives:

$$\sigma T_{IRT}^4 = A \cdot \sigma T_S^4 + (1 - A) \cdot \sigma T_M^4 \qquad (6)$$

with A[-], the fraction of vegetation cover.

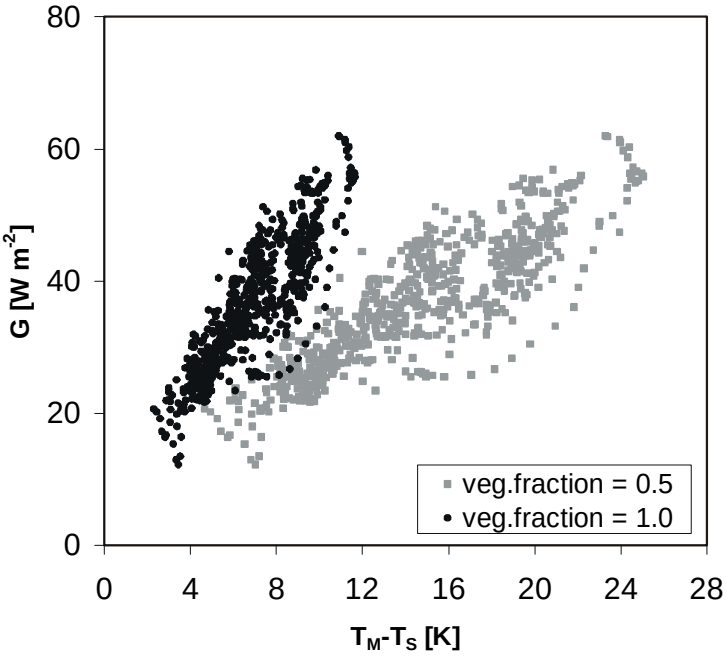

Figure 4. 9: Estimation of vegetation bulk conductance for two different fractions of vegetation cover (see text).

For a given vegetation fraction, the actual temperature of the vegetation top T_S can be calculated from the measured values T_{IRT} and T_M. Next, the value of G can be plotted as a function of $T_M - T_S$ in order to estimate the bulk conductance. In Fig. 4.9 this is applied to the CASES99 data assuming two different values for the vegetation cover.

The plots show surprisingly little scatter, given the strong empirical character of Eq. (5) not accounting for the complicated structure of real vegetation (leaf distribution/orientation). From Fig. 4.9 the following estimates for the bulk conductance are made [W m^{-2} K^{-1}]: $\lambda_m / \delta_m \approx 5$ for A=1.0, $\lambda_m / \delta_m \approx 2$ for A=0.5 (the intermediate case (not shown) gives $\lambda_m / \delta_m \approx 3.5$ using A =0.75). These 'extremes' give a range for the bulk conductance at CASES99. For comparison we note that Duynkerke (1999) found $\lambda_m / \delta_m \approx 3$ [W m^{-2} K^{-1}] for short, dense grass at Cabauw, comparable to the values given above.

Another vegetation parameter is the heat capacity C_v of the vegetation top (per unit area). This parameter, which is difficult to estimate, was given an effective value of 2

[KJ m^{-2} K^{-1}] (as in VdW(a)), based on typical biomass estimations for grasslands (Atzema, 1992), accounting for the dry and sparse character of the CASES99 grass.

The momentum roughness length z_{0m} was taken to be 0.03 [m], based on local measurements of momentum flux and wind profiles. In order to be consistent with the theoretical work it was assumed that $z_{0m} = z_{0h}$. In future work this assumption could be refined.

4.4.4 Boundary conditions

Bottom boundary condition for temperature

In the simplified model the top-soil temperature T_M (the bottom system-boundary) is assumed to be a known external variable, needed to calculate Π. T_M (at z=0.00 m) is inferred from Fourier analysis of soil temperature measurements as explained in App. 4A.

Top boundary condition for temperature

In order to estimate the radiative forcing on the SBL system, strictly speaking, a temperature T_{TOP} at the boundary layer height is needed. As a practical approach, the temperature at the top of the central mast (55m) was taken as T_{TOP}. Because, the strongest temperature gradient is usually below 55m, Π is not very sensitive to the exact height at which this top temperature is evaluated as long as it is not close to the surface.

4.4.5 Other input parameters

Boundary layer height

From sodar measurements at Beaumont, Oxford and Whitewater a composite estimate of the boundary layer height (h) was made, given in table 4.2. For a few cases, h was small enough (<55m) to compare it with flux data from the central NCAR-tower. Although, the sodar estimates showed somewhat larger values than estimates from mast data, the comparison seemed reasonable for most cases. Generally, It is stressed however, that the 6 hour averaged values of the h are rather crude estimates. In some cases (e.g. Oct. 24) h showed considerable variation during the averaging period, responding to changing intensity of SBL turbulence. It is noted that the final results are not very sensitive to the exact value for h.

4.4.6 Summary

The total set of input parameters is given in table 4.2. Only days with a complete set of input parameters, derived from various instruments, could be analysed, which limited the number of days. Additionally, the following constants were used: ε_s = 1.0 [-], ε_a =0.8 [-], $z_{0h} = z_{0m}$ =0.03 [m], $T_{ref} = (T_{TOP} + T_M)/2$, C_v = 2 [KJ m^{-2} K^{-1}]. Unless stated otherwise, physical constants like Boltzmann's are given the same values as in VdW(a). Based on this input data, Π has been computed for two cases: λ_m / δ_m = 5 (case 1) and 2 (case 2) [W m^{-2} K^{-1}]. Results are discussed below.

Doy	Date	Time	Class	u_*^2/h	Q_i	h	T_{TOP}	T_M	Π λ_m/δ_m =5	Π λ_m/δ_m =2
[-]	[-]	LST[hr]	[-]	[m s^{-2}]	W m^{-2}	[m]	[K]	[K]	[-]	[-]
279	6-Oct.	0 - 6	**Int.**	7.5E-05	-77.2	75	290.01	284.31	23.8	2.1
280	7-Oct.	0 - 6	**Turb.**	1.3E-03	-80.8	145	290.59	286.98	268.3	258.6
281	8-Oct.	0 - 6	**Int.**	1.7E-04	-56.0	115	290.78	287.48	19.2	-20.2
283	10-Oct.	0 - 6	**Rad.**	6.8E-06	-67.3	70	294.15	287.53	86.0	56.0
284	11-Oct.	0 - 6	**Turb.**	7.4E-04	-73.5	175	291.39	288.86	202.3	142.9
286	13-Oct.	0 - 6	**Non**	7.5E-04	-78.2	150	295.03	291.28	152.1	102.9
287	14-Oct.	0 - 6	**Rad.**	1.0E-05	-73.9	90	284.76	285.10	80.5	46.5
288	15-Oct.	0 - 6	**Turb.**	1.2E-03	-84.5	200	294.82	290.05	366.5	358.5
290	17-Oct.	0 - 6	**Turb.**	5.0E-03	-29.3	70	283.39	285.72	254.7	301.7
291	18-Oct.	0 - 6	**Int.**	1.8E-04	-63.4	50	281.81	282.05	19.3	0.2
292	19-Oct.	0 - 6	**Rad.**	1.6E-05	-70.2	70	282.98	283.28	56.9	31.4
293	20-Oct.	0 - 6	**Int.**	8.1E-05	-73.0	61	284.50	281.63	22.5	3.4
294	21-Oct.	0 - 6	**Non**	1.1E-04	-79.8	120	285.99	283.72	21.7	-18.5
295	22-Oct.	0 - 6	**Non**	2.0E-04	-83.0	70	291.49	284.54	13.8	-8.0
296	23-Oct.	0 - 6	**Non**	2.9E-04	-78.1	100	281.79	282.63	44.9	-5.2
297	24-Oct.	0 - 6	**Int.**	1.0E-04	-70.1	52	280.89	281.01	20.9	2.7
298	25-Oct.	0 - 6	**Turb.**	8.6E-04	-80.0	102	284.15	282.71	127.8	90.7
299	26-Oct.	0 - 6	**Rad.**	1.1E-05	-83.8	30	291.05	283.04	40.5	27.1
300	27-Oct.	0 - 6	**Int.**	2.5E-04	-85.3	100	291.89	285.83	16.9	-17.3
301	28-Oct.	0 - 6	**Non**	4.1E-04	-71.4	130	290.83	287.28	55.0	0.9

Table 4. 2: Overview of input parameters for the evaluation of Π. The calculated Π-values are given for two values of λ_m/δ_m .

4.5 Comparison of theory and observations

4.5.1 *Using full theory (Π)*

In Fig. 4.10 the critical contour line $\Pi=1$ from Fig. 4.8 is replotted. As before, this contourline is valid for a single location with a certain set of local parameters. Fig. 4.10 (also the example in Fig. 4.8) is calculated for the CASES99-site using local parameter estimations (like z_{0m}) as given in the previous section. Because some of the parameters are not true physical constants like T_M, T_{TOP} and h they had to be given fixed values in order to plot this theoretical contourline. In Fig. 4.10 we assumed $T_M = T_{TOP}$ =285[K] and h =80 [m]. For comparison, the CASES99 nights are plotted in Fig. 4.10, according to their values of u_*^2/h and Q_i. The nights are marked with different symbols according to their a priori time-series classification described in section 4.3.

If we take the theoretical figure to be representative for the CASES99 location (although, strictly speaking each night should have a slightly different contour-line, due to the fact that each night has it own value of T_M, T_{TOP} and h), then the observed nights with intermittent turbulence should be located within the contour line, and the non-intermittent nights should lie outside this contour line. Fig. 4.10 shows that this is indeed the case, favoring the theoretical predictions (although the number of data points is limited). On the other hand, it is not clear how robust this result is in view of

the assumptions and uncertainties in the parameter estimations. Therefore, a *sensitivity example* of the results in Fig. 4.10 is discussed below. First, however, some quantitative characteristics will be investigated.

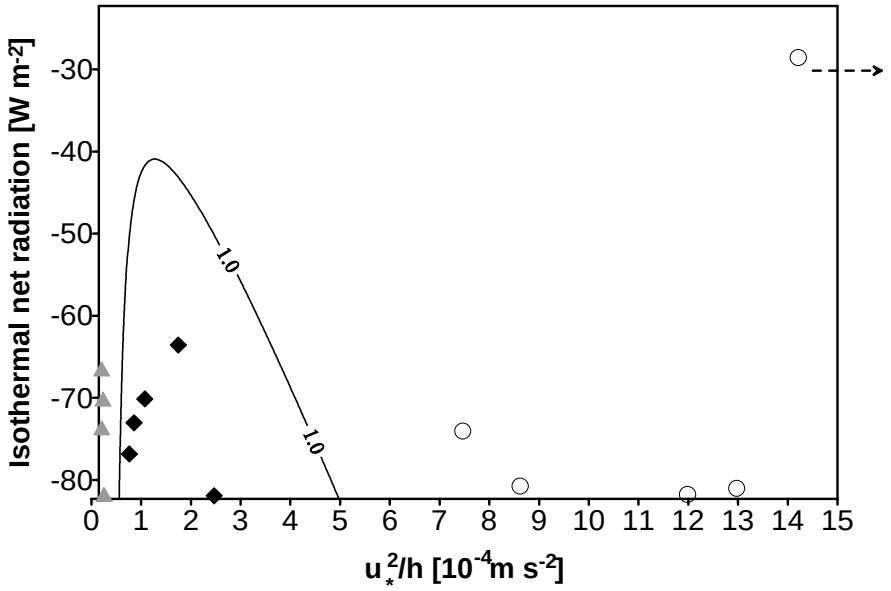

Figure 4. 10: Critical contourline $\Pi = 1$ for the CASES99 site predicted by theory. Observed nights are located in this graph according to their values of Q_i and u_*^2/h. The nights are marked with different symbols according to their a priori time-series classification described in section 4.3: gray triangles = radiative nights, black diamonds = intermittent nights, and open circles = continuous turbulent nights (as Fig.11).

Fig. 4.10 represents a single contour line of a bowl-shaped figure (intermittent cases at the bottom of the bowl) showing Π as a function of u_*^2/h and Q_i. It would be interesting to know the exact Π values in Fig. 4.10, i.e.: what is the height of the observation-points compared to the critical level (Π=1)? First we may simplify the representation of Fig. 4.10, by recognizing the fact that during CASES99 clear sky conditions prevailed over cloudy conditions. Thus, the isothermal net radiation was very similar for most of the nights, indicating that the dynamical differences between the nights are mainly caused by differences in u_*^2/h.

Therefore we limit the parameter-space by looking at Π as a function of u_*^2/h (Fig. 4.11a). Effectively, a horizontal slice is made in Fig. 4.10. The intersection of this slice with the contourline of Fig. 4.10 predicts the two pressure gradient values for which Π=1 in Fig. 4.11a. Again,different symbols are used according to the á priori classification of section 4.3. In Fig. 4.11a it is shown that the non-intermittent nights show Π values larger than its critical value 1, and Π values below or just around the critical level coincide with observed intermittent nights, confirming the theoretical predictions of VdW(a,b). The data points do not exactly collapse on one single curve, due to small differences in Q_i, and differences in T_M, T_{TOP} and h. But, roughly speaking, Fig. 4.11a and 4.10 indicate comparable results, confirming the predictive character of Π.

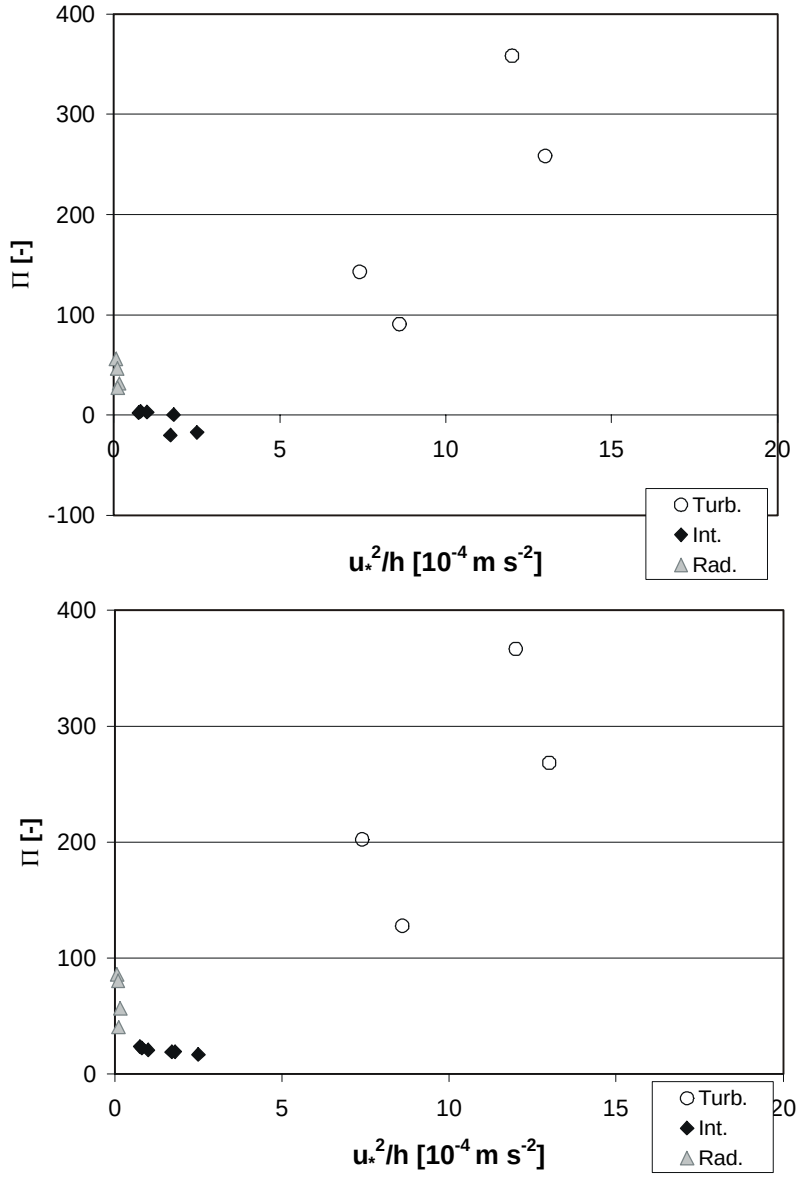

Figure 4. 11a,b: Calculated Π values as a function of u_*^2/h for various CASES99 nights (upper graph, **a**,: with λ_m/δ_m =2). Different symbols are used according to the a priori classification (as Fig. 10). Lower graph ,**b**, with λ_m/δ_m =5.

In Figure 4.11b the calculations of Π are identical to 4.11a, except for the fact that a bulk conductance λ_m/δ_m of 5 [W m^{-2} K^{-1}] is used, corresponding to a vegetation fraction of 1.0, instead of λ_m/δ_m =2 (veg. fract. of 0.5). Although the qualitative shape of 4.11b is similar to 4.11a, its quantitative features are rather different. Fig. 4.11b shows that, although the predicted Π values are low for the intermittent cases, they are not below the theoretical critical level of $\Pi = 1$, below which intermittency is predicted. Thus, although the observed intermittent cases are predicted to be most unstable (mathematically) of all, they are predicted just not unstable enough to be intermittent. The implications of this result for the general classification figure 4.10 becomes clear in Fig. 4.12, showing two theoretical classifications for CASES99 site, using two different values of the bulk conductance.

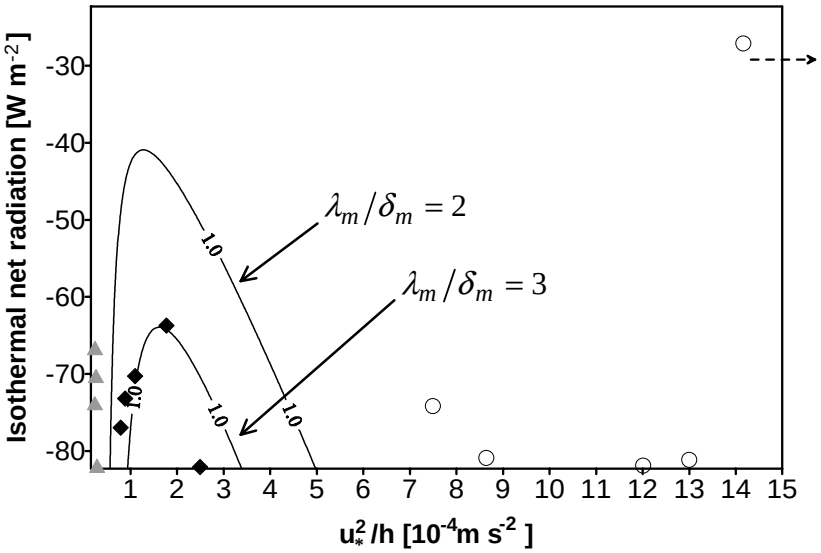

Figure 4. 12: as Fig. 4.10, but for two value of λ_m/δ_m , viz. λ_m/δ_m =2 and λ_m/δ_m =3 [W m^{-2} K^{-1}].

It is observed that the case with the highest bulk conductance (λ_m/δ_m =3) results in the smallest area with intermittent turbulence. The large value of λ_m/δ_m of 5 [W m^{-2} K^{-1}] (not shown) would not give a single Π value below the critical level 1 for any value of u_*^2/h and Q_i. As such it could not be plotted as a contour line $\Pi = 1$. On the other hand it is noted that even in this case of λ_m/δ_m =5, the most unstable cases are located in the same area as in the case of λ_m/δ_m =2 (as with 4.11a and 4.11b), indicating that the qualitative bowl shaped dependence of Π remains unchanged. It is noted that the importance of the bulk conductance on the system stability was recognized/discussed in the previous studies of VdW(a,b).
In summary: although the predictions by Π are robust and discriminative in a qualitative sense, the exact quantitative features have to be interpreted with caution, because of uncertainties in the parameter estimations.

4.5.2 A simplified approach

Theoretical background

A disadvantage of the Π parameter of VdW(b) is its complexity, which limits its applicability. Furthermore, due to this complexity this parameter does not provide insight in the physical cause of instability that generates intermittency. Therefore, in VdW(b), a less exact but simpler stability/classification criterion was given, which allows a physical interpretation. In this section this simplified criterion is applied to the CASES99 data set.
The Approximate stability Criterion (denoted as: A-Cr.) is derived by application of a Fixed Shear Criterion for Instability (FSCI, Derbyshire, 1999) to the surface energy balance equation. Here only the result is given. The system is found to be mathematical/physical unstable (causing intermittency) when:

$$\left(\frac{R_b}{R_c}\right)_{eq} > \frac{K+1}{3} \qquad (7)$$

This criterion depends on two dimensionless groups:

1) The normalised equilibrium bulk Richardson number: $(R_b/R_c)_{eq}$.

2) The partitioning parameter: K

Both groups are calculated from external variables. As expected, the equilibrium value of the bulk Richardson number is primarily determined by Q_i and by the effective pressure gradient. The second group, the so-called *partitioning parameter*, is physically interpreted as the ratio of the summed radiative and soil/vegetation conductance/exchange coefficient compared to the exchange coefficient for turbulent heat transport (VdW(b)). If turbulent heat exchange were the only process involved, the criterion $(R_b/R_c)_{eq} > 1/3$ would imply a sufficient condition for system instability (assuming fixed shear). The discussion in the previous section however, learned that a large soil heat flux (and additionally, the radiative flux) tends to stabilize the system, counteracting intermittency. This effect is accounted for in the partitioning parameter, making $(R_b/R_c)_{eq} > 1/3$ a necessary but not a sufficient condition.

For the application of the A-Cr external parameters were estimated as with Π except for the following:
- T_{TOP} and T_M are not needed as input parameters.
-Instead, at the bottom boundary, G is needed as input. Because G was only available for a limited number of days (table 4.2), G is estimated from the residual of the other energy balance terms, accounting for the gap in the energy balance closure (13 [W m^{-2}]).

Results

For the available CASES99 nights, both terms in the stability criterion of Eq. 7 were calculated (Fig. 4.13). Moreover the *difference* between those two terms, $(R_b/R_c)_{eq} - (K+1)/3$ is plotted, marked differently according to the a priori classification based on the flux time-series, as in Fig. 4.11a,b. A positive difference means $(R_b/R_c)_{eq} > (K+1)/3$, predicting instability (causing intermittency). Likewise, a negative difference predicts a non-intermittent situation.

To some extent the system stability is predicted correctly: negative differences coincide with radiative and turbulent nights, and the intermittent nights show positive values. However, the 'in-between' cases show that some turbulent nights are incorrectly predicted as being unstable. Moreover, the slope between the intermittent and turbulent cases is rather flat, indicating that the figure is not very discriminative for these cases (contrary to the strong slopes in Fig. 4.11a,b). It is noted that the use of a larger bulk conductance, λ_m/δ_m of 5 instead of 2 [W m^{-2} K^{-1}], gave very similar results as with Π, i.e. leading to system stabilization.

In summary: although the approximate criterion provides useful physical insight and predicts the extreme cases correctly, its predictions are incorrect or not very discriminative for the more subtle cases. For these cases the basic fixed shear assumption is probably not correct (Derbyshire, 1999). Therefore, for these cases, the momentum equation needs to be accounted for in a coupled momentum-energy balance system as in the derivation of Π.

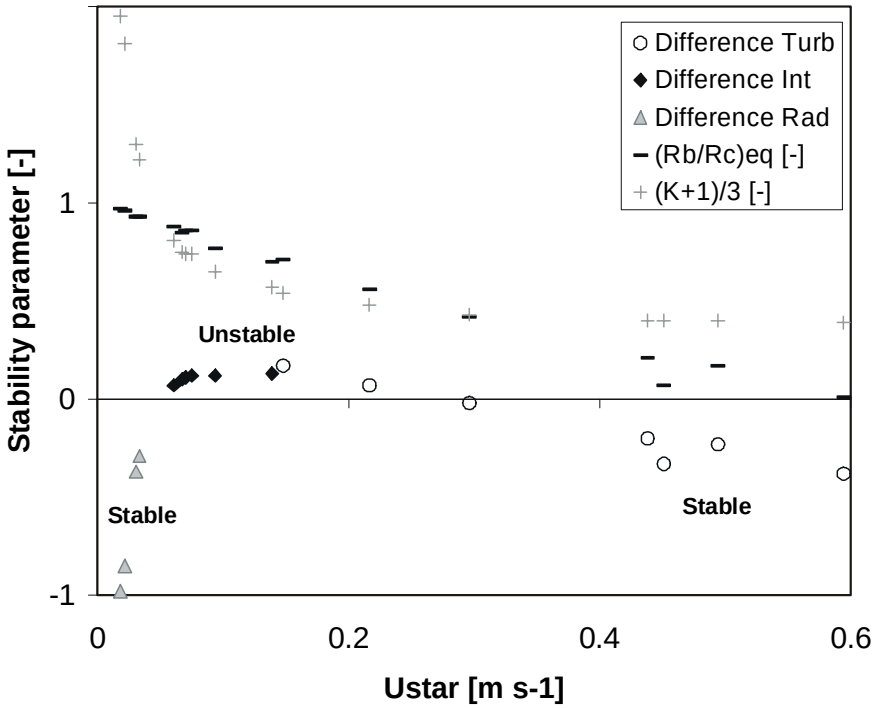

Figure 4. 13: The simplified stability parameter, indicated as the difference $(R_b/R_c)_{eq} - (K+1)/3$, as a function of u_*. Different symbols are used (as Fig. 4.10) according to the a priori classification (section 4.3). Separate terms of the stability parameter are given by dashes and crosses.

4.6 Discussion

Quantitative/qualitative features

The previous sections showed that the predictions with Π are robust in a qualitative sense: intermittency is most likely to occur under clear sky conditions in presence of a moderately/weak pressure gradient, in agreement with what is generally observed (section 4.3). This robustness can be understood from the basic mechanism (see: introduction or VdW(a,b)), which needs two basic ingredients:1) a possitive feedback of stratification on turbulent mixing, enabling decoupling, and 2) a pressure gradient that accelerates the flow after decoupling, enabling recoupling. In conditions of strong winds and/or large cloud cover the Ri-numbers are too low to generate decoupling (no intermittency). In the other extreme, in absence of a significant pressure gradient, the flow acceleration is absent, or not strong enough to generate intermittency.

Despite this qualitative robustness, our results (especially VdW(a)) indicate a large sensitivity of the Π value on some (uncertain) parameter estimations. This means that a single Π value on itself cannot be interpreted as an exact (strict) predictor of intermittent/non-intermittent SBL regimes. Rather, the *relative* value of Π compared to the Π-values of other nights at the same location (under various conditions) tells more about the probability of finding a particular regime during this night. This result indicates that the qualitative/conceptual value of the present study is more important than its direct quantitative significance. This is certainly true in the light of the rather strict model assumptions.

Other classifications

The present paper tries to express/predict different SBL regimes in terms of *external forcing parameters* such as pressure gradient and cloud cover. First, it is believed that, eventually, these external parameters determine SBL behaviour (apart from the discussion on predictability by McNider et al. (1995)). Secondly, especially in the intermittent regime, external parameters tend to vary less than internal system parameters, like wind speed, temperature, u_*, L, etc. Section 4.4 however shows, that in practice, still internal input parameters (averaged over a long period) such as u_*^2, h, T_M and T_{TOP} are needed to calculate Π. By inclusion of more model complexity in future studies, some of these internal variables could be related to external parameters. For example, inclusion of Coriolis effects (separate U and V equations) translates the *effective* pressure gradient into a 'real' pressure gradient as input parameter.

In literature SBL classifications have been proposed using *internal system parameters* such as z/L, z/Λ, h/L and z/h, based on similarity arguments (Holtslag and Nieuwstadt, 1986). Using z/L as indicator, Mahrt et al. (1998) classified the stable surface layer into: a) weakly stable, b) moderately stable, c) very stable. Although this classification proved to be very useful as a guideline to look at surface layer observations, it is not meant as an *exact* predictor of different SBL regimes (here, especially the intermittent regime). Generally speaking, the studies mentioned above indicate that intermittent turbulence is most likely at large stability conditions, i.e. large values of Ri, z/Λ,z/L or h/L. This fact is confirmed by the present study and others (e.g. Kondo et al., 1978; Howell and Sun, 1999). Additionally, the present study stresses the importance of other heat exchange processes (besides turbulence) such as soil/radiative heat flux, that may prevent SBL intermittency even at larger Ri-values.

Future research

It would be interesting to extend the present analysis on SBL regimes in relation to external forcings to larger data sets. The present study only partly addressed the parameter space in the direction of radiative forcing due to the limited number of cloudy nights. Also, it is tempting to assess the effect of different types of land cover (with different surface properties) on SBL regimes.

Apart from the present system analysis approach using a simplified model, there is need for more detailed studies on intermittency dynamics. Although the intermittency mechanism arising from a positive feedback between stratification and mixing efficiency in shear flow is an important candidate explaining the observed intermittency in SBL's, it is not clear whether this intermittency is caused by a direct surface-atmosphere interaction (present work), is formed in shear layers higher up (e.g. Coulter, 1990, Ha and Mahrt, 2001), or by a combination of both. It is challenging to extend the present work to the more general case, allowing both atmosphere-surface interaction and interaction with higher shear layers.

4.7 Conclusions

In this paper a classification of intermittent and non-intermittent turbulence is presented based on observations of near surface turbulence during CASES99. It is found that the different nights can be subdivided in three subclasses:

a) A turbulent regime
b) An intermittent regime
c) A radiative regime

These classes reflect different SBL dynamics. Moreover, the existence of three regimes confirms the findings of VdW(a), who simulated three different SBL regimes with a simplified model.

This bulk model of VdW(a) showed both intermittent and non-intermittent SBL behaviour for different parameter ranges. In VdW(b) analysis of the model equations resulted in a dimensionless number (Π), which is a function of external forcing parameters such as the (effective) pressure gradient and the radiative forcing. With this number the model behaviour (i.e. intermittent or non-intermittent) could be predicted.

The present study uses this parameter to classify/predict intermittent and non-intermittent nights at CASES99. To this end Π was evaluated from detailed analysis of the available data. Comparison of the predictions/classification using Π, with the actual observed regimes shows generally good agreement:

-Those nights predicted to be most (mathematically) unstable to disturbances, turned out to be intermittent.

-The most stable (mathematically) nights turned out to be non-intermittent, i.e. continuously turbulent or radiative.

The qualitative features mentioned above are very robust and discriminative. Thus, under the assumptions made, the Π-concept could be useful as a classification tool.

The exact quantitative value of Π shows to be rather sensitive to local parameters such as
the bulk conductance of the vegetation layer, which is difficult to estimate exactly a priori. In practice, this makes Π unsuitable as an *absolute* predictor of stability/SBL-regimes. However, useful information about the stability/regime of a particalar night is obtained by comparing its Π-value *relative* to other nights under different conditions.

In VdW(b) an approximation for the rather complex Π was derived. As in the Π-case, regime-predictions are compared with the observed regimes. The approximate parameter shows less discriminative than the original Π parameter: although extreme case are predicted correctly, more delicate cases showed to be less decisive or even incorrect.

The present work focusses on a special type of atmosphere-surface intermittency, without accounting for interaction with the air aloft. This limits the generality of the present results. It is challenging to study (the system dynamics of) this interaction in the future, and compare the present mechanism with other intermittency generating mechanisms.

Appendix 4A: Fourier analysis of soil temperature- and flux measurements

To solve the surface energy balance one would like to measure the soil heat flux (SHF) directly at the soil surface. In practice this is often not possible without disturbing the surface properties, due to the presence of vegetation/roots. Therefore, the SHF is often measured a few centimeters below the soil surface. Thus, the measured values need to be extrapolated to the surface in a consistent way. A method is given below. It is noted that similar method, developed simultaneously by Heusinkveld et al. (2002) showed a large improvement on the closure of the surface energy budget over a desert area. For a detailed background of the theory we refer to Van Wijk et al. (1963).

In the analysis data from thermometers at -3 and -8 cm and a SHF-plate at -5.4 cm are used, available during DOY 289-301. The time series of the 3 cm temperature is decomposed in 150 Fourier components, which results in a nearly perfect fit (Fig. 4A1). Using standard theory of heat conduction (assuming homogeneity) the temperature signal at 8 cm depth is reconstructed (Fig. 4A1) using a 'best fit' thermal diffusivity value κ_{th}. For our set this gave κ_{th} =0.155 * 10^{-6} [m^2 s^{-1}], comparable to values for dry sand (0.24* 10^{-6} [m^2 s^{-1}]) and clay (0.18* 10^{-6} [m^2 s^{-1}]), Oke (1978). Knowing this κ_{th} –value, T(z,t) is known for every z,t assuming homogeneity of soil properties in space/time. In this way $T_M(t)$ was found substituting $z = 0$ (section 4.4).

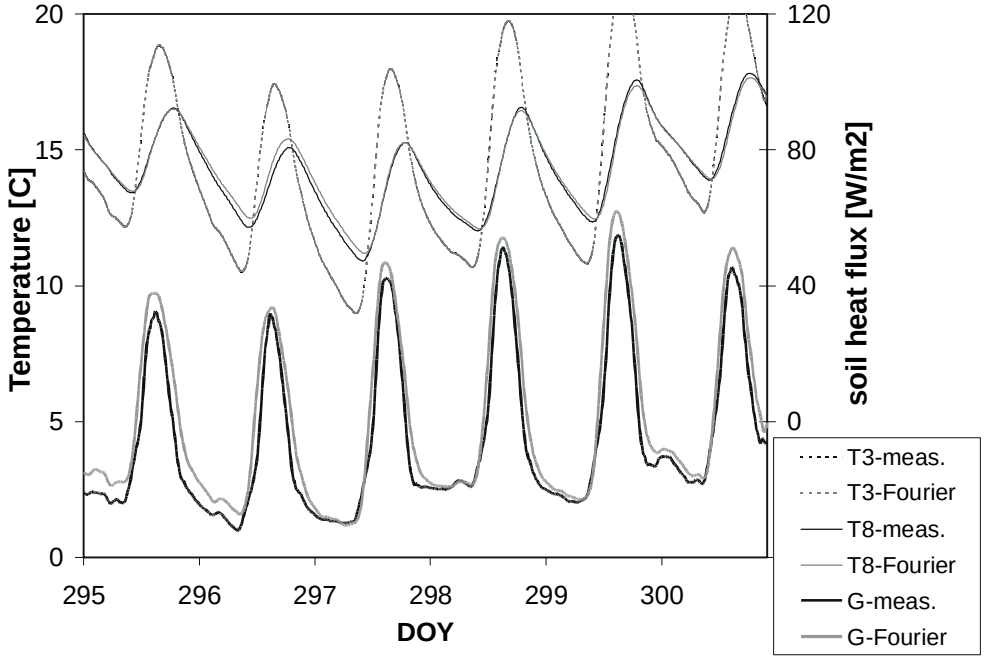

Figure 4A1: Measured and modelled soil temperatures/fluxes (see: text).

Next the SHF at 5.4 cm depth is reconstructed (Fig. 4A1) by differentiating T(z,t) with respect to z, assuming a 'best fit' value for the soil conductivity λ_S of 0.6[W m^{-1} K^{-1}]. With this λ_S-value G(z,t) is known and the SHF at the surface G(0,t) is found by substituting $z = 0$. The result is shown in Fig. 4A2, which gives an overview of the energy balance for three typical nights. Comparing Figs. 4A2 and 4A1 learns that both the magnitude and the shape of G(0,t) has changed a lot compared to the original measured G(-0.054,t), indicating the importance of the extrapolation.

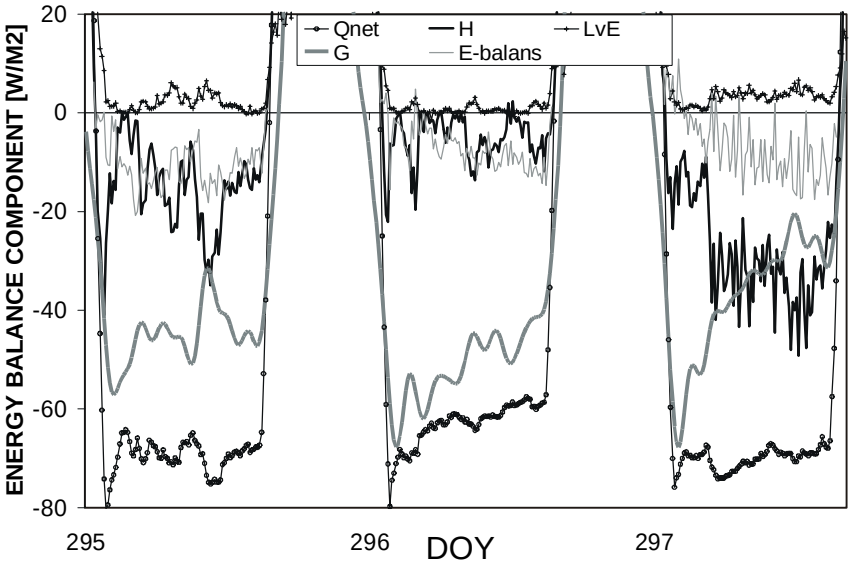

Figure 4A2: Energy balance components in three typical nights.

An innovative element of this study are large temporal changes in G(0,t), which are realistic features: the soil heat flux not only reacts on the peak value of the net radiation at the beginning of the night, but also reflects the intermittent behaviour of the turbulent heat flux at DOY 296, and the 'jump' in the heat flux at DOY 297. As such, strong fluctuations cancel out in the final energy balance budget. Apparently, the intermittent character in the turbulent flux is transferred into the soil and is still noticable in the temperature measurements, despite of its apparent smooth timeseries (4A1).

Chapter 5

Summary

5 Summary

Thesis summary

As the title of this thesis indicates, our main subject of interest is: "Intermittent turbulence and oscillation in the stable boundary layer over land". As such, this theme connects the different chapters. Here, intermittent turbulence is defined as a sequence of events were 'burst' of increased turbulence activity are followed by relatively quiet periods with low turbulence levels. This intermittent turbulence affects the mean structure of the SBL, in a sense that it may cause alternations on the nocturnal evolution of wind speed and temperature. In this way the time series of these quantities may show an oscillatory-type of behavior, referring to the title. Intermittency is commonly observed, especially in conditions of strong stratification. As such, several observed examples of this intermittent behavior are given in this thesis (chapter 3 and 4). Despite of the fact that it is ubiquitous relatively is known about intermittency: e.g. what physical mechanism causes intermittency? What are its typical statistical characteristics (e.g. regarding time-scales and amplitudes of the turbulent events)? Under what conditions can we expect intermittency to occur?

From a number of studies with atmospheric column models (e.g. Welch et al., 1986; Lin, 1990, Revelle, 1993; Vukelic and Cuxart, 2000) it appears that an intermittent behavior of turbulence is found in some specific parameter ranges. However, from these studies no general picture explaining the essential physics behind this behavior is available. Furthermore, some of these studies (e.g. Lin, 1990, Revelle, 1993) indicate that different regimes are simulated upon varying the pressure gradient: besides the intermittent regime two non-intermittent regimes emerge. From an observational point of view also, the existence of non-intermittent regimes (e.g. the continuous turbulent regime) is well known. On the other hand, it is not clear what external conditions cause the stable boundary layer to end up in one regime or another.

The large number of unanswered questions, about the intermittency phenomenon in particular and stable boundary layer dynamics in general, largely motivated the present work. In relation to the problems posed above, the following research questions are addressed in this thesis:

I) - What is the physical essence of this intermittent behaviour?
   - Is it possible to simulate both intermittent and non-intermittent regimes with a simple model?

II) - What external forcing parameters control the transitions between the different regimes?
   - Can we *predict* the occurrence of intermittent and non-intermittent regimes?

III) - What regimes are actually observed in the field? Under which conditions do they occur?

The present work consists of three parts: the first part is a numerical study (chapter 2), the second part an analytical study (chapter 3) and the third part is an observational study (chapter 4).

The study focuses on an intermittency mechanism first qualitatively described by Turner (1973) and Businger (1973): on clear nights over land in presence of weak winds, strong surface radiation may built up a strong surface inversion, such that

turbulence is suppressed effectively. This causes the atmosphere to decouple from the underlying surface. Soon, however, due to the reduced friction, the air in the lower atmosphere will be accelerated by the omnipresent pressure force, until shear is strong enough to break through the stratification. Because of this mixing, shear is reduced largely and soon a new stratification is built up by surface cooling. Thus, the situation has returned to its 'initial' state and the mechanism starts over again, causing intermittent bursts of turbulence.

In chapter 2 it is shown that the essence of this intermittency mechanism can be captured by a 1D bulk model consisting of three coupled nonlinear differential equations. According to the authors, the bulk model considers the essential elements of the SBL: surface cooling by longwave radiation, supply of mechanical energy by the synoptic pressure gradient, and the limiting effect of stratification on mixing efficiency. In the simplified model structure only direct interaction of the lower atmosphere (first tens of meters) with the vegetation surface was considered, with no interaction with the air aloft. Consequently, this type of assumptions may limit the generality of the results.

It appears that this bulk model is able to mimic the intermittent behavior described above. Surprisingly (in view of model simplicity), model simulations predict both intermittent and non-intermittent SBL to occur for different external forcings, confirming the results of others with more detailed model configurations (e.g. Lin, 1990, Revelle, 1993). It appears that three regimes occur (two non-intermittent and one intermittent) when the pressure gradient is varied.
Model results show that intermittent turbulence is most likely to occur over land surfaces with low vegetation under clear sky conditions in presence of a low synoptical pressure gradient. The results indicate that the existence of a vegetation layer has a strong influence on intermittency dynamics: due to its small heat capacity, the vegetation temperature is able to respond quickly to rapid changing conditions. This, in turn, affects the stability of the lower atmosphere, causing an important feedback mechanism (see also: chapter 4). In addition it is found that intermittent behavior in SBL models occurs for various first-order closure schemes with different stability functions (as in Derbyshire, 1999). On the other hand we find that 'broad tail' stability functions that allow turbulent transport beyond the critical Richardson number effectively suppress intermittent/oscillatory behavior. Currently, these types of broad tail stability functions are often used in numerical weather prediction to prevent excessive SBL cooling in very stable conditions. Furthermore it is noted that, strictly speaking, time-averaged flux-profile relationships will not be valid in intermittent flows. In those conditions, average flux-profile relations cannot be unique due to their nonlinear nature.

The advantage of using a simplified SBL model, as proposed in chapter 2, is that it allows an analytical study of the system. Such analytical study is presented in chapter 3, were the governing equations of the bulk model are studied from a system dynamics point of view. In this way the transition between the different flow regimes is identified as a Hopf bifurcation. At the Hopf bifurcation point the stability of the equilibrium solution of the system changes such that a stable non-oscillatory solution alters in an unstable oscillatory solution (or vice versa). This property is used to derive a dimensionless parameter (denoted as Π), which is a function of external forcing parameters such as the pressure gradient and the radiative forcing, and of local

parameters such as the aerodynamic roughness, heat capacity and bulk conductivity of the vegetation layer. With this dimensionless parameter the equilibrium behavior of the system (i.e. intermittent or non-intermittent) can be predicted exactly. As such this parameter is proposed as a classification tool to predict SBL regimes. The proposed classification parameter provides different information than classical parameters such as z/L and Ri. The main difference lies in the fact that the Π considers the stability of the system as a whole, including feed-backs from the turbulence-, soil heat flux-, and the radiation scheme, whereas z/L and Ri are scaling parameters for turbulence only. Because Π has a rather complicated structure, a less exact but simpler stability criterion is also derived, based on a fixed shear criterion for instability (Derbyshire, 1999). This, more practical criterion allows a clear physical interpretation. It is found that the main cause of instability is the positive feedback between stratification and mixing which occurs under strong stratified conditions. Furthermore it is shown that the heat exchange due to longwave radiation (outside the atmospheric window region) and by the soil heat flux imply strong negative feedbacks counteracting instability. According to the simplified criterion, the Π parameter can be approximated by two dimensionless groups: a bulk Richardson number and a so-called partitioning parameter. The latter is interpreted as the ratio of the summed radiative and soil heat exchange coefficient compared to the exchange coefficient for turbulent heat transport (or, alternatively, the ratio of fluxes). As such, this partitioning parameter represents the competition between the positive and negative feed-backs described above.

In chapter 4 SBL classification is studied from an observational point of view. In this chapter observations of the extensive CASES99 field experiment are presented (CASES: Cooperative Atmospheric Surface-Exchange Study). This field experiment, carried out by various groups from the U.S. and Europe, was specially designed to quantify the physical characteristics of the stable boundary layer over land, with a variety of observational tools. It took place in Kansas (U.S.) over a relatively flat area with dry, open prairie-grass, and lasted for a whole month (Oct. 1999), under various meteorological conditions. This makes the experiment very suitable for studying the different SBL regimes in relation to external forcings.

In chapter 4, first a classification of stable boundary layer regimes is presented based on time-series observations of near surface turbulence during CASES99. It is found that the different nights can be divided in three subclasses: a turbulent regime, an intermittent regime and a radiative regime. The existence of these three regimes is in agreement with the theoretical findings of chapter 2 and 3.

Secondly, this classification based on flux time series is compared with the theoretical predictions using Π (based on external parameters). To this end, for the CASES99 nights, this Π is evaluated from a detailed analysis of the available data. Such evaluation from real data is not a trivial task, due to the number of assumptions in the equations on which Π is based (e.g. the estimation of an effective value for the pressure gradient). The comparison between the theoretical predictions and the actual observed time-series shows generally good agreement. Also, the results are robust and discriminative in a qualitative sense. As such, it is e.g. shown that intermittent turbulence often occurs in clear sky conditions with a moderately weak (effective) pressure gradient. Similarly, in clear sky conditions, radiative and continuous turbulent regimes occur during conditions of very weak pressure gradients and strong pressure gradients respectively. This robustness is explained from the main ingredients of the mechanism described in chapter 2. On the other hand, the quantitative features of the theoretical Π classification are rather sensitive to (often uncertain) local parameter estimations, such as the bulk heat conductance of the

vegetation layer. Due to this sensitivity, the relative value of Π for a certain night compared to other nights at the same location, provides more information about the SBL regime to be expected than a single Π value by itself.
As a practical test case also the simplified criterion of chapter 3 is applied to the CASES99 data set. The approximate parameter shows less discriminative than the original Π parameter: although the extreme cases are predicted correctly, more subtle cases showed to be less decisive or even incorrect. This is probably caused by the neglection of important feed-backs between wind shear and stratification in the momentum and heat budget equations. Thus apart from its clear conceptual value (chapter 4) its practical value is limited to more extreme cases.

Generally, we reflect that the analytical approach in this thesis, using a truncated set of equations, has clear advantages: e.g. internal relations between various processes can be made explicit, and equilibrium system behaviour can be expressed a priori in terms of the external forcing parameters. As such, this type of system analysis provides a fruitful way for continuation of the present research on SBL dynamics. Additionally, there is a need for detailed studies on the instability mechanisms that may generate intermittent bursts, using more complex model configurations with higher resolution and less strict assumptions. Such models are useful in simulating individual bursting events selected from observational case-studies. Also, as a continuation of the present observational work, it is interesting to test the proposed classification under different climatological conditions. In this observational respect, there is also a need for long-term measurement campaigns providing an accurate statistical climatology/characterization about the typical time-scales and amplitudes of the intermittent bursts under different conditions. Regarding practical applications, it is shown that the equilibrium solutions presented in the thesis provide a useful starting point for parameterization studies. Because, especially with stable boundary layers, many practical problems are a consequence of its scientific counterparts, future theoretical progress may directly benefit practical applications.

Chapter 6

Perspectives

6 Perspectives

In this chapter suggestions for future continuation of the present work are given based on the findings and discussions presented in this thesis. The following subjects are discussed subsequently: -modeling issues, -observational issues and –practical issues in relation to parameterizations.

Modeling

As shown in the previous chapters and outlined in the summary, the analysis in the present work is built on a *simplified* model structure. This approach clearly showed some advantages:

1) Mutual interactions between different processes as radiation, (soil) heat conduction and turbulent heat transport are made explicit (chapter 3).
2) Results from numerical integration of the governing equations are generalized: the equilibrium solution for the system and its stability is calculated directly from analytical solutions, so that no long-time (strictly: infinite) numerical integrations are needed to obtain such information.
3) The functional relationship between internal variables such and wind speed and temperature and external forcings is made explicit.
4) Apart from the original research-objectives, new insights may emerge from additional analytical deduction. For example, previous theoretical findings on Hopf-bifurcations by others (App. B), predict the initial period of the oscillations at the bifurcation point. As such, this could help further analysis on time-series characteristics. Another example is given in the next section, where the results of a new analytical relation between the surface scaling variables u_* and θ_* are presented.

At the same time the use of such simple model structure limits the generality of the outcome, since a lot of assumptions are made (App. A). It is likely that simulations with a more complex model structure show a closer resemblance to observed stable boundary layer dynamics. From a system-dynamics point of view it would be interesting to assess the impact of introducing more degrees of freedom to our original model. Some possible physical consequences are discussed:

1) In chapter 2 modeled time series of intermittent turbulence show a single characteristic time scale in the order of 1-2 hours, whereas observed time series of intermittent turbulence reveal a multitude of time scales. The observed richness of time scales compared to the modeled situation may have *'external'* causes such as: horizontal heterogeneity in topography or surface properties, or simply a non-stationary character of the external forcings. On the other hand this variety of time scales may be a consequence of more complex *internal* dynamics, with more degrees of freedom. In this respect, we mention the results of a preliminary, suggestive study (not shown) were we added an extra diagnostic equation for the boundary layer height (Zilinkevic, 1972; although a prognostic equation would have been more appropriate, cf. Nieuwstadt and Tennekes, 1981) in stead of taking a fixed value (this thesis). As a result of this extra equation a variety of time-scales was introduced (i.e. within a single night, under fixed external forcings) spreading typically between ½ hour-5 hours. Although, this example, using a diagnostic equation for the boundary layer depth for a (prognostic) transient run, is not very realistic, it clearly demonstrates the possible effect of more complex internal

dynamics. Even so, the inherent irregular character of turbulence itself will cause intermittency to show irregular stochastic behavior on different scales, rather than pure deterministic behavior in a strict sense (i.e. as in our model).

2) In the discussions of chapters 3 and 4 the results of two studies that use a simplified model configuration are compared (i.e. the work of McNider et al. 1995 and the present work). Although quite similar model descriptions were used, in some cases different results were obtained: multi-valued solutions, as addressed by McNider et al. (implying predictability problems) were not found in the present study. Similarly, the pure oscillatory behavior (implying intermittent character of turbulence) was not found in McNider et al. (for details: see chapter 3). Some of these differences could still be attributed to differences in process description (e.g. inclusion of a vegetation layer with small heat capacity in the present work, which favors instability), but other differences were attributed to the use of different and rather specific (i.e. non-general) boundary conditions in both models. As such, these studies may reveal a complementary view of different and coexisting characteristics of the dynamics present in real stable boundary layers.

In view of the discussion above, it is tempting to 'relax' the rather strict assumptions and boundary conditions in the simplified models. This may result in a more realistic description of the complex dynamics occurring between the real atmosphere and the land surface. Of course, model complexity makes analytical analysis cumbersome or unfeasible, such that it is difficult to generalize individual model outcome. Therefore, a fruitful strategy could be to use the outcome of realistic case studies using *sophisticated models and observations*, to improve on the *conceptual models*, which in turn could be used for a system dynamics analysis. As such more insight is obtained by switching forth and back between model hierarchies.

From the outcome of the present study it appears that, in order to study SBL dynamics with detailed 1-D column models, the following aspects need attention:
-As longwave radiation is an important process in the SBL, it needs to be described explicitly in the model (for example by a parameterization using an emissivity approach or narrow band approach-see: app. A).
-Investigate the impact of different turbulent closure schemes. (e.g. comparing results of local first order closure with the outcome using higher order closure, e.g. prognostic TKE, or second order).
-Inclusion of Coriolis effects
-For the stable boundary layer a fine resolution is recommended (say O(5m)), especially near the surface. In this respect, it is worthwhile assessing the effect of different resolutions on the model outcome.
-Ensure that the height of the model domain is large enough (say O(1km)) to capture the whole SBL, enabling realistic boundary conditions beyond the region of interest.
-Include a vegetation-layer in the model description.
-Fine numerical resolution in the soil:
From chapter 2 it appears that the heat capacity and the conductivity of the surface are important parameters. As intermittent turbulence acts on rather short time-scales, the 'e-folding' depths of temperature fluctuations are small. This implies that an accurate numerical representation of the soil heat flux processes near the surface require a fine resolution (O(mm), possibly increasing logarithmically with depth). The alternative,

use of thick layers (course resolution), implies large heat capacity of the layers suppressing large temperature fluctuation. In this context, the results of App. A in chapter 4 show a considerable change in shape and magnitude of the soil heat flux graph (strong divergence) in the first 3 cm below the surface.

Apart from these types of column models, future theoretical progress is expected from so-called Large-Eddy Simulation (LES) of stable boundary layers. LES models aim to resolve the dominant large scale structures, while parameterizing the so-called subgrid processes. Currently, Large-Eddy Simulation of stable boundary layers is often applied to rather idealistic cases where geostrophic wind speed and the surface heat flux (e.g. Cederwall and Street, 2002; Jiménez and Cuxart, 2002) or surface cooling rate (e.g. Kosovic and Curry, 2000) are given fixed values. As such, these are considered as external forcing parameters. The present study, however, shows that both the surface heat flux and the surface cooling rate are dependent, internal variables and thus part of the system itself. They are strongly influenced by feed-back mechanisms between the lower atmosphere and the vegetation/soil surface (chapter 3). As such, naturally, a case with intermittent turbulence close to the surface is not correctly simulated by a constant surface flux boundary condition. Therefore it would be interesting to couple a LES model to a simple surface energy balance using a resistance law for heat transport in a thin vegetation layer, as used in the present study (see also: discussion by Derbyshire, 1999b).

Although Large Eddy Simulation has proven to be successful in convective boundary layer studies (Nieuwstadt, 1992), its current use for SBL simulations is not trivial. In SBL's, especially at high stability and close to the surface, the size of the (anisotropic) energy containing eddies is so small that computational expense may cause LES to have inadequate spatial resolution. Consequently, near the surface, the subgrid-model represents a considerable part of the energy-containing scales of vertical velocity fluctuations, which may have strong influence on the LES predictions (Sullivan et al., 2002). As such the LES of the near-surface SBL depends critically on the subgrid-model (Sullivan et al. 2002; Kosovic and Curry, 2000; Cederwall and Street, 2002). Also, in current LES models, the effects of longwave radiative processes on SBL development are neglected, despite of its relevance in real SBL's (especially in the very stable case; e.g. André and Mahrt, 1982; Estournel and Guadalia, 1985). On the other hand it is recognized that, on the longer term, large eddy simulations of stable boundary layers have a high potential as to describe realistic case-studies in an accurate way.

Observations

One of the key-questions to be answered in future work is: how are these intermittent bursts generated? Are the bursts generated close to the surface by means of a direct surface-atmosphere interaction, as studied in the present work? Are they generated in shear layers higher up, and transported downwards (as e.g. in Vukelic and Cuxart (2000) and in Ha and Mahrt (2001)). Or, do both mechanisms coexist?

It is clear that these type of process/event-oriented questions, looking for the cause of the instabilities, put a large demand on the spatial and temporal resolution of the data, especially when computation of vertical structure of turbulence budgets is desired. As noted before (chapter 3), the recent data-set obtained during the CASES99 provides an excellent data-set for these type of studies, as it was designed for the purpose of studying stable boundary layer events (Poulos et al., 2002). During this large

cooperative experiment, a vast array of instruments was deployed during one month (Poulos et al., 2002). In the analysis, the data-classification in chapter 4 can be used a starting point to select a particular night (and eventually a particular event) that can be investigated in detail.

Apart from these process oriented studies focussed on individual events, there is also a large need for a statistical climatology of intermittent events. As a logical continuation of the present work (chapter 4), it would be interesting to apply the Π-concept to different types of climates (e.g. arctic, ocean, desert) with different surface characteristics, and classify the different regimes as a function of the external forcings. Furthermore, little is known at present about the temporal structure of these intermittent events. What are the typical time-scales and amplitudes of the turbulence bursts? What does the statistical distribution look like (e.g. Poison)? In other words: there is a need for an objective statistical characterization of the time-series describing intermittent events, preferably in relation to the external forcings.
In this perspective, so-called wavelet analysis could be a promising tool in characterizing time-series of intermittent turbulence. Because wavelet analysis characterizes turbulent events both in time and in frequency space, it is suitable for describing non-stationary time series typically for intermittent flow (Handorf and Foken, 1997;Van Dijk, Pers. Comm. 2001;Oosterhuis et al., 2000).

In addition, we note that conventional methods measuring turbulent quantities have problems in providing a statistically representative fluxes in intermittent flows, because sampling/averaging periods are usually short. Therefore, as outlined by Hartogensis et al. (2002), an alternative approach is obtained by using so-called scintillometry for measuring turbulence characteristics. A scintillometer measures a path integral of refractive index fluctuations. As a result temporal averages are effectively interchanged for spatial averages (at least in a homogeneous situation) so that shorter averaging times are required to arrive at a representative flux.

In the present study we have not considered heterogeneous situations. Recently, Acevedo and Fitzjarrald (2002) analyzed observations from intermittent turbulence over an area of 30 km x 30 km. It was shown that both surface heterogeneity and differences in topography affects the way in which turbulence bursts occur: generally, higher open areas are preferred locations for events to occur (except in weakly stable conditions). Also, similarly to its temporal counterpart discussed in chapter 2, it was shown that the use of area averaged flux-profile relationships in weather/climate models underestimate the ‘real’ area-average fluxes (see also: Mahrt, 1987).

Practical issues/parameterizations
For many meteorological applications (e.g. in relation to air quality) an estimation of surface fluxes under stable conditions is needed. However, often no direct flux measurements are available since they put a relative high demand on their operation and maintenance. Instead, routine weather data, such as wind speed and temperature on a single level and cloud cover, are often available from which fluxes have to be derived. A practical method to derive fluxes from routine weather data was developed by Holtslag and Van Ulden (1982) and extended in Van Ulden and Holtslag (1985) and Holtslag and De Bruin (1988).

In the work of Holtslag and Van Ulden (1982: HvU), point of departure are the results of Venkatram (1980), who found that, under clear sky conditions, the surface layer temperature scale, θ_*, attains an (almost) constant value of about 0.1 [K]. HvU realized that in this case fluxes may easily be obtained, from a single wind speed measurement, using $H = -\rho c_p u_* \theta_*$, $L = f(u_*, \theta_*)$ and:

$$u_* = \kappa \cdot U \cdot \left[ln\left(\frac{z}{z_0}\right) + \beta \frac{z}{L} \right]^{-1}$$

with κ the Von Kármán constant ($\kappa \approx 0.4$), and β the constant of the log-linear law ($\beta \approx 5$).

Furthermore they found that the value of this 'constant' θ_*-level decreases for increasing cloud cover and that it also depends on u_* when the latter attained rather small or large values. Therefore, some semi-empirical rules, based on observations from Cabauw, were defined, so that the flux-estimation framework could be extended to the more general case.

Below it is shown that the functional dependence of θ_* on u_* and cloud cover can be made explicit. The result was obtained from a mathematical derivation using our system equations, as defined in chapter 2. More precisely: we combined the definitions of the turbulent heat flux and the surface stress, with the linearized surface energy budget (chapter 2). Here only the result is given:

$$\theta_* = C \cdot A^{-1} \cdot u_*^3 \cdot \left[\left[\left(1 + \frac{B}{u_*}\right)^2 - A\left(\frac{Q_i + G}{u_*^4}\right) \right]^{1/2} - \left(1 - \frac{B}{u_*}\right) \right]$$

with A, B, and C representing groups of physical constants such as, z_{0m}, z_{0h}, R_c and ρc_p (it is beyond the scope of this chapter to discuss the exact details). From this result it occurs that the relation between u_* and θ_* not only depends on cloud cover (via Q_i, see definition in chapter 2), but also explicitly depends on the soil heat flux.

In figure 6.1 below, θ_* is plot against u_*, using CASES99 data (5 min. averaged fluxes, Oct. 5-28th, 1999). In this example data were selected according to $-80 < Q_i < -70$ [W m^{-2}], indicating clear sky cases only.

θ_* seems to be fairly constant, except for small and large values of u_*, in agreement with the Cabauw observations by Holtslag and Van Ulden (1982). For comparison theoretical curves according to the equation above are given. As mentioned in chapter 4, accurate measurements of the soil heat flux were not always available, so that an estimation for the whole data set was made. Assuming typical values for the soil heat flux (i.e. between 25-45 [W m^{-2}]), a few curves are given representing clear sky conditions (e.g. $Q_i = -80$ [W m^{-2}]).

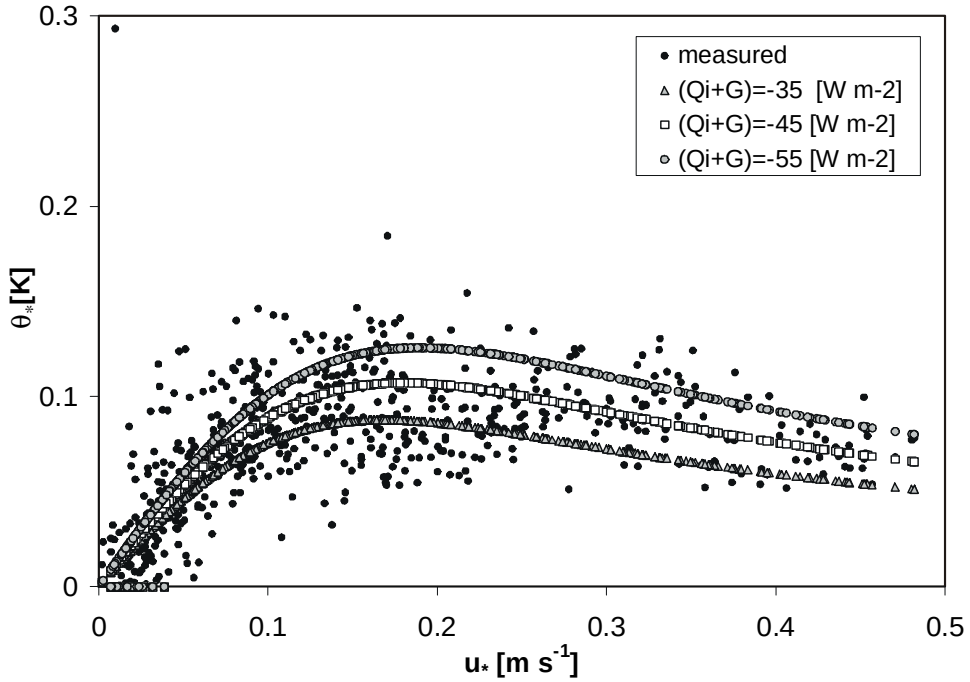

Figure 6. 1: θ_* plotted against u_* (five minute averages) for clear sky conditions , as observed during CASES99. For comparison, three theoretical curves are given for different values of $Q_i + G$.

Although the agreement between the theoretical predictions and the observed values is very good, it is noted that the actual curves are sensitive to the choice of the parameters used (e.g. $z_{0m} = 0.03$ [m], $z_{0h} = z_{0m}/10$, ε_a=0.8, etc,…). On the other hand the typical shape of the θ_*-u_* curve is explained in a physical consistent way by the internal relationships present in the governing equations. In this way, the present framework can be useful in this type of parameterization studies.

Instead of predicting surface fluxes in terms of available information on an internal variable (i.e. observed wind speed) and the external radiative forcing (i.e. observed cloud cover) as in the case above, we may go a step further by trying to predict the surface fluxes in terms of external parameters *only*. This means that, in addition to the radiative forcing, information about the mechanical forcing is needed, that is information about the pressure gradient. In that case, it was shown in chapter 3 (App. B) that an equilibrium solution of our system is available expressing the internal bulk variables U, T_a and T_S in terms of local parameters, like z_{0m}, and the forcing parameters Q_i and $-1/\rho \cdot \partial P/\partial s\big|_{effective}$. The problem with this equilibrium solution is that its practical use is still limited, mainly due to the following reasons: 1) an effective value of the pressure gradient (in the direction of the mean wind) is needed as input parameter, and 2) the boundary layer height is assumed to be a known external parameter. Unfortunately, both parameters are often not easy to estimate in practice. These problems can however be circumvented by the following model extensions:

1) inclusion of Coriolis effects in the model equations
2) adopting an equation (prognostic or diagnostic) for the boundary layer depth in terms of known quantities.

A simple diagnostic equation for the boundary layer depth could be for example the (equilibrium) relation proposed by Zilitinkevic (1972), expressing h in term of u_*, f, and L, or equivalently (using similar parameterization as in chapter 2), in terms of U, V, f, and $T_a - T_S$. In this way, a new set of 5 system equations is constructed describing:
$\partial U/\partial t = ...$, $\partial V/\partial t = ...$, $\partial T_a/\partial t = ...$, $\partial T_S/\partial t = ...$, and $h = ...$ (or rather $\partial h/\partial t = ...$ as in Nieuwstadt and Tennekes, 1981) , as a function of five unknown variables: U, V, T_a, T_S, and h. As such this forms a closed set of equations, describing the evolution of the bulk quantities of the SBL, in terms of external forcing parameters. It can be solved for the equilibrium situation by assuming the time derivatives to be zero.

Of course, many theoretical objections can be made to this rather straightforward approach. Apart from the assumptions made in the parameterizations, especially the assumption requiring a (strictly) stationary SBL is probably not realistic (Nieuwstadt and Tennekes, 1981). Nevertheless, it is worthwhile investigating the practical potential of such approach since it has low computational demands (or even analytical solutions) and its results may be of acceptable accuracy for some applications.

Thesis Closure

At the end of this thesis we reflect to the introduction by stating that many practical problems in stable boundary layer research are a direct consequence of our lack of knowledge about stable boundary layer physics. Therefore, especially in this field, future theoretical progress may directly benefit practical formulations.

Appendix A: Background to the basic equations

Since in chapters 2,3 and 4 the conservation equations are introduced only in their truncated form, we present here a more complete set of conservation equations, often used as a point of departure in atmospheric boundary layer studies (Stull, 1990; Nieuwstadt, 1992; Holtslag 2001).

We start with the basic equation describing the conservation of momentum for an incompressible, Newtonian fluid (N.S. on rotating reference frame):

$$\frac{\partial U_i}{\partial t} + U_j \frac{\partial U_i}{\partial x_j} = -\delta_{i3} g + f_c \varepsilon_{ij3} U_j - \frac{1}{\rho}\frac{\partial P}{\partial x_i} + \nu \frac{\partial^2 U_i}{\partial x_j{}^2}$$

where common notational convention is used. On the l.h.s. the storage and advection of momentum and on the r.h.s. the acceleration/deceleration terms due to the forces acting on the fluid: gravity-, Coriolis-, pressure gradient- and frictional (by viscosity) forces.

The second equation of interest is the conservation equation for heat:

$$\frac{\partial \theta}{\partial t} + U_j \frac{\partial \theta}{\partial x_j} = v_\theta \frac{\partial^2 \theta}{\partial x_j{}^2} - \frac{1}{\rho c_p}\frac{\partial R_j}{\partial x_j} - \frac{L_v E}{\rho c_p}$$

with R_j the net longwave radiative flux in the j-direction, v_θ the thermal diffusivity of dry air, and common notation otherwise. The two terms on the l.h.s. represent the storage and the avection of heat respectively. The first term on the r.h.s describes the transport of heat by molecular diffusion, followed by the net longwave radiation divergence term and evaporation/condensation term being a source/sink of heat.

Next, going back to the momentum equation, common practice is to subdivide the instantaneous velocity U into: a mean velocity $\overline{U}$ averaged over a time period (indicated by the overbar; ergodicity assumed), and a turbulent fluctuation u':

$$U = \overline{U} + u'$$

This is the so-called Reynold decomposition of the instaneous velocity U. This decomposition is applied to the instanteous velocity and pressure and substituted in the equation above. Next the result is averaged over time, applying the well-known Reynolds postulates (e.g. $\overline{u'} = 0$), which gives:

$$\frac{\partial \overline{U_i}}{\partial t} + \overline{U_j}\frac{\partial \overline{U_i}}{\partial x_j} = -\delta_{i3} g + f_c \varepsilon_{ij3} \overline{U_j} - \frac{1}{\overline{\rho}}\frac{\partial \overline{P}}{\partial x_i} + \nu \frac{\partial^2 \overline{U_i}}{\partial x_j{}^2} - \frac{\partial(\overline{u_i' u_j'})}{\partial x_j}$$

This equation describes the time evolution of the *mean* velocity.

It immediately occurs that this equation for the mean wind looks very similar to the equation above, except for the extra term on the r.h.s. (last term). This term can physically be interpreted as the (turbulent) transport in the j-direction, of momentum in the i-direction (per mass). It is often called the Reynolds' stress term, since it has the same effect as a stress on a surface of a fluid element. The term shows that turbulence must be considered in forecasting mean quantities of the turbulent boundary layer.

Same decomposition procedure can be followed for the conservation equation of heat, which gives:

$$\frac{\partial \overline{\theta}}{\partial t} + \overline{U_j}\frac{\partial \overline{\theta}}{\partial x_j} = \nu_\theta \frac{\partial^2 \overline{\theta}}{\partial x_j{}^2} - \frac{1}{\rho c_p}\frac{\partial \overline{R}}{\partial x_j} - \frac{L_v E}{\rho c_p} - \frac{\partial(\overline{u_j'\theta'})}{\partial x_j}$$

As with the equation for the mean momentum an extra term appears. This term is the divergence of turbulent heat, representing the contribution of turbulence to the mean heat budget.

Turbulence closure

In the previous section it was mentioned that the Reynolds' terms describe the influence of turbulent motions on the mean quantities. It must be realised that these terms originate from the non-linear advection term in the original heat and momentum budget equations. It is just this non-linear character of the original equations that makes these equations so interesting and reflects the fascinating non-dynamics of turbulence itself. On the other hand this non-linear behaviour of the equations leads to the so-called 'closure problem' which is discussed next.

The problem is that these Reynolds' terms are new unknowns in the budget equations of the mean quantities $\overline{U_i}$ and $\overline{\theta}$. As a result the number of unknown variables is larger than the number of equations. Thus, extra equations are needed to solve (close) the system. A logical step is to construct prognostic equations for the turbulent fluxes $(\overline{u_i'u_j'})$ and $(\overline{u_j'\theta'})$ in the Reynolds' terms. Such equations can be constructed from the prognostic equations for the turbulent deviations u' and θ', which, in turn can be derived by substraction of the prognostic equations for the mean variables from the orgininal prognostic equations for the instanteneous variables. However, it can be shown that these prognostic equations for the turbulent fluxes contain new unknowns of the order $(\overline{u_i'u_j'u_k'})$. Thus the set of equations cannot be closed in this way. This is the well-know 'closure problem', one of the central problems in turbulence theory. It can be shown that any finite set of these type of equations is not closed (Nieuwstadt, 1992).

In order to make the physical/mathematical description of turbulence tractable, one common approach is to use only a finite number of equations and then approximate/parameterize the remaining unknowns in terms of known quantities. The closure approximations are named by the highest order of prognostic equations that are retained (Stull, 1990). The closure assumption adopted in the present study is related to the well-known first-order local clossure. First order closure parameterizes turbulent fluxes directly in terms of the local gradients of the mean quantities, such as:

$$\overline{u_j'\xi'} = -K\frac{\partial \overline{\xi}}{\partial x_j}$$

were the variable ξ could be either U or θ. K is the so-called 'eddy diffusivity' (in this thesis often denoted as the turbulent exchange coefficient). It is a property of the flow rather than a material constant (as with its laminar counterpart). It is noted that although this type of local closure is simple and useful in practice, it is certainly not universal because turbulence is often non-local in its character (see: Nieuwstadt, 1992). In stable boundary layer models the local eddy diffusivity is often expressed in terms of the local (gradient) Richardson number, i.e. $K(Ri)$, with:

$$Ri = \frac{\frac{g}{\theta_0}\frac{\partial \overline{\theta}}{\partial z}}{\left(\frac{\partial \overline{U}}{\partial z}\right)^2 + \left(\frac{\partial \overline{V}}{\partial z}\right)^2}$$

This gradient Richardson number Ri can be related to the so-called flux Richardson number R_f. The latter is a key-parameter for turbulence in stratified flow and it represents the competition between the generation of turbulent kinetic energy by shear and the destruction by buoyancy forces. Thus, the basic principle behind $K(Ri)$ is that mixing efficiency is limited by increased stratification strength (see chapter 1). This Ri dependence of the 'eddy diffusivities' in the momentum and heat budget equations cause these equations to form a coupled system. This is an important aspect and may lead to interesting dynamic behaviour of the SBL as discussed qualitatively in chapter 1 and more quantitatively in the remaining chapters.

As before; although the type of local $K(Ri)$ closure can be shown to be valid in specific type of flows (in case of local equilibrium of TKE), it has no general validity. This is certainly true for the so-called bulk-approach adopted in this thesis. In this approach turbulent fluxes at the boundaries are parameterized in terms of the bulk properties of the SBL. Its formulations resemble the profile-integrated forms of the local closure discussed above, using $K(Ri)$. However, in stead of a gradient Richardson number the stability dependence $K(R_b)$ is parameterized with the help of a discretized bulk Richardson number (see: chapter 2). This type of simple closure formulations are adopted in the present study, because they allow analytical treatment (this has clear advantages, as indicated below and in chapter 3) and because they are able to describe the main feed-back mechanism between stratification and mixing (chapter 1).

Further assumptions

Starting from the complete momentum- and heat budget equations, additional assumptions are made in order to reduce the complexity of the system under study. The advantage of such reduced complexity, is that non-linear interactions between the coupled momentum and heat budget equations can be studied more easily in an analytical way. As showns in chapter 3 this may lead to explicit equilibrium solutions in terms of forcing parameters, which can be usefull for practical applications such as in parameterisation studies, and for theoretical work. Such analytical analysis may also provide information about stability aspects of the system which can be usefull in prediction of SBL regimes (chapter 3)

Simplification of the analysis by neglection of certain processes like: advection, slope effects and moisture effects, does not mean these processes are not important in real SBL's. On the contrary: a credible fog prediction in a valley area for example, cannot be made without considering the processes mentioned above. Thus, it must be kept in mind that the present analysis can only be an idealized study of real atmospheric complexity.

Starting with the momentum equation some main assumptions are listed shortly:

-assumption of horizontal homogeneity: horizontal advection is not considered.

-neglection of vertical advection (subsidence).
-neglection of Coriolis effects. Only horizontal motions in the mean wind direction are modelled (see: chapter 2). This also means that only the pressure gradient component in the mean wind direction is considered.
-the direct effect of viscous forces on the mean wind is neglected (i.e. Reynolds numbers are high).
In the heat conservation equation the following assumptions are made additionally:
-the atmosphere is assumed to be dry. Thus no phase changes of water such as evaporation/condensation occur (also no effect of moisture on the long wave radiative budgets).
-the influence of heat transport due to molecular diffusion is neglected.

Application of these assumptions to the (mean) conservation equations for heat and momentum leaves the following equations:

$$\frac{\partial \overline{U}}{\partial t} = -\frac{1}{\overline{\rho}}\frac{\partial \overline{P}}{\partial x} - \frac{\partial(\overline{u'w'})}{\partial z}$$

$$\frac{\partial \overline{\theta}}{\partial t} = -\frac{1}{\rho c_p}\frac{\partial \overline{R}}{\partial z} - \frac{\partial(\overline{w'\theta'})}{\partial z}$$

These equations are used as a starting point for chapter 2, together with the surface energy balance for a small vegetation layer:

$$C_{veg}\frac{\partial T_{veg}}{\partial t} = Q_{net} + G_0 - \rho c_p(\overline{w'\theta'})_0$$

with , the temperature T_{veg} [K] and the heat capacity C_{veg} [W m^{-2} K^{-1}] of the vegetation layer, Q_{net} the net radiation [W m^{-2}] , G_0 the soil heat flux [W m^{-2}] and surface heat flux represented by $\rho c_p(\overline{w'\theta'})_0$. For a detailed description of the parameterization of the different terms we refer to chapter 2.

So far we have mainly discussed the impact of turbulence closure/parameterization in the governing equations. From the heat budget equations for the vegetation surface and the atmosphere it becomes clear that another key-process besides turbulent transport is the heat transport due to longwave radiation. Longwave radiation is important, since it is the engine behind the surface cooling, which causes a near surface inversion to develop. Also, from several SBL studies it became clear that radiative cooling can give a comparable contribution to the heat budget as turbulent heat flux divergence (e.g. André and Mahrt, 1982; Garratt and Brost, 1982; Estournel and Guedalia, 1985). As with turbulence it is posible to describe/parameterize longwave radiative processes with several degrees of complexity: from complex spectral line models describing emission as a function of wavelength, to band methods describing emission/absorbtion over a smaller number of wave length bands (e.g. as in Tjemkes and Duynkerke, 1989), to the rather simple emissivity or grey-body approach that assumes that each atmospheric layer can be represented by a single emissivity/transmissivity (Rodgers, 1967). For simplicity a grey-body approach was followed in the present study. As with the turbulence parameterization the parameterization of longwave radiation is such that the fluxes are related to the mean quantities (temperatures) in order to close the system. A detailed description of the model parameterization using this method is given in chapter 2.

Appendix B:Outline Hopf-bifurcation technique

Because the Hopf bifurcation technique is not commonly used in atmospheric sciences, and because of the fact that it forms the core of the work presented in this article, it will be explained rather basically. The condensed explanation is based on the introductionary book of Seydel (1988).

As an example a system with two coupled non-linear ordinary differential equations is considered:

$$\frac{dy_1}{dt} = f_1(y_1, y_2)$$
$$\frac{dy_2}{dt} = f_2(y_1, y_2) \qquad (1)$$

Equilibrium points of this system are reached when the time derivatives are zero. The system presented above is solved for this condition, which gives the values of the equilibrium points y_1^{eq} and y_2^{eq} . One could get (local) information about the behaviour of the system near the equilibrium by disturbing the equilibrium values. Now it are the differential equations which decide whether the trajectories, or $y_1(t)$ and $y_2(t)$, starting in the vicinity of y_1^{eq} and y_2^{eq} remain near the equilibrium (attraction) or depart from it. To start a local analysis of the behaviour of the equations a Taylor series expansion of f_1 around (y_1^{eq}, y_2^{eq}) gives:

$$\frac{dy_1}{dt} = f_1(y_1, y_2) = f_1(y_1^{eq}, y_2^{eq}) + \frac{\partial f_1(y_1^{eq}, y_2^{eq})}{\partial y_1} \cdot (y_1 - y_1^{eq}) + \frac{\partial f_2(y_1^{eq}, y_2^{eq})}{\partial y_2} \cdot (y_2 - y_2^{eq}) + h.o.t. \qquad (2)$$

Expanding also the f_2 of the second differential equation, observing that $f_1(y_1^{eq}, y_2^{eq}) = f_2(y_1^{eq}, y_2^{eq}) = 0$ and dropping the higher order terms, gives two differential equations that are *linear* in $(y_1 - y_1^{eq})$ and $(y_2 - y_2^{eq})$. Because the equations are linear, they can easily be solved with the help of standard theory as we will show. The linearized system is easily written down in matrix notation if one uses the derivative or *Jacobian* matrix:

$$\mathbf{J} = \begin{bmatrix} \frac{\partial f_1(y_1^{eq}, y_2^{eq})}{\partial y_1} & \frac{\partial f_1(y_1^{eq}, y_2^{eq})}{\partial y_2} \\ \frac{\partial f_2(y_1^{eq}, y_2^{eq})}{\partial y_1} & \frac{\partial f_2(y_1^{eq}, y_2^{eq})}{\partial y_2} \end{bmatrix} \qquad (3)$$

If the vector $\mathbf{h}$ is represented by:

$$h_1(t) \approx y_1(t) - y_1^{eq}(t)$$
$$h_2(t) \approx y_2(t) - y_2^{eq}(t) \qquad (4)$$

Then the above mentioned *linearized* system can be written as:

$$\frac{d\mathbf{h}}{dt} = \mathbf{J} \cdot \mathbf{h} \qquad (5)$$

So this equation describes how the system evolves when the initial state deviates slightly from it's equilibrium values. Like in standard theory about systems of linear ordinary differential equations one tries to solve the system by stating the following hypothesis about the form of it's solution:

$$\mathbf{h}(t) = \begin{bmatrix} h_1(t) \\ h_2(t) \end{bmatrix} = \begin{bmatrix} C_{11} \\ C_{12} \end{bmatrix} \cdot e^{\mu_1 t} + \begin{bmatrix} C_{21} \\ C_{22} \end{bmatrix} \cdot e^{\mu_2 t} \tag{6}$$

By inserting this solution in (5) it can be shown that this problem is equivalent to a eigenvalue problem. The two eigenvalues μ_1 and μ_2 that meet the above stated hypothesis are the solutions of the characteristic equation:

$$\det(\mathbf{J} - \mu \cdot \mathbf{I}) = 0 \tag{7}$$

Now several situations can occur:

- μ_1 and μ_2 are positive. Then the argument of the exponents in equation (6) are positive, any disturbance grows with time, which will give rise to an *unstable* equilibrium.
- μ_1 and μ_2 are both negative. In a similar way this leads a *stable* equilibrium.
-either μ_1 or μ_2 is negative and the other positive. The equilibrium point will be a so-called *saddle point*.
- μ_1 and μ_2 are both complex. Then any trajectory close to the equilibrium resembles a *spiral*.

Parameter dependence

Usually a differential equation describing a real meteorological problem involves one or more parameters. Denoting one such parameter by λ, the differential equations read:

$$\begin{aligned} \frac{dy_1}{dt} &= f_1(y_1, y_2, \lambda) \\ \frac{dy_2}{dt} &= f_2(y_1, y_2, \lambda) \end{aligned} \tag{8}$$

Because this system depends on the actual value of λ we speak of a *family* of differential equations. So solutions $\mathbf{y}(t;\lambda)$ of the system now depend both on t and λ.

Consequently, equilibrium points, Jacobian matrices, and the eigenvalues μ depend on λ:

$$\mu(\lambda) = \alpha(\lambda) + i\beta(\lambda) \tag{9}$$

It is very important to notice that, upon the varying parameter λ, the position and the stability of a stationary point can vary! For example when λ passes some critical value λ_{crit} the real part of $\alpha(\lambda)$ may change sign and the stable equilibrium point may turn into an unstable point. This qualitative change of the equilibrium solution when passing λ_{crit} is called branching or *bifurcation*. The type of bifurcation that connects a *stable* equilibrium with a *periodic* motion is called a *Hopf-bifurcation.*

In figure B1, taken from Seydel (1988), an example of a Hopf-bifurcation is given. One sees the stable solution "splits" up in a cyclic solution when λ passes a certain value.

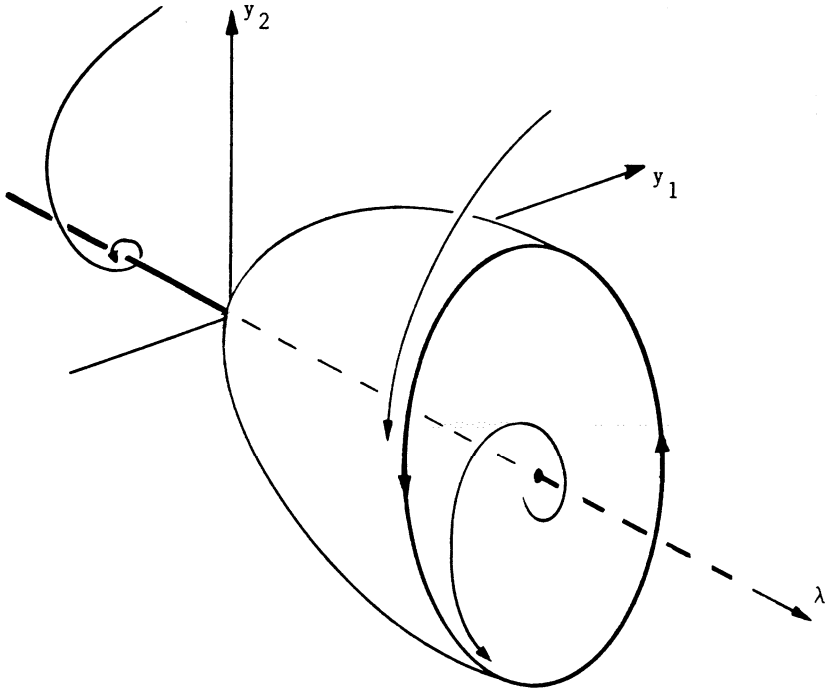

Figure B1: trajectories showing $y_1(t)$ and $y_2(t)$ (towards the equilibrium point/circle) as a function of a certain physical parameter λ. At the critical value of λ, the equilibrium solution changes from an equilibrium point to an equilibrium circle. This is the Hopf bifurcation point (Fig., after Seydel, 1988).

The Jacobian evaluated at the Hopf bifurcation point has a pair of purely imaginary eigenvalues $\pm i\beta$ which denotes the beginning of a cycle. It can be shown that the existence of a Hopf bifurcation leads to two consequences:

1) The initial period (of zero amplitude at $(y_1^{eq}, y_2^{eq}, \lambda_{crit})$) is: $\frac{2\pi}{\beta}$.

2) The limit cycle has an amplitude proportional to: $\sqrt{\lambda - \lambda_{crit}}$.

We mention that the validity of these statements close to the bifurcation points was verified for our system (not shown).

Bibliography

Acevedo, O. C., and D. R. Fitzjarrald, 2000: Relating temporal and spatial structure of the nocturnal surface layer to landscape heterogeneity. *Proc. 14th. Symp. on Bound. Layer and Turb.* Aspen, Amer. Meteor. Soc., 596-599.

Acevedo, O., and R. Fitzjarrald, 2002: In the core of the night – effects of intermittent mixing on a horizontally heterogeneous surface. *Bound. Layer Meteor.*, **105**, 1-33.

André, J. C., and L. Mahrt, 1982: The nocturnal surface inversion and influence of clear-air radiative cooling. *J. Atmos. Sci.*, **39**, 864-878.

Atzema, A. J., 1992: A model for the drying of grass with realtime weather data., *J. Agric. Eng. Res.*, **53**, 231-247.

Beljaars, A. C. M., and A. A. M. Holtslag, 1991: Flux parametrization and land surfaces in atmospheric models. *J. Applied Meteor.* **30**, 327-341.

Beljaars, A. C. M., and P. Viterbo, 1998: Role of the boundary layer in a numerical weather prediction model. *Clear and Cloudy Boundary Layers*, Holtslag A. A. M., P. G. Duynkerke, and P. J. Jonker Eds., Royal Netherlands Ac. Of Arts and Sci., Amsterdam, 287-304.

Best, M. J., 1998: A model to predict surface temperatures. *Bound. Layer Meteor.*, **88**, 279-306.

Blackadar, A. K., 1957: Boundary-layer wind maxima and their significance for the growth of nocturnal inversions. *Bull. Amer. Meteor. Soc.*, **38**, 283-290.

Blackadar, A. K., and H. Tennekes, 1968: Asymptotic similarity in neutral barotropic planetary boundary layers. *J. Atmos. Sci.*, **25**, 1015-1020.

Blackadar, A. K., 1979: High-resolution models of planetary boundary layer., *Advances in Environmental Science and Engineering*, J.R. Pfafflin and E.N. Ziegler, Eds., Gordon and Breech Sci. Pub., Inc., 50-85.

Businger, J. A., J. C. Wyngaard, Y. Izumi, and E. F. Bradley, 1971: Flux-profile relationships in the atmospheric boundary layer. *J. Atmos. Sci.*, **30**, 788-794.

Businger, J. A., 1973: Turbulent transfer in the atmospheric surface layer. *Workshop on the Planetary Boundary Layer*, D.A. Haugen Ed., Amer. Meteor. Soc., 67-98.

Caughey, S. J., J. C. Wyngaard, and J. C. Kaimal, 1979: Turbulence in the evolving stable boundary layer., *J. Atmos. Sci.*, **36**, 1041-1052.

Cederwall, R. T., and R. L. Street, 2002: Investigation of episodic enhancement of turbulence in the stable boundary layer using Large-Eddy Simulation. *Proc. 15th. Symp. on Bound. Layer and Turb.*, Wageningen, Amer. Meteor. Soc., 469-472.

Coulter, R. L., 1990: A case study of turbulence in the stable nocturnal boundary layer. *Bound. Layer Meteor.*, **52**, 75-91.

Coulter, R. L., and J. C. Doran, 2000: Intermittent turbulence events observed with a sonic anemometer and minisodar during CASES99. *Proc. 14th. Symp. on Bound. Layer and Turb.* Aspen, Amer. Meteor. Soc., 622-625.

Csanady, G. T., 1967: On the "Resistance Law" of a turbulent Ekman layer. *J. Atmos. Sci.*, **24**, 467-471.

De Bruin, H. A. R., 1994: Analytic solutions of the equations governing the temperature fluctuation method. *Bound. Layer Meteor.*, **68**, 427-432.

De Bruin, H. A. R., R. J. Ronda, and B. J. H. van de Wiel, 2000: Approximate solutions for the Obukhov length and the surface fluxes in terms of bulk Richardson numbers. *Bound. Layer Meteor.*, **95**, 145-157.

Deardorff, J. W., 1978: Efficient prediction of ground surface temperature and moisture, with inclusion of a layer of vegetation. *J. Geophys. Res.*, **83**, 1889-1903.

Delage, Y., 1997: Parameterising sub-grid scale vertical transport in atmospheric models under statically stable conditions. *Bound. Layer Meteor.*, **82**, 23-48.

Derbyshire, S. H., 1999: Boundary-layer decoupling over cold surfaces as a physical boundary instability. *Bound. Layer Meteor.*, **90**, 297-325.

Derbyshire, S. H., 1999b: Stable boundary layer modelling: established approaches and beyond. *Bound. Layer Meteor.*, **90**, 423-446.

Duynkerke, P. G., 1991: Observation of a quasi-periodic oscillation due to gravity waves in shallow radiation fog. *Quart. J.R. Met. Soc.*, **117**, 1207-1224.

Duynkerke, P. G., 1999: Turbulence, radiation and fog in Dutch stable boundary layers. *Bound. Layer Meteor.*, **90**, 447-477.

Duynkerke, P. G., S. R., de Roode, 2001: Surface energy balance and turbulence characteristics observed at the SHEBA Ice Camp during FIRE III. *J. Geophys. Res.*, **106**, 15313-15322.

Estournel, C., and D. Guedalia, 1985: Influence of geostrophic wind on atmospheric nocturnal cooling. *J. Atmos. Sci.* **42**, 2695-2698.

Garratt, J. R., and R. A. Brost, 1982: Radiative cooling effects within and above the nocturnal boundary layer. *J. Atmos. Sci.* **38**, 2730-2746.

Ha, K.-J., and Mahrt, L., 2001: Simple Inclusion of Z-less turbulence within and above the Modelled Nocturnal Boundary Layer. *Mon. Wea. Rev.*, **129**, 2136-2143.

Handorf, D., and Th. Foken, 1997: Structuranalyse der atmosphärische Turbulenz mittels Wavelett-Verfahren zur Bestimmung von Austauschprozessen über den antarktischen Schelfeis. Arbeitsergebnisse (Sci. Rep.), **47**, Deutscher Wetterdienst, 49pp.

Hartogensis, O. K., H. A. R. De Bruin, and B. J. H. van de Wiel, 2002: Displaced-Beam Small Aperture Scintillometer test. Part II: CASES-99 stable boundary layer experiment. *Bound. Layer Meteor.*, **105**, 149-176.

Heusinkveld, B. G., A. F. G. Jacobs, A. A. M., Holtslag, and S. M. Berkowicz, 2002: The surface energy balance over a desert, and the relevance of soil heat flux measurements. *Proc. 15th. Symp. on Bound. Layer and Turb.*, Wageningen, Amer. Meteor. Soc., 143-146.

Högström, U., 1988: Nondimensional wind and temperature profiles in the atmospheric surface layer: A reevaluation. *Bound. Layer Meteor.*, **42**, 55-78.

Högström, U., 1996: Review of some basic characteristics of the atmospheric surface layer. *Bound. Layer Meteor.*, **78**, 215-246.

Holtslag, A. A. M., and A. P. van Ulden, 1982: Simple estimates of nighttime surface fluxes from routine weather data. Scientific Report., **82-4**, Royal Netherlands Meteor. Inst., De Bilt.

Holtslag, A. A. M., and F. T. M. Nieuwstadt, 1986: Scaling the atmospheric boundary layer. *Bound. Layer Meteor.*, **36**, 201-209.

Holtslag, A. A. M., and H. A. R. de Bruin, 1988: Applied modelling of the nighttime surface energy balance over land. *Bound. Layer Meteor.*, **27**, 689-704.

Holtslag, A. A. M., 2001: Atmospheric Turbulence. In: *Encyclopedia of Phys. Sci. and Techn.*, 3rd Ed., Academic Press, **Vol. 1**, 707-719.

Hopf, E., 1942: Abzweigung einer periodischen Lösung von einer stationären Lösung eines Differentialsystems. *Bericht der Math.-Phys. Klasse der Sächsischen Akademie der Wissenschaften zu Leipzig*, **94**.

Howell, J. F., and J. Sun, 1999: Surface-layer fluxes in stable conditions. *Bound. Layer Meteor.*, **90**, 495-520.

Hunt, J. C. R., J. C. Kaimal, and J. E. Gaynor, 1985: Some observations of turbulence structure in stable layers. *Quart. J.R. Met. Soc.*, **111**, 793-815.

Jiménez, M. A., and J. Cuxart, 2002: Large-Eddy Simulations of stable boundary layer: exploration of ranges of applicability. *Proc. 15th. Symp. on Bound. Layer and Turb.*, Wageningen, Amer. Meteor. Soc., 333-334.

Kondo, J., O. Kanechika, and N. Yasuda, 1978: Heat and momentum transfers under strong stability in the atmospheric surface layer. *J. Atmos. Sci.* **35**, 1012-1021.

Kosovic, B., and J. A. Curry, 2000: A Large Eddy Simulation study of a quasi-steady, stable stratified atmospheric boundary layer. *J. Atmos. Sci.* **57**, 1052-1068.

Lin, J.T. 1990: The effect of inertial and turbulence oscillations in the stable boundary layer and their role in horizontal dispersion. M.S. thesis, Dept. of Mathematics, University of Alabama in Huntsville, 82 pp.

Louis, J-F., 1979: A parametric model of vertical eddy fluxes in the atmosphere. *Bound. Layer Meteor.*, **17**, 187-202.

Louis, J-F., M. Tiedtke, and J. F. Geleyn, 1982: A short history of the PBL parameterization at the ECMWF. *Proc. Workshop on BL-parameterization*, ECMWF, Reading, 59-79.

Mahrt L., C. Heald, D. H. Lenschow, B. B. Stankov, and L. B. Troen, 1979: An observational study of the structure of the nocturnal boundary layer. *Bound. Layer Meteor.*, **17**, 247-264.

Mahrt, L., 1987: Grid-averaged surface fluxes. *Mon. Wea. Rev.,* **104**, 1403-1407.

Mahrt L., 1989: Intermittency of atmospheric turbulence. *J. Atmos. Sci.,* **46**, 79-95.

Mahrt L., J. Sun, W. Blumen, T. Delany, and S. Oncley, 1998: Nocturnal boundary layer regimes. *Bound. Layer Meteor.*, **88**, 255-278.

Mahrt L., 1999: Stratified atmospheric boundary layers. *Bound. Layer Meteor.*, **90**, 375-396.

Mahrt L., and Vickers, D., 2002: Constrasting vertical structures of nocturnal boundary layers., *Bound. Layer Meteor. (to appear).*

Malhi, Y. S., 1995: The significance of the dual solutions for heat fluxes measured by the temperature fluctuation method in stable conditions. *Bound. Layer Meteor.*, **74**, 389-396.

Marsden, J. E., and M. McCracken, 1976: *The Hopf Bifurcation and its Applications*. Springer, New York.

McNider, R. T., and R. A. Pielke, 1981: Diurnal boundary layer development over sloping terrain. *J. Atmos. Sci.* **38**, 2198-2212.

McNider, R. T., D. E. England, M. J. Friedman, and Shi, X., 1995: Predictability of the stable atmospheric boundary layer. *J. Atmos. Sci.* **52**, 1602-1614.

Miles, J. W., 1961: On the stability of heterogeneous shear flows. *J. Fluid Mech.,* **10**, 496-508.

Monteith J. L., 1981: Evaporation and surface temperature. *Quart. J.R. Met. Soc.*, **107**, 1-27.

Nappo C., 1991: Sporadic breakdown of stability in the PBL over simple and complex terrain. *Bound. Layer Meteor.*, **54**, 69-87.

Nieuwstadt, F. T. M., and H. Tennekes, 1981: A rate equation for the nocturnal boundary-layer height. *J. Atmos. Sci.* **38**, 1418-1428.

Nieuwstadt, F. T. M., 1984: The turbulent structure of the stable, nocturnal boundary layer. *J. Atmos. Sci.* **41**, 2202-2216.

Nieuwstadt, F. T. M., 1992: *Turbulentie: inleiding in the theorie en toepassingen van turbulente stromingen*. Epsilon Uitgaven, Utrecht, 202 pp.

Oke, T. R., 1978: *Boundary Layer Climates*., Methuen & Co Ltd, 372 pp.

Oosterhuis, G., J. Sun, and S. Burns, 2000: Wavelett analysis of thermocouple measurements during CASES-99. *Proc. 14th. Symp. on Bound. Layer and Turb.* Aspen, Amer. Meteor. Soc., 590-592.

Paltridge, G. W., and C. M. R. Platt, 1976: Radiative processes in meteorology and climatology. *Developments in Atm. Sc.* ,No. 5, Elsevier Sc. Pub. Company, 318 pp.

Poulos, G. S., D. C. Fritts, W. Blumen, and W. D. Bach, 2000: CASES-99 field experiment: an overview. *Proc. 14th. Symp. on Bound. Layer and Turb.* Aspen, Amer. Meteor. Soc., 618-621.

Poulos, G. S., W. Blumen, D. Fritts, J. L. Lundquist, J. Sun, S. P. Burns, C. Nappo, R. Banta, R. Newsom, J. Cuxart, E. Terradellas, B. Balsey, and M. Jensen, 2002: CASES-99: A comprehensive investigation of the stable nocturnal boundary layer. Bull, Amer. Meteor. Soc., **83**, 555-581.

Revelle, D. O., 1993: Chaos and "bursting" in the planetary boundary layer. *J. Applied Meteor.*, **32**, 1169-1180.

Rodgers, C. D., 1967: The use of emissivity in atmospheric radiation calculations. *Quart. J. R. Met. Soc.*, **93**, 43-54.

Ronda, R. J., and H. A. R. De Bruin, 1999: A note on the concept of 'effective' bulk exchange coefficients for determination of surface flux densities. *Bound. Layer Meteor.*, **94**, 155-162.

Seydel, R., 1988: *From equilibrium to chaos: practical bifurcation and stability analysis*., Elsevier Sc. Pub. Co., Inc. 367 pp.

Sullivan, P. P., T. W. Horst, D. H. Lenschow, C.-H. Moeng, J. C. Weil, 2002: Analysis of subfilter-scale fluxes in the atmospheric surface layer. *Proc. 15th. Symp. on Bound. Layer and Turb.*, Wageningen, Amer. Meteor. Soc., 440-443.

Smedman, A-S., 1988: Observations of a multi-level turbulence structure in a very stable atmospheric boundary layer. *Bound. Layer Meteor.*, **44**, 247-264.

Stull, R. B., 1983: Integral scales for the nocturnal boundary layer. Part 1: Empirical depth relationships. *J. Clim. Appl. Meteor.*, **22**, 673-686.

Stull, R. B., 1990: *Introduction to Boundary Layer Meteorology*. Kluwer Academic Pub., 670 pp.

Thorpe, A. J., and T. H. Guymer, 1977: The nocturnal jet. *Quart. J.R. Met. Soc.*, **103**, 633-653.

Tjemkes, S. A., and P. G. Duynkerke, 1989: The nocturnal boundary layer: model calculations compared with observations. *J. Applied Meteor.*, **28**, 161-175.

Turner, J. S., 1973: *Bouyancy effects in fluids.*, Cambridge University Press, 368 pp.

Van den Hurk, B. J. J. M., and A. A. M. Holtslag, 1997: On the bulk parameterization of surface fluxes for various conditions and parameter ranges. *Bound. Layer Meteor.*, **82**, 119-134.

Van de Wiel, B. J. H., R. J. Ronda, A. F. Moene, H. A. R. De Bruin, and A. A. M. Holtslag, 2000: Intermittent turbulence and oscillations in the stable boundary layer: a system dynamics approach. *Proc. 14th. Symp. on Bound. Layer and Turb.* Aspen, Amer. Meteor. Soc., 593-595.

Van de Wiel, B. J. H., R. J. Ronda, A. F. Moene, H. A. R. De Bruin, and A. A. M. Holtslag, 2002: Intermittent turbulence and oscillations in the stable boundary layer. Part I: A bulk model. *J. Atmos. Sci*., **59**, 942-958.

Van de Wiel, B. J. H., A. F. Moene, R. J. Ronda, H. A. R. De Bruin, and A. A. M. Holtslag, 2002: Intermittent turbulence and oscillations in the stable boundary layer. Part II: A system dynamics approach. *J. Atmos. Sci.*, **59**, 2567-2581.

Van de Wiel, B. J. H., A. F. Moene, O. K. Hartogensis, H. A. R. De Bruin, and A. A. M. Holtslag, 2002: Intermittent turbulence and oscillations in the stable boundary layer. Part III: A Classification for observations during CASES99. *J. Atmos. Sci., Submitted.*

Van Ulden, A. P., A. A. M. Holtslag, 1985: Estimation of atmospheric boundary layer parameters for diffusion applications, *J. Climate Appl. Meteor.*, **24**, 1196-1207.

Van Wijk, W. R., and D. A. De Vries, 1963: Periodic temperature variations. *Physics of Plant Environment*, Van Wijk, W. R., Ed. , Interscience Publ., Amsterdam, pp. 133-138.

Venkatram, A., 1980: Estimating the Monin-Obukhov length in the stable boundary layer for dispersion calculations. *Bound. Layer Meteor.*, **19**, 481-485.

Viterbo, P., A. C. M, Beljaars, J-F. Mahfouf, and J. Teixeira, 1999: The representation of soil moisture freezing and its impact on the stable boundary layer. *Quart. J. R. Met. Soc.*, **125**, 2401-2426.

Vukelic, B., and J. Cuxart, 2000: One-dimensional simulations of the stable boundary layer as observed in SABLES99. *Proc. 14th. Symp. on Bound. Layer and Turb.* Aspen, Amer. Meteor. Soc., 579-580.

Welch, R. M., M. G. Ravichandran, and S. K. Cox, 1986: Prediction of quasi-periodic oscillations in radiation fogs. Part I: comparison of simple similarity approaches. *J. Atmos. Sci.*, **43**, 633-650.

Yamada, T., 1976: On the similarity functions A, B and C of the planetary boundary layer. *J. Atmos. Sci.*, **33**, 781-793.

Zilitinkevic, S. S., 1972: On the determination of the height of the Ekman boundary layer. *Bound. Layer Meteor.*, **3**, 141-145.

Samenvatting

De titel van dit proefschrift luidt: “Intermittent turbulence and oscillations in the stable boundary layer over land”, oftewel “Over oscillaties en het intermitterend gedrag van turbulentie in de stabiele grenslaag boven land”. Dit is het overkoepelende thema van het proefschrift welke de verschillende hoofdstukken met elkaar verbindt. Onder intermitterend gedrag van turbulentie wordt hier verstaan: een zekere opeenvolging van beurtenissen bestaande uit periodes met intensieve turbulentie gevolgd door periodes met nauwelijks turbulentie, danwel relatief zwakke turbulentie. Dit intermitterend gedrag van de turbulente fluxen (intermittency) beïnvloedt het gedrag van de gemiddelde grootheden in de stabiele grenslaag zoals windsnelheid en temperatuur zodanig, dat deze schommelingen gaan vertonen ten opzichte van hun ‘onverstoorde’ nachtelijke trend. Als gevolg hiervan vertonen de tijdreeksen van dergelijke grootheden een soort oscillatorisch gedrag (zie titel). Intermittency wordt relatief vaak waargenomen, vooral tijdens sterk gestratificeerde omstandigheden van de nachtelijke grenslaag. Verschillende voorbeelden van intermitterende nachten worden dan ook getoond in dit proefschrift (met name hoofdstuk 3 en 4). Hoewel dergelijk intermitterend gedrag dikwijls wordt waargenomen, is er vrij weinig bekend over dit gedrag: hoe wordt het veroorzaakt? Wat zijn de typische statistische karakteristieken van intermitterende turbulentie (m.b.t. de tijdschalen en de amplitudes). En vooral: onder wat voor omstandigheden kunnen we dit soort intermittency verwachten?

In de literatuur zijn een aantal voorbeelden van studies met atmosferische kolom-modellen bekend, waarbij een bepaalde mate van intermitterend gedrag van turbulentie wordt gesimuleerd onder verschillende meteorologische conditions (bv. Welch et al., 1986; Lin, 1990; Revelle, 1993; Vukelic and Cuxart, 2000). In deze studies wordt echter geen algemene verklaring geven voor de achterliggende fysica van een dergelijk gedrag. Bovendien laten Lin (1990) en Revelle (1993) zien dat verschillende stabiele grenslaag regimes worden gesimuleerd bij variatie van de synoptische drukgradient: naast het intermitterende regime worden ook twee totaal andere regimes waargenomen. Vanuit de experimentele hoek is het algemeen bekend dat er verschillende regimes kunnen optreden in de stabiele grenslaag (e.g. Mahrt et al., 1998). Geen van de genoemde studies kan echter verklaren onder wat voor condities de stabiele grenslaag in het ene, dan wel het andere regime terecht zal komen. De motivatie voor het huidige werk kan voor een groot deel worden toegeschreven aan dit type onbeantwoorde vragen.

Naar aanleiding van de bovengenoemde problemen worden (onder andere) de volgende vragen behandeld in dit proefschrift:

I) -Wat zijn de essentiële fysische principes achter dit intermitterende gedrag van turbulentie?
-Is het mogelijk om zowel een intermittent regime als niet-intermittent regimes te simuleren met een eenvoudig model?

II) -Welke externe forceringsparameters zijn bepalend voor de regime-transities?
-Is het mogelijk om de verschillende regimes a priori te voorspellen?

III) -Wat voor typen regimes worden er in het veld waargenomen? Onder welke omstandigheden treden zij op?

Het huidige werk bestaat uit drie kerndelen: het eerste deel is een numerieke studie (hoofdstuk 2), het tweede deel is een analytische studie (hoofdstuk 3) en het derde deel is een experimentele studie (hoofdstuk 4).

De intermittency-studie richt zich op een mechanisme, waarvan het principe eerder kwalitatief beschreven is door Turner (1973) en Businger (1973): tijdens heldere nachten boven land kan zich nabij het aardoppervlak een sterke inversie ontwikkelen als gevolg van de langgolvige uitstraling van dit oppervlak. Deze inversie zorgt ervoor dat de turbulentie-intensiteit sterk wordt onderdrukt. Hierdoor raakt de atmosfeer ontkoppeld van het aardoppervlak. Aangezien in deze situatie oppervlaktewrijving sterk gereduceerd is, zal de aanwezige drukkracht op een gegeven moment de lucht in het onderste gedeelte van de grenslaag gaan versnellen, tot het moment dat de ontstane windshering sterk genoeg is om door de stratificatie heen te breken. Dit veroorzaakt een intensieve menging welke de aanwezige windschering en oppervlakte-inversie sterk reduceert. Weldra zal er weer een nieuwe inversie worden opgebouwd door de continue afkoeling van het aardoppervlak. Op deze wijze is de situatie weer teruggekeerd naar de beginsituatie en zal het mechanisme weer van voren af aan beginnen, hetgeen resulteert in een intermitterend karakter van de turbulentie.

In hoofdstuk 2 wordt aangetoond dat de essentie van dit intermittency mechanisme beschreven kan worden door middel van een simpel 1-D model bestaande uit drie gekoppelde niet-lineaire differentiaalvergelijkingen. Dit zogenaamde ‘bulkmodel’ bevat volgens de auteurs de meest essentiële elementen van de stabiele grenslaag: koeling nabij en van het aardoppervlak als gevolg van langgolvige uitstraling, de input van kinetische energie door (arbeid verricht door) de synoptische drukkracht en het feit dat stratificatie on stabiele omstandigheden in de regel een effectieve menging van verschillende luchtlagen vermoeilijkt. In de vereenvoudigde modelopzet wordt alleen de directe interactie tussen de onderste luchtlagen van de atmosfeer (enkele tientallen meters) en de vegetatie beschouwd, zonder te kijken naar interactie met hogere luchtlagen. Uiteraard limiteren dergelijke aannames de algemene geldigheid van de resultaten.

Het blijkt dat het eenvoudige bulkmodel in staat is om het bovengenoemde intermitterende gedrag van turbulentie te simuleren. Daarnaast laten de resultaten zien dat *zowel* intermitterende *als* niet-intermitterende regimes gesimuleerd worden onder verschillende externe forceringen: bij een veranderende drukgradiënt treden drie regimes op (twee niet intermitterend en één intermitterend). Dit is verrassend te noemen gezien de eenvoud van het model. Niettemin bevestigt dit de uitkomsten van eerdere studies met meer complexe modelconfiguraties (e.g. Lin, 1990; Revelle, 1993).

Uit de modelresultaten komt naar voren dat de kans op intermittency het grootst is bij heldere hemel en een tamelijk zwakke synoptische drukkracht, met name boven landoppervlakken met een lage vegetatie. Het blijkt dat de aanwezigheid van een vegetatielaag van sterke invloed is op de dynamica van intermittency: de temperatuur van een dunne vegetatielaag kan sterk reageren op snelle atmosferische

veranderingen. Deze temperatuurverandering van de vegetatie zelf echter, beïnvloed op haar beurt weer de stabiliteit van de onderste lagen van de atmosfeer. Derhalve kan er een belangrijke terugkoppeling ontstaan tussen de atmosfeer en het onderliggend oppervlak (zie H4). Uit een gevoeligheidsstudie met verschillende stabiliteitsfuncties blijkt dat intermitterend gedrag optreedt voor verschillende eerste-orde-sluiting schema's met verschillende stabiliteitsfuncties (zie ook Derbyshire, 1999). Daarbij wordt overigens wel aangetoond dat stabiliteitsfuncties met 'brede staarten' (d.w.z. stabiliteitsfuncties welke een aanzienlijk turbulent transport toestaan boven het kritische Richardsongetal) een mogelijk intermitterend gedrag sterk onderdrukken. Deze laatstgenoemde type stabiliteitsfuncties worden tegenwoordig gebruikt in weersvoorspellingsmodellen om excessieve koeling van het aardoppervlak onder stabiele condities tegen te gaan. Als laatste wordt opgemerkt dat gemiddelde flux-profiel relaties, strict gesproken, niet geldig kunnen zijn voor intermitterende stromingen. Dit ligt aan het feit dat de relaties niet lineair zijn, en dus hun tijds hun unieke karakter (d.w.z. één op één) verliezen in dergelijke stromingen wanneer tijds-gemiddelden worden gehanteerd.

Het gebruik van een vereenvoudigd model, zoals in hoofdstuk 2, heeft als voordeel ten opzichte van complexe modellen dat het een analytische studie van het systeem toestaat. Een dergelijke analytische studie wordt gepresenteerd in hoofdstuk 3, waarin de drie basisvergelijkingen van het bulkmodel geanalyseerd worden door middel van een systeem-dynamische aanpak. Op deze wijze worden de transities tussen de verschillende stromingsregimes geïdentificeerd als zijnde zogenaamde Hopf-bifurcaties van het systeem. Bij het Hopf-bifurcatiepunt verandert de stabiliteit van de evenwichtsoplossing namelijk zodanig dat een stabiele, niet oscillerende (en niet-intermitterende) oplossing verandert in een instabiele, oscillerende (en intermitterende) oplossing (en vice versa). Deze eigenschap wordt vervolgens gebruikt in de afleiding van een nieuw dimensieloos getal (aangegeven met het symbool Π), welke een functie is van externe forceringsparameters zoals de drukgradiënt en de stralingsforcering, en van locale parameters zoals de aërodynamische ruwheidslengte, de warmtecapaciteit en het bulk-geleidingsvermogen van de vegetatielaag. Met dit dimensieloos getal is het mogelijk om voorspellingen te doen over het gedrag van het systeem (d.w.z. of het systeem intermitterend of niet-intermitterend gedrag zal vertonen) in een evenwichtssituatie. Als zodanig wordt het getal gebruikt als hulpmiddel bij de classificatie van verschillende stabiele grenslaagregimes in termen van externe forceringparameters. Tevens wordt aangetoond dat deze classificatieparameter (Π) andere informatie verschaft dan klassieke classificatieparameters als z/L en Ri. Het verschil zit 'm hoofdzakelijk in het feit dat Π de stabiliteit van het systeem als geheel voorspelt, rekening houdend met terugkoppelingen in zowel het turbulentieschema als in de bodemwarmtestroom- en het stralingsschema, terwijl z/L en Ri bedoeld zijn als schalingsparameters van enkel turbulentie. Aangezien Π een behoorlijk gecompliceerde vorm heeft, is in hoofdstuk 3 ook een minder exact, maar stuk eenvoudiger stabiliteitscriterium afgeleid, waarbij gebruik gemaakt is van het zogenaamde 'fixed-shear criterion for instability' (zie ook: Derbyshire, 1999). Als zodanig laat dit praktische, meer doorzichtigere criterium een duidelijke fysische interpretatie toe (i.t.t. Π). Instabiliteit van het systeem blijkt te worden veroorzaakt door een positieve terugkoppeling tussen stratificatie en mengingsefficiëntie welke optreedt onder sterk gestratificeerde condities. Bovendien wordt aangetoond dat een mogelijke instabiliteit van het systeem tegengewerkt wordt door sterke negatieve terugkoppelingen afkomstig van warmtetransportprocessen door

geleiding in de bodem en door langgolvige straling in de lucht. Volgens het vereenvoudigde criterium kan het oorspronkelijke dimensieloze Π getal benaderd worden door twee dimensieloze groepen: een bulk Richardsongetal en een zogenaamde partitieparameter. Deze laatste kan worden geïnterpreteerd als de ratio van de gesommeerde coëfficiënten voor warmteflux door langgolvige straling en bodem/vegetatie-geleiding ten opzichte van de uitwisselingscoëfficiënt voor turbulente warmtestroom (N.B. een equivalente interpretatie in termen van fluxen van de genoemde processen is ook mogelijk). Als zodanig beschrijft deze partitieparameter de competitie tussen de eerder genoemde positieve en negatieve terugkoppelingen.

Hoofdstuk 4 behandelt de classificatie van stabiele grenslagen vanuit het experimentele gezichtspunt. Hiervoor wordt gebruik gemaakt van metingen verkregen tijdens CASES99 (Cooperative Atmospheric Surface-Exchange Study). Dit experiment, uitgevoerd door verschillende groepen uit de U.S.A. en Europa (waaronder de meteorologiegroep uit Wageningen), is specifiek opgezet met het doel om een beter begrip te krijgen van fysische grenslaagprocessen onder stabiele omstandigheden boven land. Het experiment vond plaats in Kansas (U.S.A.) in een relatief vlak gebied begroeid met tamelijk open prairie-gras. Het experiment werd uitgevoerd gedurende een volledig maand (oct. 1999) onder wisselende meteorologische condities. Dit maakt het experiment bijzonder geschikt om de verschillende stabiele grenslaagregimes te bestuderen in relatie tot externe forceringen.
Hoofdstuk 4 begint met een classificatie van verschillende regimes in de stabiele grenslaag, gebaseerd op waargenomen tijdreeksen van turbulente fluxen nabij het aardoppervlak gedurende CASES99. Als resultaat blijkt dat de bestudeerde nachten kunnen worden onderverdeeld in drie verschillende subklassen/regimes: een turbulent regime, een intermitterend regime en een stralingsregime. Dit resultaat is in overeenstemming met de theoretische bevindingen van hoofdstukken 2 en 3, waarin het bestaan van drie regimes werd voorspeld. Vervolgens wordt in hoofdstuk 4 deze classificatie op basis van flux-tijdreeksen vergeleken met de theoretische classificatie gebaseerd op het Π -concept. Hiertoe is voor al de verschillende CASES99 nachten een waarde voor Π geschat, door middel van een grondige analyse/parameterschatting met behulp van de beschikbare data. Een dergelijke evaluatie van Π op basis van werkelijke gegevens is niet triviaal, gezien het aantal theoretische aannames in de basisvergelijkingen waarop Π gebaseerd is (zo moet bv. de *effectieve* waarde van de drukgradiënt moet worden geschat i.p.v. de drukgradiënt sec). In het algemeen is er een goede overeenkomst tussen de voorspelde regimes met het Π -concept en de 'werkelijk opgetreden' regimes zoals waargenomen in de tijdreeksen. De resultaten blijken voldoende onderscheidend en robuust, zeker in kwalitatieve zin. Als zodanig wordt uit zowel de theoretische voorspellingen als uit de waargenomen tijdreeksen duidelijk dat intermittency in de regel optreedt ondere wolkenloze hemel in de aanwezigheid van een geringe/tamelijk zwakke drukgradiënt. Op gelijksoortige wijze blijkt dat, in wolkenloze condities, het stralings en het turbulente regime te verwachten zijn bij een respectievelijk zeer zwakke dan wel een tamelijk sterke drukgradiënt. De robuustheid van de resultaten kan op logische wijze worden verklaard uit de basisingrediënten van de stabiele grenslaag zoals beschreven in hoofdstuk 2. Aan de andere kant zijn de exacte *kwantitatieve* karakteristieken van de theoretische classificatie met Π tamelijk gevoelig voor (vaak onzekere) schattingen van locale parameters zoals het bulkgeleidingsvermogen van de vegetatielaag. Als

gevolg van deze gevoeligheid, zegt de *relatieve* Π -waarde voor een bepaalde nacht, ten opzichte van andere nachten op dezelfde locatie, meer dan een individuele waarde van Π . In hoofdstuk 4 wordt ook het vereenvoudigde criterium uit hoofdstuk 3 getest op de dataset van CASES99. Het blijkt dat dit criterium minder onderscheidend is dan het Π -criterium: hoewel tamelijk extreme gevallen juist worden voorspeld, zijn de voorspellingen voor de subtiele gevallen weinig onderscheidend of zelfs incorrect. Het is waarschijnlijk dat dit veroorzaakt wordt door de verwaarlozing van terugkoppelingsmechanismen tussen windschering en stratificatie, welke van belang zijn in de subtiele gevallen. Zodoende is het directe praktische nut van het vereenvoudigde criterium beperkt, ofschoon zij conceptueel gezien, sterk verhelderend is ten opzichte van het originele Π -criterium (H3).

Terugblikkend kunnen we stellen dat de analytisch aanpak in dit proefschrift voordelen heeft: interne relaties tussen de verschillende processen worden expliciet en evenwichtsoplossingen kunnen worden uitgedrukt in termen van externe forceringsparameters. Als zodanig is een dergelijke analytische aanpak nuttig bij toekomstig onderzoek naar de dynamica van de stabiele grenslaag. Daarnaast is er ook een behoeft aan onderzoek waarbij modellen met een hoger detailniveau (en minder stringente aannames) worden toegepast met het doel om precieze instabiliteitsmechanismen tijdens intermitterende turbulentie te kunnen ontrafelen. Zodoende zouden ‘bursting events’ kunnen bestudeerd m.b.t. geselecteerde case-studies. Als een continuering van het experimentele werk in deze studie kan gedacht worden aan het testen van de voorgestelde klassificatie onder verschillende climatologische omstandigheden. Daarnaast is er ook een behoefte aan lange-termijn meetcampagnes om een statistische klimatologie van intermittency vast te stellen. Daarbij moet gedacht worden aan een karakterisering van de tijdschalen en amplitudes van de turbulente bursts onder verschillende atmosferische condities. Met betrekking tot praktische toepassingen van het huidige werk merken we op dat de evenwichtsoplossingen uit hoofdstuk 3 als vertrekpunt zouden kunnen dienen voor toekomstige parameterizatie-studies. Aangezien gebleken is dat veel van de huidige praktijkproblemen met betrekking tot de stabiele grenslaag sterk verbonden zijn met een gebrek aan wetenschappelijke kennis, zal de praktijk in de toekomst vrij direct kunnen profiteren van een mogelijke wetenschappelijke vooruitgang.

Curriculum Vitae

Ik, Bas Johannus Henricus ben op 6 december 1972 geboren te Nijmegen. Kort daarna verhuisde we (terug) naar Tilburg waar ik tot mijn achttiende zou wonen. Via basisschool de Vlashof, die met veel plezier werd doorlopen, ging ik naar het St. Pauluslyceum waar het Gymnasium-β diploma werd behaald (cum laude). Daarna vertrok ik naar Wageningen om de studie Bodem-Water en Atmosfeer te gaan volgen. Tijdens de Wageningse studie werden er interessante bijvakken gevolgd in Eindhoven en vooral in Wenen, waar ik een onvergetelijke tijd doormaakte. Het eerste afstudeervak in de richting hydrologie, samen met Sander Bakkenist, betrof een studie naar de verspreiding van fabriekslozingen temidden van waterbeweging en sediment in het Rotterdamse havenestuarium (beloond met scriptieprijs). Daarna werd een tweede afstudeervak gedaan, samen met Martin van den Akker, naar mogelijke verbeteringen in de hoogwatervoorspellingen voor de Rijn met behulp van een aantal hybride methoden (gecombineerd fysisch-statistische aanpak).
Daarbij ben ik met name de docenten van deze studies, Jan Verhagen en Paul Torfs, dankbaar, omdat ze me fysisch/mathematisch inzicht bijgebracht hebben vanuit een (ogenschijnlijk) eenvoudige aanpak met conceptuele modellen. Vervolgens werd het doctoraalexamen Bodem-Water-Atmosfeer, specialistatie hydrologie/hydraulica aan de Landbouwuniversiteit behaald (cum laude). Via co-promotor Henk de Bruin belandde ik in een uitdagend promotieonderzoek in een aanverwant vakgebied: de grenslaagmeteorologie. Gedurende een vijftal jaren heb ik , in combinatie met enkele onderwijsactiviteiten, onderzoek gedaan naar de dynamica van de nachtelijke grenslaag. Het resultaat van deze werkzaamheden is (grotendeels) samengevat in het voorafgaande.

Cover illustrations thesis: The ‘Green Flash’ at sunset by Peter Pammer.

Thesis printing by: Grafisch Service Centrum Van Gils B.V., Wageningen

Sponsoring thesis: Meteo Consult Wageningen & Wageningen University